

MULTISCALE RESERVOIR SIMULATION: LAYER DESIGN, FULL FIELD  
PSEUDOIZATION AND NEAR WELL MODELING

A Dissertation

by

SONG DU

Submitted to the Office of Graduate Studies of  
Texas A&M University  
in partial fulfillment of the requirements for the degree of

DOCTOR OF PHILOSOPHY

Approved by:

Chair of Committee,	Michael J. King
Committee Members,	Akhil Datta-Gupta
	Duane McVay
	Yalchin Efendiev
Head of Department,	A. Daniel Hill

December 2012

Major Subject: Petroleum Engineering

Copyright 2012 Song Du

## ABSTRACT

In the past decades, considerable effort has been put into developing high resolution geological models for oil and gas reservoirs. Although the growth of computational power is rapid, the static model size still exceeds the model size for routine reservoir simulation. We develop and apply a variety of grid coarsening and refinement algorithms and single and multiphase upscaling approaches, applied to tight gas and conventional reservoir models.

The proposed research is organized into three areas. First the upgridding of detailed three dimensional geologic models is studied. We propose an improved layer design algorithm with considerations of accuracy and efficiency. This involves developing measures of reservoir heterogeneity and using these measures to design an optimal grouping of geologic model layers for flow simulation. The optimal design is shown to be a tradeoff between the desire to preserve the reservoir heterogeneity and a desire to minimize the simulation time. The statistical analysis is validated by comparison with flow simulation results.

Accurate upgridding/upscaling of single-phase parameters is necessary. However, it does not always satisfy the accuracy requirements, especially for the model which is aggressively coarsened. We introduce a pseudoization method with total mobility and effective fractional flow as the major targets. This pseudoization method helps to push upgridding/coarsening degree to the limit but still be able to reproduce the fine scale field performance. In practice, it is common to not use a different set of pseudos for every coarse cell; only a limited number of pseudo functions should be generated for different “rock types” or geological zones. For similar well patterns and well control conditions, applying pseudo is able to reproduce the fine scale performance for different simulation runs. This is the second proposed research area.

Finally, it is necessary to increase flow resolution for precise field history matching and forecasting. This has received increasing attention, especially when studying hydraulically fractured wells in unconventional reservoirs. We propose a multiscale reservoir simulation model combining local grid refinement (LGR) and pillar-based upscaling for tight gas reservoir performance prediction. Pillar-based coarsening away from the wells is designed for tight gas reservoirs. It compensates for the extra computational cost from LGR, which is used to represent hydraulic fractures. Overall reservoir performances, including the accuracy and efficiency, are evaluated.

## DEDICATION

To my parents Guihua Du and Ping Li for their love, support, and encouragement.

## ACKNOWLEDGEMENTS

I would like to express my deep gratitude to my graduate advisor Dr. Michael King for his inspiration, thoughtful advice, academic guidance, financial support, time and efforts contributed to this project. This work would not have been possible without him for sure.

I would like to thank Dr. Akhil Datta-Gupta for imparting some of his knowledge to me through our many meetings, discussions and classes.

I would like to thank Dr. McVay and Dr. Efendiev for serving on my committee. I acknowledge their helpful comments and suggestions in shaping this dissertation.

I would like to thank my colleagues in the model calibration and efficient reservoir imaging group for their precious help and discussion. Thank you for making my years in Texas A&M enjoyable.

I would like to acknowledge financial support from members of the Joint Industry Project. The facilities and resources provided by the Petroleum Engineering Department, Texas A&M University, are gratefully acknowledged.

## NOMENCLATURE

$a$	= hydraulic fracture extension
$A$	= cell area
$c_t$	= total compressibility
$B$	= between cell variance
$BHP$	= bottom hole pressure
$DX$	= cell length in x axis
$DY$	= cell length in y axis
$DZ$	= cell length in z axis
$f^*$	= Buckley-Leverett frontal speed
$F$	= flow capacity
$F_w$	= fractional water flow
$F_w^{Outlet}$	= fractional water flow at the outlet
$h$	= the cell thickness
$H$	= total heterogeneity
$k$	= permeability vector
$k_f$	= fracture permeability
$k_{ro}$	= oil relative permeability
$k_{rw}$	= water relative permeability
$\tilde{k}_x$	= pseudo permeability in x direction
$\tilde{k}_y$	= pseudo permeability in y direction
$L$	= cell length along the flux direction
$Lc$	= Lorenz coefficient
$n_{i,j,k}$	= bulk rock volume
$N$	= the total cell number
$NX$	= number of cells in x axis
$NY$	= number of cells in y axis

$NZ$	= number of cells in z axis
$p$	= upscaling parameter
$p_{ijk}^C$	=the coarsened static property of each cell
$\bar{p}_{ij}$	=the column based average of the static property
$\bar{p}_{ij}$	= the column based average of the static property
$P$	= pressure
$PV$	= cell pore volume
$P_{wf}$	= wellbore pressure
$P_b$	= well block average pressure
$r_b$	= Peaceman radius
$r_w$	= wellbore radius
$S_w$	= water saturation
$S_{oir}$	= irreducible oil saturation
$\bar{S}_w$	= averaged saturation of entire model
$S_w^{Outlet}$	= water saturation at the outlet
$\overline{S_w^{Outlet}(t)}$	= averaged water saturation at the outlet
$t$	= time
$t_x$	= diffusive time in x direction
$t_z$	= diffusive time in z direction
$T$	=transmissibility
$Q$	= volumetric flux
$Q_{it}^{outlet}$	= total volumetric flux of phase "i" at the outlet
$\bar{u}$	= Darcy velocity
$w$	= fracture width
$W_i$	= cumulative of water injection
$W$	= within cell variance

$\Delta x$	= cell length in x direction
$\Delta y$	= cell width in y direction
$\delta$	= <i>difference</i>
$\zeta$	= <i>distance along streamline</i>
$\lambda$	= <i>mobility</i>
$\lambda_{\text{total}}$	= <i>total mobility</i>
$\lambda_T^{\text{Outlet}}$	= <i>total mobility at the outlet</i>
$\tau$	= <i>time of flight</i>
$\phi$	= <i>porosity</i>
$\Phi$	= <i>storage capacity</i>
$\psi$	= <i>streamline trajectory</i>
$\nabla$	= <i>gradient</i>
$\mu$	= <i>viscosity</i>



## TABLE OF CONTENTS

	Page
ABSTRACT .....	ii
DEDICATION .....	iv
ACKNOWLEDGEMENTS .....	v
NOMENCLATURE .....	vi
TABLE OF CONTENTS .....	ix
LIST OF FIGURES .....	xii
LIST OF TABLES .....	xv
1 INTRODUCTION .....	1
1.1 Motivation .....	1
1.2 Objectives of the Study .....	3
1.3 Dissertation Outline .....	5
2 EFFECTIVE SIMULATION LAYER DESIGN FOR HIGH RESOLUTION GEOLOGIC MODELS .....	7
2.1 Introduction .....	7
2.2 Literature Review .....	8
2.2.1 Upgridding .....	8
2.3 Methodology .....	10
2.3.1 Heterogeneity Evaluations .....	10
2.3.2 Upgridding Procedures .....	23
2.3.3 Optimal Number of Layers in Coarse Model .....	24
2.4 Field Applications .....	26
2.4.1 Case 1: SPE10, Model 2 .....	26
2.4.2 Case 2: Turbidite Reservoir, Deepwater Gulf of Mexico .....	36
2.5 Discussion .....	44
2.5.1 Gridding Design .....	44
2.5.2 Modified V&S .....	47
2.6 Conclusions .....	50

3	PSEUDO FUNCTIONS AND THEIR APPLICATIONS .....	52
3.1	Introduction .....	52
3.2	Literature Review .....	53
3.3	Methodology .....	55
3.3.1	JBN Methodology.....	57
3.3.2	Effective Total Mobility .....	60
3.3.3	General Workflow .....	63
3.4	Results and Discussions .....	64
3.4.1	Model Description .....	64
3.4.2	Results and Comparisons.....	66
3.4.3	Discussions .....	88
3.5	Conclusions .....	90
4	TIGHT GAS RESERVOIR MANAGEMENT: MULTISCALE SIMULATION .....	92
4.1	Introduction .....	92
4.2	Literature Review .....	95
4.2.1	Hydraulic Fracture Representation .....	95
4.2.2	Well Spacing Design and Infill Drilling Potentials .....	98
4.3	Hydraulic Fracture Representation.....	100
4.3.1	Introduction.....	100
4.3.2	Effective Permeability .....	100
4.3.3	Enhanced Transmissibility.....	101
4.3.4	Infinite Conductivity Model .....	103
4.3.5	Local Grid Refinement .....	105
4.4	Pillar Based Upscaling .....	108
4.4.1	Introduction.....	108
4.4.2	Methodology.....	109
4.5	Tight Gas Reservoir Description.....	114
4.5.1	Multiscale Modeling Results .....	114
4.5.2	Discussions .....	122
4.6	Conclusions .....	124
5	CONCLUSIONS AND FUTURE WORK .....	126
5.1	Summary and Conclusions.....	126
5.2	Suggestions for Future Work .....	130
	REFERENCES.....	132
	APPENDIX A: COMBINATION OF VELOCITY AND SLOWNESS.....	146

APPENDIX B: SWIFT .....	149
APPENDIX C: WORKFLOW OF THE MULTIPHASE UPSCALING .....	166
APPENDIX D: SWIFT_PILLAR .....	168

## LIST OF FIGURES

	Page
Figure 2-1 “Best-fit” line.....	13
Figure 2-2 Typical F-C curves .....	16
Figure 2-3 Lorenz chart for the 19 layer model described in Table 2-2 .....	17
Figure 2-4 Various velocities replaced by a single one .....	20
Figure 2-5 Standard procedure optimal upgridding .....	24
Figure 2-6 Fine scale permeability distribution of SPE10 (Model 2).....	26
Figure 2-7 Heterogeneity comparison of SPE10 case: Slowness, Velocity, “V&S” and Lorenz coefficient (A) under normalized scale (B) under Lorenz Coefficient scale.....	28
Figure 2-8 Grouping sequences for different static measures.....	30
Figure 2-9 A 3D view of the 29 layer model colored by layer thickness, designed with optimal slowness.....	31
Figure 2-10 Comparison of fine and coarse scale field predictions.....	32
Figure 2-11 Comparison of fine and coarse scale field response with different coarsened layers .....	34
Figure 2-12 Exhaustive determination of cumulative recovery vs. number of layers .....	35
Figure 2-13 Comparison of the fine and coarse scale CPU time .....	36
Figure 2-14 Reservoir structure.....	37
Figure 2-15 Water saturation profile at the same cross-section for different model resolutions at 2000 days: (A) 420 layer model, (B) 15 layer model (C) 7 layer model.....	38
Figure 2-16 Heterogeneity analysis of case2 (A) V&S (B) Slowness (C) Velocity .....	40
Figure 2-17 Heterogeneity under Lorenz coefficient scale.....	41

Figure 2-18 Field performance: oil production prediction with different layer combination.....	41
Figure 2-19 Filed performance: cumulative oil production with different layer combination.....	42
Figure 2-20 Comparison of the fine and coarse scale CPU time .....	43
Figure 2-21 Aquifer flow geometries.....	45
Figure 2-22 Oil recovery for modified SPE10 at 2000 days.....	46
Figure 2-23 Between-variation heterogeneity analysis for the SPE10 case study.....	48
Figure 2-24 Grouping sequence for: (A) original “V&S” by Kelkar and (B) modified “V&S” .....	48
Figure 2-25 QQ scatterplot of original “V&S” grouping vs. other static measure based grouping (25 layer model).....	49
Figure 3-1 Effective fractional flow illustration .....	59
Figure 3-2 Illustration of total fluid segregation .....	61
Figure 3-3 Quarter model (A) line drive pattern (B) Q5 pattern.....	65
Figure 3-4 Pseudo function bias and calibration: (A) Q5 pattern (B) line drive pattern..	68
Figure 3-5 Rate control: (A) pseudo fractional flow and (B) effective total mobility .....	70
Figure 3-6 Effective total mobility for (A) line drive models and (B) Q5 spot models (C) Coats models.....	71
Figure 3-7 Rate control injection wells, field performance: (A, B) oil production rate (C, D) cumulative oil production (E, F) water cut (G, H) field pressure .....	74
Figure 3-8 Pressure control: (A) Pseudo fractional flow and (B) effective total mobility .....	77
Figure 3-9 Effective total mobility for (A) line drive models and (B) Q5 spot models (pressure control).....	78
Figure 3-10 Pressure control injection wells, field performance: (A, B) oil production rate (C, D) cumulative oil production (E, F) water cut (G, H) field	

pressure.....	80
Figure 3-11 Field performance when injectors are under pressure control and producers are under rate control: (A, B) oil production rate (C, D) cumulative oil production (E, F) water cut (G, H) field pressure .....	83
Figure 3-12 Effective fraction flow and total mobility: $a = 2.5$ .....	86
Figure 3-13 Field performance for a two layer model (A) oil production rate (B) cumulative oil production (C) water cut (D) field pressure .....	87
Figure 4-1 Illustration of hydraulic fracture through original simulation grids.....	101
Figure 4-2 Illustration of hydraulic fracture through partial cells.....	102
Figure 4-3 Illustration of infinite-conductivity line source on (A) cell centers (B) cell edges.....	103
Figure 4-4 Sample of local grid refinement .....	106
Figure 4-5 Typical hydraulic fracture distribution.....	107
Figure 4-6 Illustration of pillar based upgridding .....	110
Figure 4-7 Diffusive time in (A) horizontal direction (B) Vertical direction. ....	111
Figure 4-8 2x4 Upscaling: Transmissibility vs. Permeability.....	113
Figure 4-9 Geologic model for Wamsutter tight gas reservoir (A) NTG (B) permeability distribution .....	114
Figure 4-10 Fracture distributions and cross-section of upscaled models .....	115
Figure 4-11 Cross-section view of the fracture representation in a multiscale model ...	116
Figure 4-12 Benchmarking of model simulation prediction from different algorithms	119
Figure 4-13 Benchmarking of model simulation prediction from different algorithms at 10 years .....	120
Figure 4-14 Benchmarking of model simulation prediction using ECLIPSE.....	121
Figure 4-15 Benchmarking of different simulator performance .....	122

## LIST OF TABLES

	Page
Table 2-1 1-D synthetic layered model .....	13
Table 2-2 Example calculation of Lorenz chart for a 19 layer model.....	17
Table 2-3 Variance based static measures.....	21

## 1 INTRODUCTION

### 1.1 Motivation

Subsurface reservoirs are characterized by strong heterogeneities occurring on a variety of scales. Data integration from different sources and scales, such as core, well log, and seismic data, generates the geologic descriptions, which are used for building flow (relative permeability and capillary pressure curves) are measured and modeled at different scales. Upscaling of these properties is necessary to preserve the impact of the small scale reservoir heterogeneity on the large scale reservoir fluid flow.

In the past decades, great effort has been put into developing high resolution geological models for oil and gas reservoirs. These models are used to capture the heterogeneity in rock properties that can affect the fluid flow, and hence the oil and gas recovery. Static reservoir models with  $10^7$  cells are routine, while models with  $10^8 \sim 10^9$  cells (Dogru, 2010) are also being created. Although the growth of computational power is rapid, the static model size still exceeds the model size for routine reservoir simulation. Significant computational power is required for flow simulation on such large models. This is especially true when multiple realizations of reservoir models are built for uncertainty analysis and reservoir performance predictions. As a consequence there are a variety of requirements which cannot be met by working at a single scale or with a single style of model. However, it is impotent to work consistently across multiple scales, which is the subject area of this dissertation. We develop and apply a variety of grid coarsening and refinement algorithms and single and multiphase upscaling approaches, applied to tight gas and conventional reservoir models. These models have sufficiently high resolution to represent hydraulically fractured wells in the tight gas reserves and sufficiently low resolution away from the wells for effective full field models.

The proposed research is organized into three areas. First the upgridding of heterogeneous three dimensional geologic models is studied. This research work



investigates novel heterogeneity measures that are able to predict optimal number of layers for convective dominated process. We design, extend, and integrate a measure which focuses on the time of flight and breakthrough response. This work also involves the development of a Petrel plug-in to build coarse reservoir simulation models, which honor geologic makers, and for arbitrary layering schemes.

Accurate upgridding/upscaling of single-phase parameters is necessary. However, it does not always satisfy the accuracy requirements, especially for the model which is aggressively coarsened. It is necessary to pseudoize the multiphase flow properties to reproduce the flow behaviors in the fine scale models. The second area includes the development of a novel multiphase upscaling technique which integrates the classic JBN method (Johnson et al. 1959) for homogeneous core flood analysis with heterogeneous large scale sector models. We presented the impact of total mobility upscaling and demonstrated the requirement of rescaling the overall permeability as part of the multiphase upscaling procedures. This research also provides a simple parameterization to upscale rock curves to reservoir scale.

Finally, it is necessary to increase flow resolution for precise field history matching and forecasting. This has received increasing attention, especially when studying hydraulically fractured wells in unconventional reservoirs. Most tight gas reservoirs need to be stimulated with hydraulic fractures for commercial production. A key issue in tight gas reservoir modeling is to represent the hydraulic fractures precisely. Traditional ways to model hydraulic fractures in 3D models are to mimic the flow behaviors with modified skin factors, modified cell permeability/transmissibility and well productivity index (PI). However, none of them can fully reproduce the critical transient physics of the flow into and through the fracture-matrix-well system. Precise representation of grids with local grid refinement is an alternative enabling realistic near wellbore modeling and flow simulation. The major drawback of applying LGRs is that the explicit gridding introduces a large number of cells and makes it impractical to use LGRs in full field

model. Multiscale reservoir modeling can be considered for solving such a problem. We proposed and tested a unique combination of using a novel unstructured coarsening algorithm, a traditional LGR structure and Nexus, the next generation “unstructured” simulator. In such a multiscale model, the low permeability region requires explicitly refined grids for temporal resolution. The higher permeability area has rapid transients to steady state, and can be modeled using effective well index or cell permeability.

In short, there exists competition between the computational efficiency and the capability of reproducing the detailed reservoir behaviors. Though much work has been done on single phase upgridding/upscaling, multiphase upscaling and multiscale modeling, there are still unsolved problems in this general field. How to reduce the computational costs of the upscaling which may be comparable to the fine scale simulation runtime? How to create a reasonable coarse model from a fine scale one? What is the coarsening limit a model can be pushed to, with/without multiphase upscaling techniques? Is it feasible to use the same upscaling techniques for both conventional and unconventional reservoirs? If not, how can they be improved? Are there any other issues need to be taken care of in tight gas reservoir modeling? This research will try to answer the questions above, while at the same time providing a fundamental review of each element of the proposed methods.

## 1.2 Objectives of the Study

This work studies upgridding for layer design, pseudoization and near-well modeling in heterogeneous reservoirs, with the emphasis on the scale manipulation from geostatistical modeling to flow simulation. Although lots of work and development has been finished in this general area, there still exist outstanding issues.

Our objectives include:

- 1) Improving layer design algorithm by introducing novel measures of

heterogeneity, with considerations of accuracy and efficiency. For accuracy, crucial flow behaviors at fine scales should be preserved. Total flow rates for given condition, breakthrough time of injection fluid, and the average pressure of the entire domain are used to evaluate the accuracy. For efficiency, computational cost would be evaluated. It consists of two parts. One is the upgridding procedure itself as a model pre-processing step, and the other is the degree of coarsening that is achieved by layer design algorithms.

- 2) Development of a pseudoization method based upon total mobility and effective fractional flow. This pseudoization method helps to push upgridding/coarsening degree to the limit but still be able to reproduce the fine scale field performance. It involves both novel local total mobility upscaling and global permeability upscaling impacts.
- 3) Development of a multiscale reservoir simulation model combining local grid refinement (LGR) and pillar-based upscaling for tight gas reservoir performance prediction. Pillar-based coarsening, designed for tight gas reservoir specifically, will compensate the extra computational cost from LGR which is used to represent hydraulic fractures. Overall reservoir performance, include the accuracy and efficiency as mentioned, is evaluated.
- 4) Development of software for layer design and tight gas reservoir modeling. Two different types of software/plugin are developed as simulation pre-processing tools.

### 1.3 Dissertation Outline

The dissertation is arranged as follows:

Chapter 2 presents the work on effective simulation layer design based on error analysis. A sequential layer design algorithm, which provides the capability of preserving the heterogeneity of the fine scale model efficiently, is introduced. We investigate novel static heterogeneity measures that are applicable for different flow scenarios and are able to predict optimal number of layers for convective dominated process. Based on the error analysis, we apply a non-uniform upgridding method to coarsen the reservoir model vertically, instead of using uniform coarsened layers. This method combines the fine-scale layers in such a way that the heterogeneity within the coarse cells is minimized while it is maximized between the coarsened cells. Within this upgridding workflow, the fine scale flow behaviors can be preserved in the coarsened models. Demonstrations of algorithm effectiveness and efficiency are presented on the SPE10 model and also a turbidite reservoir.

In Chapter 3, a general pseudoization method for multiphase upscaling is developed based on the calculation of effective relative permeability, effective total mobility and global permeability upscaling. The effective relative permeability calculation follows the modified JBN method (Johnson et al. 1959). This multiphase upscaling method also considers both the local total mobility upscaling and the global absolute permeability upscaling impacts. This pseudoization method is suitable especially for the progressively coarsened models. A model calibration method is introduced to avoid calculation of unrealistic pseudo relative permeabilities. Sensitivity studies are performed to investigate the impacts from total mobility under different flow scenarios. The pseudoization method is validated on SPE10 case with different injection conditions.

In Chapter 4, our research focuses on multiscale tight gas reservoir modeling. First, different methods representing hydraulic fractures are reviewed. The pillar-based adaptive coarsening algorithm is then introduced to improve the computational efficiency. Due to the special geologic descriptions of tight gas reservoirs, the adaptive coarsening breaks the concept of “layer” and reconstructs the model in such a way that pay and non-pay cells are never merged. For the first time, a multiscale tight gas reservoir model, combining a novel pillar-based upscaling technique and the traditional local grid refinements, is built and tested with the next generation simulator. Only with the high resolution near wells, can the engineers study the pressure and stress change which affects the future infill drillings. Low resolution far away from the well and fractures helps to maintain the simulation efficiency. The multiscale reservoir modeling was demonstrated with a full field U.S. on-shore reservoir model.

In Chapter 5, we draw conclusions and present our recommendations for future research in coarse scale modeling of flow and transport and tight gas reservoir modeling and management.

Finally, in Appendix A, a simple illustration of error calculation of “V&S” method is presented. Comparison to Hosseini et al.’s work (2008) is also reviewed. A Petrel plug-in for effective layer design is introduced in Appendix B. In appendix C, a general workflow of pseudoization procedures is reviewed. In appendix D, an Internal Programming Language (IPL) based script for tight gas reservoir coarsening is introduced.

## 2 EFFECTIVE SIMULATION LAYER DESIGN FOR HIGH RESOLUTION GEOLOGIC MODELS

### 2.1 Introduction

In this chapter, we present our work on effective simulation layer design which is based on a static error analysis. Layer design is a widely applied form of reservoir coarsening and is a necessary procedure for reservoir flow simulation. We utilize a sequential layer design algorithm that provides the capability of efficiently preserving the heterogeneity of the fine scale model. We investigate novel heterogeneity measures that are able to predict optimal number of layers for convective dominated process.

This work applies high resolution upscaling techniques to model flow in heterogeneous reservoirs. The current work differs from these previous efforts in that there is no need to reference actual wells, their locations, or rates. Finally, we utilize an a priori analysis of the upscaling error as a guide to the required resolution of the simulation grid. The error analysis utilized in this study relies upon a variance analysis of “Velocity”, ”Slowness”, modified “V&S” and Lorenz coefficient. The modified “V&S” focuses on the time of flight and breakthrough response simultaneously. Lorenz coefficient provides an evaluation of the model heterogeneity in a wide distribution, and it takes care of the flow capacity and the storage capacity at the same time.

In this chapter, we first review the previous studies on upgridding and upscaling techniques and then present the upgridding methodology for the geologic models. Algebraic upscaling techniques will not be emphasized since in general, the numerical flow based calculations provide a better characterization of the reservoir’s heterogeneity. Further, flow based calculations can be performed quite effectively, with, for instance, local or extended local flow based upscaling of a 20 million cell geologic model taking approximately five minutes on a current laptop. All of the approaches are validated using

the SPE10 Model 2 (Christie and Blunt 2001) and a full field deepwater Gulf of Mexico case.

## 2.2 Literature Review

### 2.2.1 Upgridding

Several papers have been published regarding both the upgridding and assigning effective properties for coarsened grid block (Li and Beckner 1999, 2000; Li and Lake 1995; Stern and Dawson 1999; Testerman 1962; Zhang et al. 2006).

Statistical approaches applied to the layer coarsening use the geological reservoir properties to generate the new property. Early in 1963, Testerman first developed the application of a statistical approach on zonation scheme. In his work, Testerman focused on how to zone individual wells and how to build up a reservation zonation scheme from multiple wells. His approach is better described as a refinement method because he started with treating the reservoir as a single layer and sequentially separated this reservoir into layers based on calculation of “Between” and “Within” variation. His ideas about grouping layers based on the permeabilities, minimizing the variance within each layer and maximizing the variance between layers were later further developed by other researchers (Li and Beckner 2000; Li and Lake 1995).

Li et al. (1995) presented a global permeability scale-up method which attempted to preserve the variance and the spatial correlation within an entire permeability field. Li and Beckner (2000) focused directly on grouping fine scale layers into coarsen scale for the reservoir simulation. Rather than using permeability only, they proposed a new uplayering (upgridding) property, which was a combination of porosity, permeability and facies (in term of relative permeability, endpoint saturation and various facies rules),

as a static measure. A residual curve was generated as a function of the number of simulation layers from a given initial number of layers to the number of geologic layers. The residual curve is able to show all potential upgridding scenarios for a given geological model, and it provides reservoir engineers with quantitative knowledge on the amount of the loss of reservoir heterogeneity.

Stern and Dawson (1999) developed a sequential coarsening algorithm which included: selecting optimal locations for simulation model layer boundaries and determining the number of layers required. Starting from the bottom of a geological model, they sequentially combined the layers in such a way that can minimize the changes in geological model properties. They defined two types of objective functions which are combinations of permeability, porosity and thickness of the fine grid cells. The first one is the change in the time required for single-phase breakthrough in both fine and coarse grid. The second one focuses on the difference of flux between fine and coarse grids. The adjacent layers were combined so as to minimize the increase in the objective function. To determine the optimal number of layers that preserved, they calculated sweep efficiency for unit mobility displacements. This iterative method is able to provide a quantitative way for selecting an optimal layer number.

King et al. (2005) proposed the upgridding method that utilizes the local velocity as the static measure of heterogeneity. The local velocity is the product of Buckley Leverett velocity and interstitial flow velocity within each layer. This local velocity is directly related to the fluid flow in the porous media. The preservation of heterogeneity was maximized in the reservoirs by combining the layers that minimize the deviation from the original fine scale variance.

From Darcy's steady state equation, Hosseini and Kelkar (2008) derived a criterion that incorporated thickness and size of the grid blocks into account for upgridding. They used pressure profile to combine layers while maintaining the variation in permeabilities.



They also introduced a total error term which was the multiplication of various errors terms, including the effect of cross flow, adverse mobility ratios and so on. Besides, Hosseini and Kelkar provided two different parameters for choosing the optimum number of layers. The first one was a design factor representing the quality of the layering design and reservoir. The second one was the change of error per layer calculated at each step of the coarsening. These parameters are able to evaluate the level of the heterogeneity preserved in the reservoir and to propose possible optimum layer combinations. Instead of proposing one optimal number of layers, they suggested various numbers for users.

Another important upscaling approach that has been studied for years is flow-based method in which the pressure equation is solved for each cell and flux properties are determined later (Chen and Durlofsky 2007; Chen et al. 2003; Efendiev and Durlofsky 2003; Stern and Dawson 1999; White and Horne 1987; Wu et al. 2007; Zhang et al. 2006). Our effective layer design algorithm is to minimize the requirement for flow based upscaling which may be time consuming.

## 2.3 Methodology

### 2.3.1 Heterogeneity Evaluations

The reservoir properties such as permeability, porosity, fluid saturation, lithology and others vary in space both vertically and laterally. Therefore the petroleum reservoirs rocks are heterogeneous in nature. In a static statistical study, there are different ways of evaluating the heterogeneity of a reservoir model or the heterogeneity preserved during the upscaling procedures.

We utilize traditional static heterogeneity measures ignoring correlation (Dykstra and Parsons 1950; Lake and Jensen 1989; Schmalz and Rahhme 1950; Shook and Mitchell 2009; Testerman 1962). These measures are based on measured samples (usually core plugs) taken from the reservoir. The spatial relationships of the samples are ignored. The samples are treated as independent and representative data all coming from one population. Permeability and (exceptionally) porosity data are used in the calculation. Three typical static heterogeneity measures are: the coefficient of variation, the Dykstra-Parsons coefficient, and the Lorenz coefficient. The major advantages of the three traditional static measures are the relatively low cost of estimation and their effectiveness in conveying heterogeneity effects in models (Lake and Jensen 1989). However, while the Dykstra-Parsons and Lorenz Coefficients give measures of the permeability variation, they provide no information on the spatial relationship between the permeability values (Peters 2012). Dynamic methods of measuring heterogeneity, such as fast simulation (Ballin et al. 1992; Deutsch and Srinivasan 1996), permeability-connectivity estimates (Ballin et al. 2002; Hird and Dubrule 1998), and streamline simulation (Datta-Gupta and King 2007; Shook and Mitchell 2009) can better account for permeability connectivity.

#### 2.3.1.1 Dykstra-Parsons Coefficient

The original Dykstra-Parsons coefficient (Dykstra and Parsons 1950),  $V_{DP}$ , is a measure of heterogeneity based on the permeability variations only. The “permeability variation” is determined from the median and variance of an ordered set of permeability data. The method used to calculate  $V_{DP}$  has the assumption that permeability data are drawn from a log normal distribution. The permeability data are ranked in a decreasing order, and then the frequency distribution of the permeability data are plotted on log-normal probability paper. A “best-fit” straight line is used to represent an “equivalent” reservoir having a log-normal permeability distribution. Lake and Jensen (1989) and Peters (2012) suggested to use the central portion of the data if the points do not fall approximately on

a straight line. This “best-fit” line is used to determine the 84<sup>th</sup> percentile permeability,  $k_{0.84}$ , which is the one standard deviation from the mean and the log mean permeability,  $k_{0.5}$ . The Dykstra-Parsons coefficient is defined as:

$$V_{DP} = \frac{k_{0.5} - k_{0.84}}{k_{0.5}} \quad \mathbf{2-1}$$

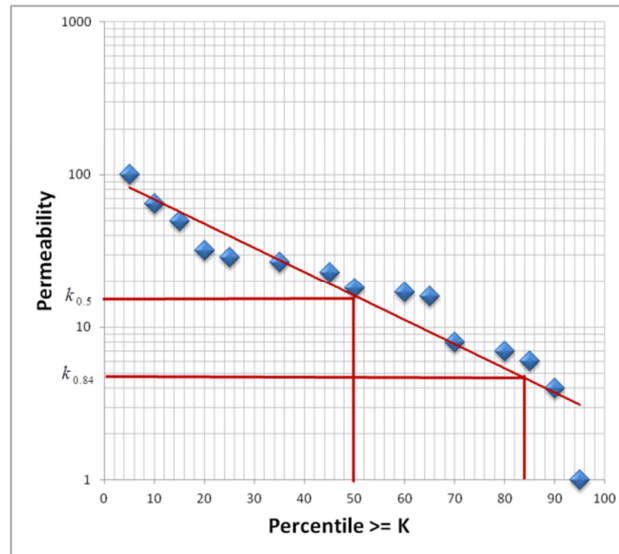
A simple illustration is presented in Figure 2-1 and the sorted permeability values are presented in Table 2-1.  $k_{0.5} = 22.3md$ ,  $k_{0.84} = 3.6md$  and  $V_{DP} = \frac{22.3 - 3.6}{22.3} = 0.8386$ .

Dykstra-Parsons coefficient of variation is a dimensionless number that ranges from 0 to 1. A homogeneous reservoir has a coefficient of permeability variation that approaches 0 whereas an extremely heterogeneous reservoir has a coefficient of permeability variation that approaches 1.

The above procedures have another assumption that each permeability datum represents the same quantity (e.g., thickness or bulk rock volume) of formation. Jensen and Lake (1988; 1989) pointed out the misfit in behavior is influenced by the subjective element in drawing the “best-fit” line. They also demonstrated that Dykstra-Parsons coefficient is non-unique: several “equivalent” reservoirs have quite different performances. In other words: multiple static models could have the same  $V_{DP}$ , although, dynamically, they are different. Another disadvantage is a little subtle:  $V_{DP}$  has low sensitivity of models, when  $V_{DP} < 0.5$  and high sensitivity of models when  $V_{DP} > 0.5$  (Tang and Liu 2008). While the Dykstra-Parsons coefficient gives a measure of the permeability variation, it provides no information on the spatial correlation between the values. It is also known that the permeability and other petrophysics properties (like porosity) are not randomly distributed. Another measure of heterogeneity, Lorenz coefficient, takes into account both the permeability and porosity distributions.

**Table 2-1 1-D synthetic layered model**

k (md)	$\Phi$	h(ft)	No of Samples $\geq k$	Percentile $\geq k$
250	0.25	5	1	5
178	0.24	5	2	10
135	0.23	5	3	15
130	0.22	5	4	20
82	0.21	5	5	25
45	0.21	5		
45	0.21	5	7	35
36	0.21	5		
36	0.21	5	9	45
19	0.21	5	10	50
17	0.21	5		
17	0.21	5	12	60
16	0.21	5	13	65
8	0.1	5	14	70
7	0.1	5		
7	0.1	5	16	80
6	0.05	5	17	85
4	0.05	5	18	90
2	0.05	5	19	95

**Figure 2-1 “Best-fit” line**

### 2.3.1.2 Lorenz Coefficient

The Lorenz coefficient measure of heterogeneity is developed based on ‘flow capacity – storage capacity’ diagrams which were studied in the past decades (Gunter et al. 1997; Lake 1989; Schmalz and Rahhme 1950; Stiles 1949). The original ‘flow capacity – storage capacity’ diagrams are used for 1D, vertical cross section and isolated multilayer reservoirs and are known as the  $F - C$  curves. Lorenz coefficient emphasizes the correlation between porosity and permeability. As a model is increasingly homogenized, this correlation is lost. Therefore, we can use LC as a heterogeneity measure while upscaling.

A general procedure to generate the  $F - C$  curve for 1D layer model is going to be reviewed here and detailed applications on 1D are presented after that. Here, we consider a model with multiple layers, each having a different permeability,  $k$ , porosity,  $\phi$ , and thickness,  $h$ . The flow capacity and storage capacity of the individual layers can be identified in the following steps:

**Step 1:** The layers are ordered according to decreasing fluid velocity which is defined as  $k_i / \phi_i$ .

**Step 2:** Calculate individual layer flow capacity which is defined as the volumetric flow of that layer, divided by the total volumetric flow:

$$f_j = \frac{q_i}{\sum_1^N q_i} \quad 2-2$$

Applying Darcy’s Law:

$$q_i = -\frac{kA}{\mu} \frac{\Delta P}{L} \quad 2-3$$

We simply have

$$f_j = \frac{q_i}{\sum_1^N q_i} = \frac{(kh)_i}{\sum_1^N (kh)_i} \quad 2-4$$

**Step 3:** Calculate fractional storage capacity for each layer. The storage capacity is defined as the layer pore volume divided by the total pore volume:

$$c_j = \frac{PORV_j}{\sum_1^N PORV_j} = \frac{(\phi h)_i}{\sum_1^N (\phi h)_i}$$

**Step 4:** Plot the cumulative distribution of flow capacity and storage capacity and the accumulations which are defined as following:

$$F_i = \frac{\sum_{j=1}^i q_j}{\sum_1^N q_i} = \frac{\sum_{j=1}^i (kh)_j}{\sum_1^N (kh)_j} \quad 2-5$$

$$C_i = \frac{\sum_{j=1}^i PORV_j}{\sum_{j=1}^N PORV_j} = \frac{\sum_{j=1}^i (\phi h)_j}{\sum_{j=1}^N (\phi h)_j} \quad 2-6$$

N is the total number of layers.  $F_i$  is the volumetric flow capacity from the velocities greater than that of layer i and  $C_i$  is the corresponding storage capacity. The cross-plotted diagram reveals the relationship between the flow capacity and storage capacity. A simple synthetic illustration is presented in Figure 2-2. A pure homogeneous case is shown in a blue corner-to-corner straight line. For a highly heterogeneous case, the flow capacity increases rapidly at the beginning with limited storage capacity.

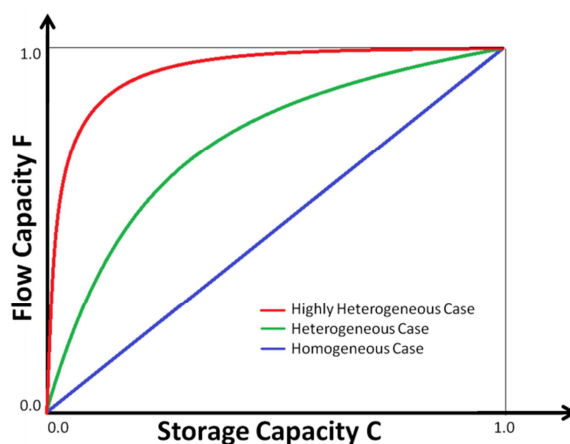


**Figure 2-2 Typical F-C curves**

$F - C$  curve can be used to generate Lorenz Coefficient (Lake 1989; Schmalz and Rahhme 1950) and it's defined as:

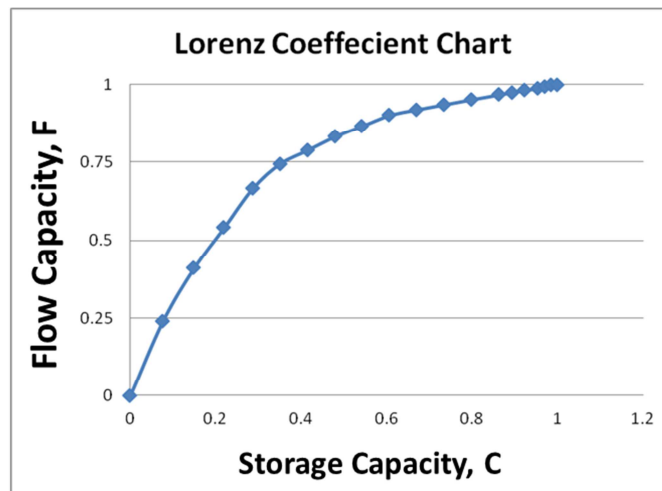
$$L_C = 2 \int_0^1 (FdC - 0.5) \quad 2-7$$

The original Lorenz coefficient concerns 1D layered model. We have 3D heterogeneous reservoir simulation model in actuality. We calculate the Lorenz coefficient on such 3D models in a map based sense. For each grid column, one Lorenz coefficient is calculated, and then the values are summarized over the horizontal plane for the 3D model. As a result, a 2D Lorenz map for the 3D heterogeneous model is preserved. The maximized summation of the Lorenz coefficient indicates that two adjacent vertical layers shall be upgridded.

Calculations for the same 19-layer model are given in Table 2-2 below, and the resulting Lorenz Chart is given in Figure 2-3.

**Table 2-2 Example calculation of Lorenz chart for a 19 layer model**

k (md)	$\Phi$	h(ft)	kh	$\Phi h$	F	C
					0	0
250	0.25	5	1250	1.25	0.2404	0.0762
178	0.24	5	890	1.2	0.4115	0.1494
135	0.23	5	675	1.15	0.5413	0.2195
130	0.22	5	650	1.1	0.6663	0.2866
82	0.21	5	410	1.05	0.7452	0.3506
45	0.21	5	225	1.05	0.7885	0.4146
45	0.21	5	225	1.05	0.8317	0.4787
36	0.21	5	180	1.05	0.8663	0.5427
36	0.21	5	180	1.05	0.9010	0.6067
19	0.21	5	95	1.05	0.9192	0.6707
17	0.21	5	85	1.05	0.9356	0.7348
17	0.21	5	85	1.05	0.9519	0.7988
16	0.21	5	80	1.05	0.9673	0.8628
8	0.1	5	40	0.5	0.9750	0.8933
7	0.1	5	35	0.5	0.9817	0.9238
7	0.1	5	35	0.5	0.9885	0.9543
6	0.05	5	30	0.25	0.9942	0.9695
4	0.05	5	20	0.25	0.9981	0.9848
2	0.05	5	10	0.25	1	1
			5200	16.4		

**Figure 2-3 Lorenz chart for the 19 layer model described in Table 2-2**



From an upgridding point of view, the original fine scale geological model retains the maximum amount of heterogeneity. In other words, it is far away from the straight corner-to-corner line (as the blue curve in Figure 2-2). During the coarsening procedures, heterogeneity is gradually removed from the system. The model becomes more and more homogeneous, and it is close to the pure homogeneous case. Ultimate layer coarsening would result in a big layer to represent the whole model vertically, but the areal resolution would be preserved.

The concepts of the 1D Lorenz curves can also be generalized to 3D dynamic curve (Shook and Mitchell 2009) using 3D streamline tracing to calculate the fluid flow and reconstruct the Lorenz curve for 3D. The major disadvantage of the dynamic Lorenz coefficient calculation is that it requires simulation runs until steady state is reached. It may induce more computational cost and uncertainty due to the streamline tracing.

### 2.3.1.3 Coefficient of Variation

The earliest application of statistical techniques to zonation was by Testerman (1962). Testerman worked on the permeability data for a vertical well and grouped the permeabilities to minimize the variance within each group and maximize the variance between groups. The most useful measure of variability around the central value is the variance defined for sample data as:

$$Var(p_1, \dots, p_n) = \frac{1}{N-1} \sum_1^N (p_i - \bar{p})^2 \quad 2-8$$

Different from Testerman's work, this upgridding algorithm relies on the analysis of "total variation" in a property  $p$ , instead of variance, as a measure of heterogeneity during coarsening. The total heterogeneity measure is developed from a sum over the entire reservoir volume.

$$H = \sum_{ijk=1}^{NX, NY, NZ} n_{ijk} \cdot (p_{ijk} - \bar{p}_{ij})^2 \quad 2-9$$

Here

$n_{ijk}$  is the bulk rock volume of each cell

$p_{ijk}$  is the static property of each cell at the fine scale

$\bar{p}_{ij} = \sum_{k=1}^{NZ} n_{ijk} \cdot p_{ijk} / \sum_{k=1}^{NZ} n_{ijk}$  is the column based average of the static property

We define a modified “between cell” variation (B) as:

$$B = \sum_{ijk=1}^{NX, NY, NZ} n_{ijk} \cdot (p_{ijk}^C - \bar{p}_{ij})^2 \quad 2-10$$

Here,

$C$  represents the coarsened static property of each cell

$p_{ijk}^C$  is the transitional static property that is calculated after every merging of adjacent layers. Differ from the previous between cell variations (Kim and Datta-Gupta 2009; King et al. 2005),  $p_{ijk}^C$  is no longer defined as  $\sum_k n_{ijk} \cdot p_{ijk} / \sum_k n_{ijk}$ . For local velocity

measure,  $p_{ijk}^C = \frac{\sum_k n_{ijk} \cdot k_{ijk} / \sum_k n_{ijk}}{\sum_k n_{ijk} \cdot \phi_{ijk} / \sum_k n_{ijk}}$ , and for local slowness measure,

$$p_{ijk}^C = \frac{\sum_k n_{ijk} \cdot \phi_{ijk} / \sum_k n_{ijk}}{\sum_k n_{ijk} \cdot k_{ijk} / \sum_k n_{ijk}}$$

The quantity B, ‘the between cell variation’ quantifies the amount of heterogeneity preserved during upgridding. We also define W, “the within cell variation”, to quantify the variation removed from the model after upgridding. The use of the bulk rock volume weighing ensures that the calculated heterogeneity does not change if the grid is refined numerically. When merge the two cells, the total with in variation increase by the

amount:  $\delta W = -\delta B$ . The major advantage of using the  $\delta B$  is that these relationships do not refer to the fine scale properties, but only to the coarsened properties. If the calculation during the sequential coarsening has to use the fine scale information, the order of the calculation increases from  $N$  to  $N^2$ .

Selecting a proper static measure,  $p_{ijk}$ , is critical for layer grouping. During the upscaling procedures, the porosity is upscaled to preserve the pore volume and permeabilities are upscaled to preserve volumetric flux per unit pressure drop. When a column of cells is replaced by one cell, the different horizontal flow velocities in each layer are replaced by a single average value (King et al. 2006) as shown in Figure 2-4. In this study, we utilize a priori analysis of the upscaling error as a guide to the required resolution of the simulation grid. The error analysis relies upon a variance analysis of different measures, as shown in Table 2-3.

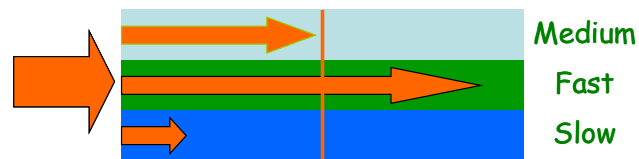


**Figure 2-4 Various velocities replaced by a single one**

**Table 2-3 Variance based static measures**

Measure	Equation	References
Difference in breakthrough time	$\tau = PV/Q$	Stern and Dawson (1999)
Difference in flux	$p = Q/PV$	Stern and Dawson (1999)
Local velocity	$p = k / \phi$	King et al. (2005)
Local permeability or Inverse of permeability	$p = k$ $p = 1/k$	Hosseini and Kelkar (2008)
V&S	$Error = \sqrt{Error_{perm} \cdot Error_{pressure}}$	Hosseini and Kelkar (2008)
Local slowness	$p = \phi / k$	Kim and Datta-Gupta (2009)
Modified V&S	$Error_{vs} = \sqrt{Error_{velocity} \cdot Error_{slowness}}$	Current Work
Lorenz Coefficient	$L_C = 2 \int_0^1 (FdC - 0.5)$	Current Work

Here,

PV is the pore volume

Q is the total volumetric flow rate

k is the permeability

$\phi$  is the porosity

$L_C$  is the Lorenz coefficient

We proposed a modified “V&S” measure which combines the errors of the local slowness and the local velocity to provide increased sensitivity to the breakthrough time and the time of flight simultaneously. For the very first time, static Lorenz coefficient, a traditional static heterogeneity measure, focusing on the storage capacity and flow capacity correlation, is used for layer grouping and has been proven to be an effective

measure. The calculation of static Lorenz coefficient does not require any numerical simulation and, therefore, is relatively inexpensive.

The general idea is to use the variation of a certain static measure around the central value to evaluate the total model heterogeneity or the loss of heterogeneity, as described in the previous sections. Concepts of local velocity and slowness measures are well accepted as the replacements for the local permeability or the inverse of the local permeability measure (Hosseini and Kelkar 2008; Kelkar and Atiq 2010; Kim and Datta-Gupta 2009; King et al. 2006). Measure of the local velocity is most sensitive to the high permeability streaks and does a good job of assessing the error in breakthrough times. Measure of the local slowness provides a good estimation of the error in time of flight, which controls the overall saturation distribution.

Hosseini and Kelkar (2008) suggested an original “V&S” which combines two errors from the difference in pressure profiles and from the permeability difference. This error measure is balanced with both  $(1/k)^2$  and  $k^2$  terms. However, the porosity and permeability correlation is ignored in Hosseini and Kelkar’s derivations. They also fail to provide a correct weighting factor to evaluate the overall heterogeneity. The newly proposed modified “V&S” measure is a combination of local velocity and slowness, which focuses on time of flight and breakthrough response respectively. This “V&S” measure concerns both the permeability and porosity contributions, and it correctly uses bulk rock volume as the weighting factor. A simple example is presented in Appendix B.

The concept of 3D dynamic Lorenz coefficient was proposed by Shook and Mitchell (2009). However, extra computational cost from simulation runs makes it infeasible to use the Dynamic Lorenz coefficient to evaluate the heterogeneity loss during the layer merging. The Dykstra-Parsons coefficient is not selected as the measure due to the disadvantages discussed in the previous section.

### 2.3.2 Upgridding Procedures

Once an error measure is selected, there are two stages in the upgridding algorithm. The first part determines which two adjacent layers should be combined together in a recursive coarsening operation to determine how much reservoir heterogeneity is preserved within the coarsened model as a function of the number of layers. The second part of the calculation analyses this curve to determine the minimal number of layers that can preserve significant amounts of heterogeneity. This is the optimal layer number.

This approach is closely related to that of the previous studies (Li and Beckner 2000; Li and Lake 1995; Stern and Dawson 1999; Wu et al. 2007) which determine the error in a *global* velocity field as a model is coarsened. However, in the current approach, the error estimate is *local* and there is no need to define typical well locations or rates for the analysis.

Our algorithm is shown in Figure 2-5. The recursion is initiated with the number of layers within the geologic model with  $W=0$  in all cells. Layer pairs are selected, recursively, to minimize the increase in  $\delta W$ . We constrain the layer grouping to preserve the geologic zonation since this is typically a major deterministic feature of the reservoir.

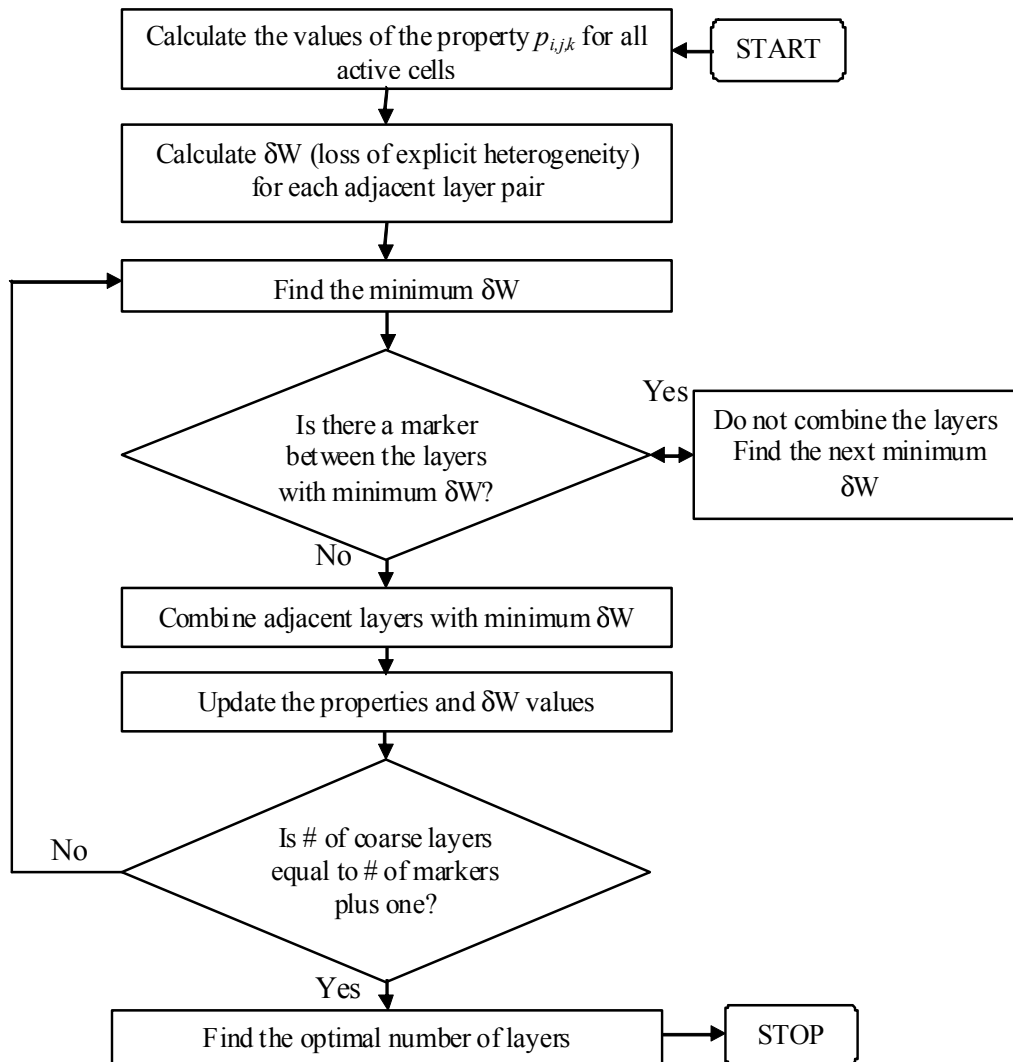


**Figure 2-5 Standard procedure optimal upgridding**

### 2.3.3 Optimal Number of Layers in Coarse Model

In addition to the finding a criterion for coarsening the geological model, another question that we should answer is: how to decide on the “Optimal” number of layers.

We followed the way proposed by King et al. (2006) for retrieving the “optimal” number and extended this concept. The shape of the curve “between cell variation (W)” exhibits a bias-variance cross over. The optimal layering scheme is obtained from this curve by identification of the number of layers beyond which the error increases rapidly.

Because defining the curvature by a local difference is unstable, the data is segmented into two portions with a straight line fit through each (King et al. 2006). The location of the split point which minimizes the root mean square error is defined as the optimal layer number. On the curve of “between cell variation (W)”, this point represents the start of a slow increase in heterogeneity with an increased number of layers. In contrast, reducing the number of layers will lead to a large decrease in the amount of heterogeneity preserved in the model. The root mean square error (RMSE) for a series of a regression lines is calculated. In the variation analysis chart, two linear regressions that fit the two sides of the curve are generated. Based on the absolute RMSE and layer number weighted RMSE calculation, we are able to calculate two RMSE curves and two different minimum mean square error which are used to label the upper and lower bound of the optimal layer number region.

The calculation of optimal layer is based on the statistical analysis and focus on finding the “breaking point” beyond which the heterogeneity reduces severally as the layer number decreases. However, this statistical analysis can be applied for predicting the strong break in terms of the dynamic field response. Different choices of measure result in various optimal choices and different grouping sequences. Examples will be shown in the following on SPE10 model 2 and the deepwater Gulf of Mexico model.



## 2.4 Field Applications

In this section, two geologic models are used to validate our statistical analysis algorithm with different static measures. The first model is the full 3D SPE 10, Model 2 and the second model is deepwater Gulf of Mexico model.

### 2.4.1 Case 1: SPE10, Model 2

#### 2.4.1.1 Model Descriptions

The upgridding analysis is applied to Model 2 of SPE10. Figure 2-6 shows the fine scale permeability distribution and its histogram. Permeability varies over four orders of magnitude.

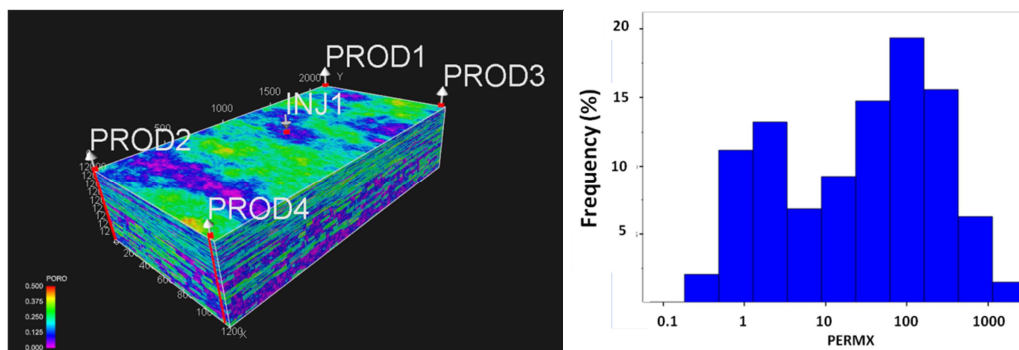


**Figure 2-6 Fine scale permeability distribution of SPE10 (Model 2)**

This is a 60x220x85 cell model, with over a million cells. The upper unit is the Tarbert. It is a heterogeneous geological unit with permeability values that are almost randomly distributed. The lower unit is the Upper Ness. It is channelized and there is a big contrast between channel/non-channel permeability values. Also these two geological units have different ranges of permeabilities, with higher permeabilities in the Upper Ness. The top 35 layers of the model are the Tarbert and the bottom 50 layers are the Upper Ness.

#### 2.4.1.2 Heterogeneity Analysis

Four different statistical error measures are compared in the same chart, as in Figure 2-7 (A). Only heterogeneity curves from slowness and “V&S” measure showed similar trend. Local velocity and Lorenz coefficient analysis presented totally different maximal curvatures and different shapes. Heterogeneity curves for slowness, velocity and “V&S” have start points of 100% with original fine scale geologic model. However, the Lorenz coefficient will never reach the value of 100%, which implies the “infinite heterogeneous”. To better evaluate the heterogeneity error introduced by coarsening procedures, the heterogeneity charts are reconstructed to fit in the same scale. The Lorenz coefficient was used as the standard measure because of its natural advantage of evaluating the overall reservoir heterogeneity without local high/low permeability bias. The normalized curves are presented in Figure 2-7 (B). In each of the grouping step, from different algorithms, the Lorenz coefficient is calculated and plotted against the number of layers preserved. In this chart, the Lorenz curve is always at the top of all four curves because we maximize the Lorenz coefficient in each of the grouping step. The second top one is “V&S” measure. “V&S” curve shows a close match to that of the Lorenz curve. Local slowness and velocity is away from the reference curve at different locations, though eventually they are close to each other and to the reference when a large number of layers are preserved. It is straight forward to visualize the effectiveness of preserving heterogeneity at the same scale. Heterogeneity comparison provides a

further guidance of predicting the field performance, which are reviewed in the following sections.

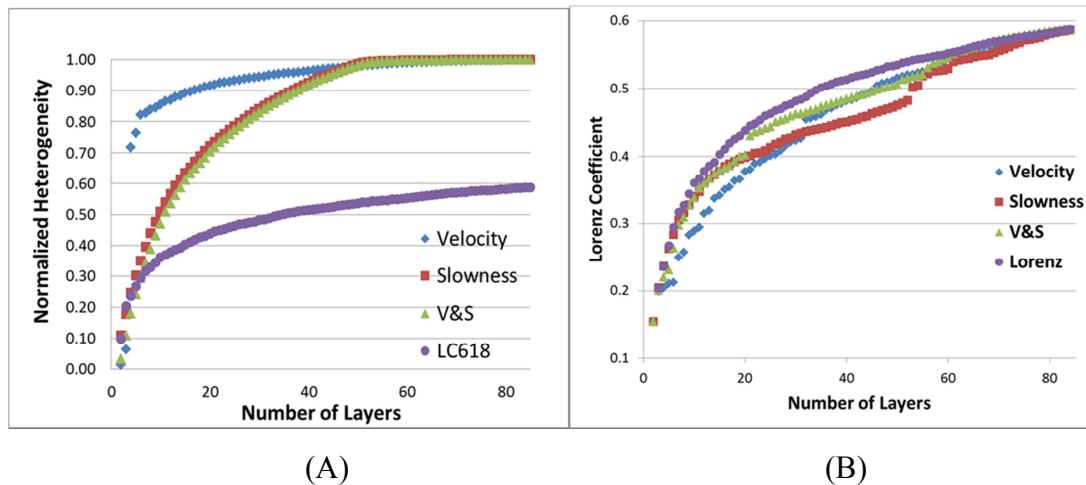


**Figure 2-7 Heterogeneity comparison of SPE10 case: Slowness, Velocity, “V&S” and Lorenz coefficient (A) under normalized scale (B) under Lorenz Coefficient scale**

Figure 2-8 shows the resulting layering schemes based upon the four algorithms. In this figure, each layer is represented by a black horizontal bar which terminates when that layer is grouped with the layer above. In other words, the white “fronts” in each figure show the specific step at which the layers are combined and the black “tails” indicate the grouping step at which the layer is no longer preserved. At the end of the calculation, only two layers remain and are presented with layer 1 and 36, since this model contains two geologic units.

Velocity, slowness and “V&S” based algorithms group the top zone (layer 1~35) first and preserved the resolutions in the lower zone because top zone is relatively more homogeneous comparing to the bottom zone. Specifically, in the top zone, the velocity

based algorithm retains vertical resolution in the higher permeability zones, while the slowness based calculation groups the higher permeability Tarbert and preserves resolution in the low permeability regions. “V&S” based algorithm groups the top zone more uniformly. On the other hand, the Lorenz coefficient based algorithm starts combining layers in both top and bottom zones because it requires data pair resorted and emphasizes on the overall reservoir performance.

The optimal ranges of final layer preserved from each algorithm are labeled in red regions in Figure 2-8. Specifically, using slowness, the maximum curvature occurs with 17 ~ 29 layers in this 85 layer model. The velocity measure indicates that a more aggressive reduction to 7 ~ 13 layers. The “V&S” shows a layer range of 12 ~ 19 layers which is between those two measures. Applying Lorenz coefficient presents a range of 12 ~ 16 layers in the final coarsened models. Lorenz coefficient based algorithm gives very similar optimal range and numbers to that of the “V&S” based method, though their combinations and grouping orders are not same. Figure 2-9 shows a 3-D view of the layer thickness of a coarsened model in which 29 layers are preserved from local slowness calculation.

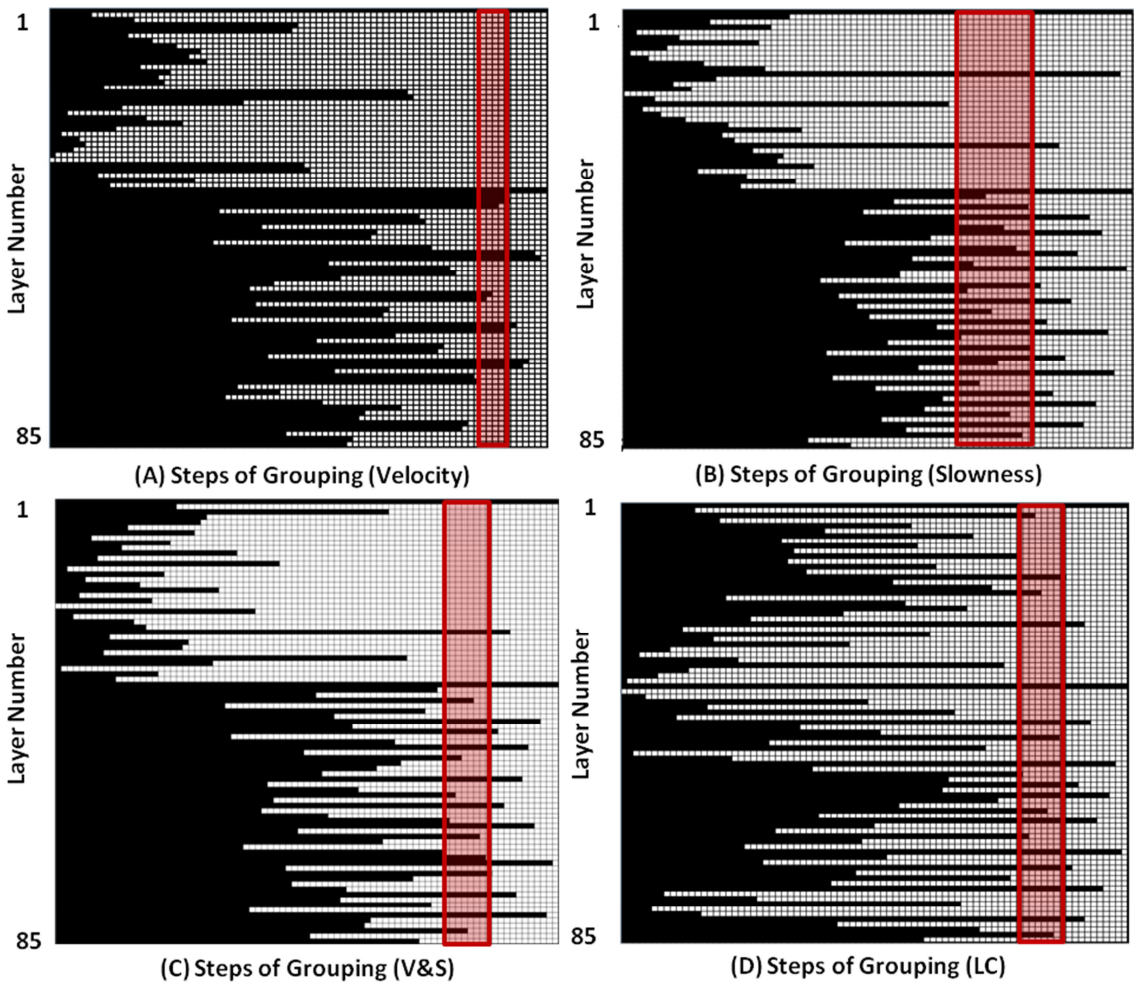
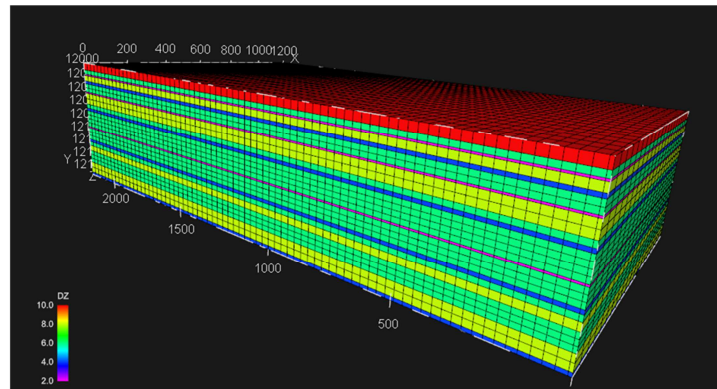


Figure 2-8 Grouping sequences for different static measures



**Figure 2-9 A 3D view of the 29 layer model colored by layer thickness, designed with optimal slowness**

#### 2.4.1.3 Simulation Results

The SPE10 model is an extremely simplified reservoir model with no structure, no faults, and no mobile water. The model has 4 producers, one at each corner of the model, and one injector at the center. All wells are fully completed throughout the thickness of the model. The injector has a injection rate of 5000 rb/day and is constrained to a maximum injection bottom hole pressure of 10000 psi. The producers operate at 4000 psi bottom hole pressure (BHP). Different heterogeneity measure results in different layer grouping combinations and various optimal number of layers preserved. After the grouping combination is selected, the property upscaling is performed within Eclipse automatically by applying “COARSEN” keyword.

Figure 2-10 shows the results of fine scale simulation and a number of coarse scale simulation runs. Figure 2-10 (A) and (B) show field cumulative oil production (FOPT), and field pressure (FPR) respectively. The cases presented utilize the layering design scheme with different static measures and have various layer combinations. There is no areal upscaling performed in those models.

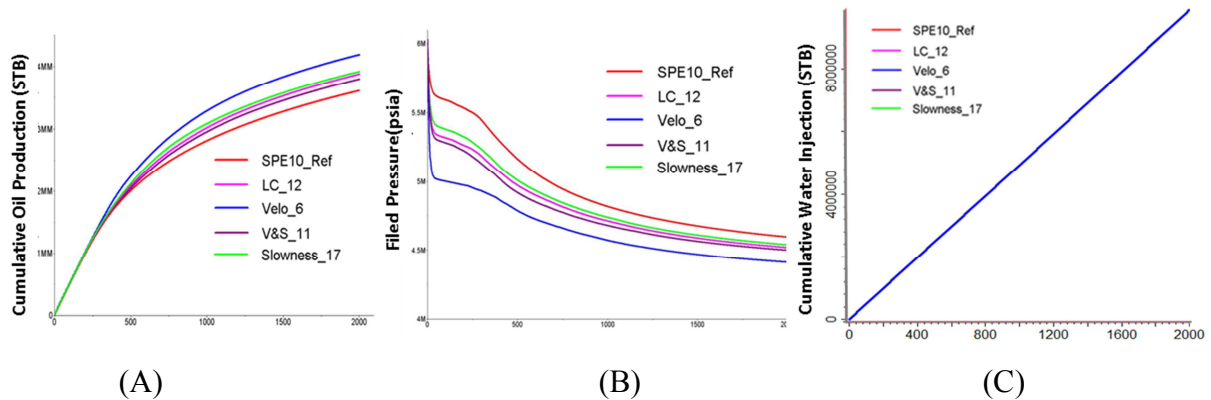


**Figure 2-10 Comparison of fine and coarse scale field predictions: Field oil production total (A), field pressure (B) and water injection volume (C)**

In general, all of the models underestimate the field pressure and overestimate the oil production. In this SPE10 model, injector is under rate control. The cumulative water injection remains the same for all different cases. In terms of cumulative oil recovery, preserving more layers in the coarsened model does not guarantee a better oil recovery simulation but shows a better field pressure estimation. For example, the optimal slowness based layering scheme with 17 layers (aggressive bound) presents the best estimation of the average field pressure among all different layer design schemes. However, it fails to show a better match for oil production compared to “V&S” or Lorenz coefficient (LC) based design which gives fewer model numbers.

Figure 2-11 shows the results of fine scale simulation and a number of coarse scale simulation runs. The figure shows field cumulative oil production (FOPT) from different optimal layer design schemes. Instead of using the traditional curves, each point represents one coarsened model with a simulation run of 2000 days, and the recovery was normalized to the reference result of the 85 layer fine scale model.

As the layer number preserved in the coarse model increases, the simulation results will eventually be close to the reference point (black, round). However, different layer design algorithms have various field responses while increasing the layer number. Generally, all upscaled calculations overestimate the oil recovery. When the number of layers is less than 10, all layer design algorithms fail to provide good reproductions of the fine scale model performance. The “V&S” based measure does not provide obviously better oil recovery when the number of layers varies from 12 to 40. Though the total cell count for a 40 layer model is greater than the one within a 12 layer model, it does not provide any significant improvement in terms of oil recovery. A strong field response “break” can be observed at layer 12 for the “V&S” based algorithm. Recall that the Lorenz coefficient based algorithm focuses on the overall reservoir behavior without knowledge of the local high/low permeability distributions. The Lorenz coefficient measure presents a clear trend that the oil recovery gets closer to the fine scale reference point as the number of layers increases.



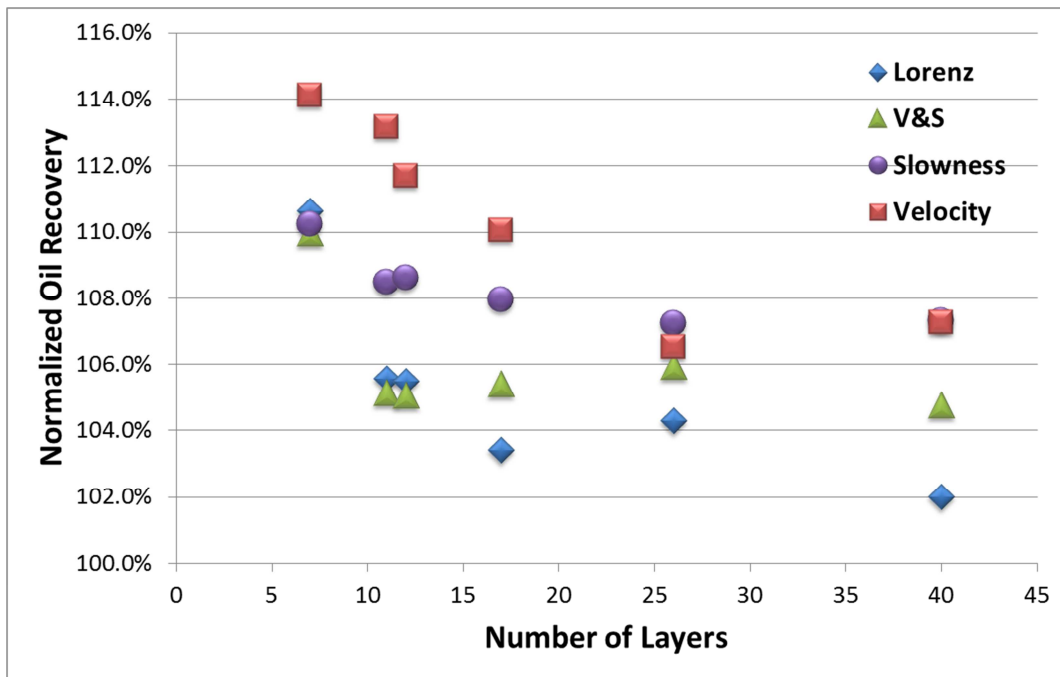


**Figure 2-11 Comparison of fine and coarse scale field response with different coarsened layers**

Figure 2-12 shows the results of the fine scale simulation run and a number of coarse scale simulation runs for “V&S” and Lorenz coefficient based algorithms. The figure shows exhaustive determination of field cumulative oil production (FOPT) with different layer numbers preserved, ranging from 2 to 40. Each point represents one simulation run of a coarsened model, and the recovery factor is compared to the reference of the 85-layer fine scale model. Compared to the “V&S” based algorithms, the Lorenz coefficient based groupings are more close to the fine scale reference point, while the number of layers preserved increases. Both “V&S” and Lorenz coefficient based calculation show obvious plateaus in terms of the normalized oil recovery. There is a strong “break” in the field response, and the turning point is the optimal number of layers preserved. The novel static measures are able to predict optimal number of layers which is a good statistical analysis based indicator of a break in the dynamic field response. Preserving less number of layers, the coarsened model fails to reproduce the fine scale performance.

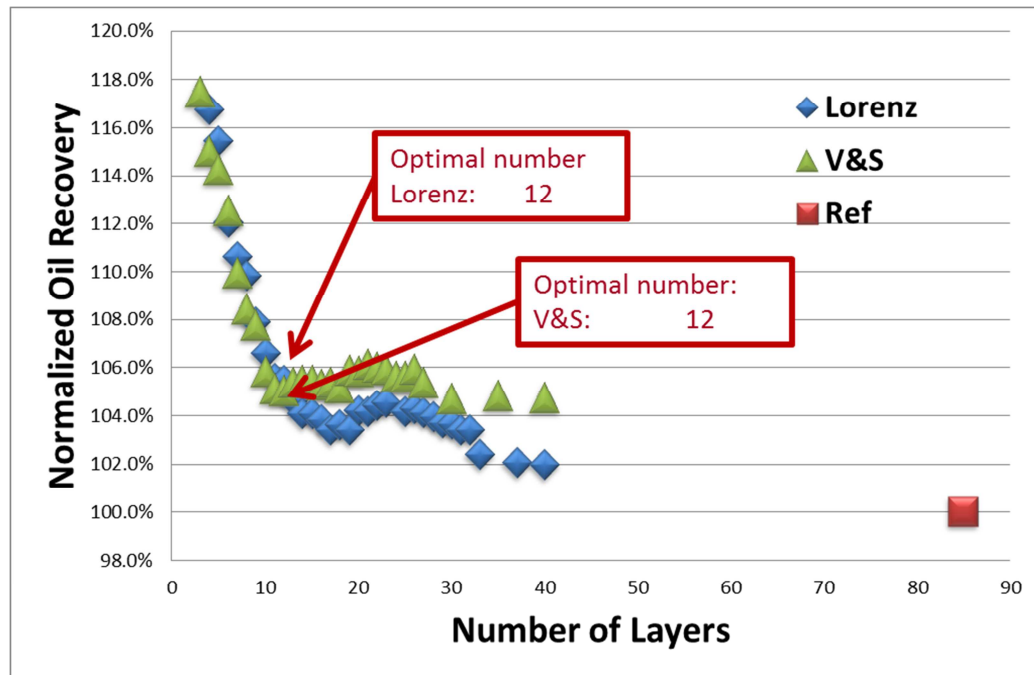


**Figure 2-12 Exhaustive determination of cumulative recovery vs. number of layers**

The CPU times for these same cases are shown in Figure 2-13. There is no dependence on the upscaling approach. The cost of the computation is essentially only a function of the number of coarse cells. With a cell ratio from 5% to 30%, the total simulation time is reduced to 2% to 20% of original CPU time. Two trend lines are generated with the exponent of 1.1652 (LC) and 1.2451 (Velocity). These two lines mark the upper bound and lower bound of the increasing trend.

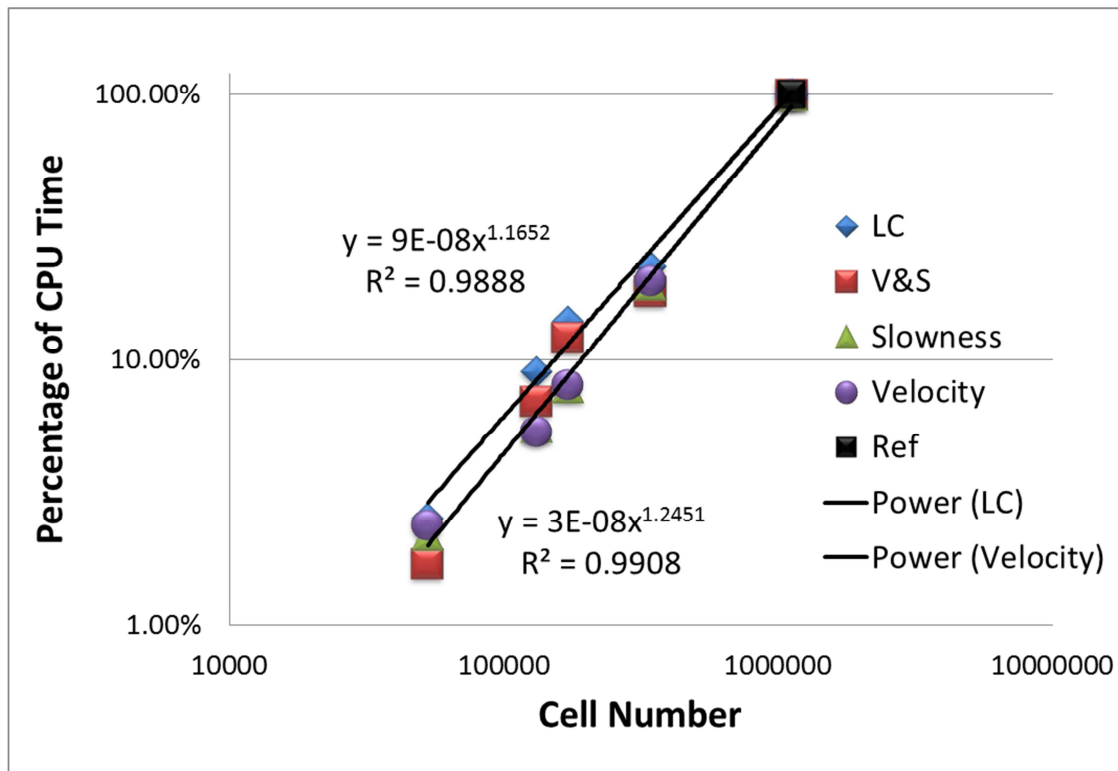


Figure 2-13 Comparison of the fine and coarse scale CPU time

## 2.4.2 Case 2: Turbidite Reservoir, Deepwater Gulf of Mexico

### 2.4.2.1 Model Descriptions

The reservoir produces oil from middle Miocene sands. The field has a combination of structural and stratigraphic traps. Figure 2-14 shows the reservoir structure of the field. This model has a dimension of 70x40x420, and the vertical resolution is close to log data. The model has 7 producers and two injectors. All wells are fully completed throughout the thickness of the model. The injector has an injection rate of 4000 rb/day and is constrained to a maximum injection bottom hole pressure of 9000 psi. The producers operate at 3000 psi bottom hole pressure (BHP). By applying effective layer

design algorithm, a simulation resolution model is built directly from the log resolution data without the intermittent processing. Similar to the SPE10 case, this model is coarsened using Eclipse and the upscaled properties are calculated by the simulator automatically.

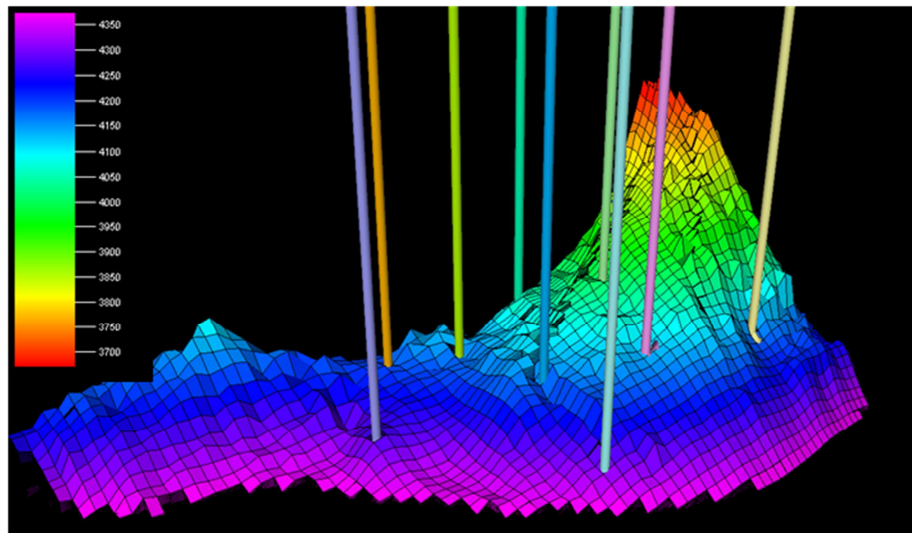


**Figure 2-14 Reservoir structure**

Here, we present a typical water saturation distribution of the high resolution and low resolution models in Figure 2-15. The water saturation pathway can be more clearly visualized at the high resolution model. However, it suggests that 420 layers may be more than sufficient to describe the detailed flow behaviors. Our effective layer design algorithm is able to provide guidance for a practical simulation model resolution.

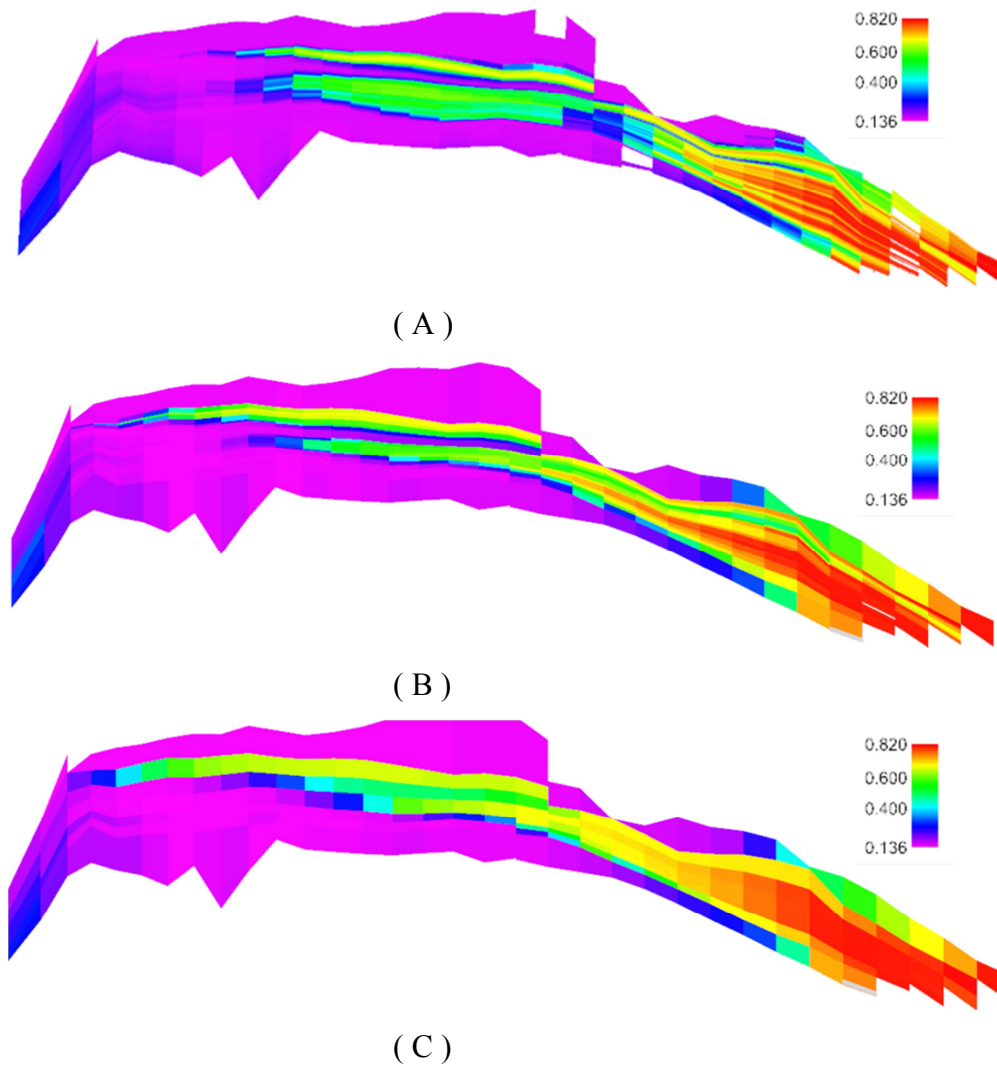


**Figure 2-15 Water saturation profile at the same cross-section for different model resolutions at 2000 days: (A) 420 layer model, (B) 15 layer model (C) 7 layer model**

#### 2.4.2.2 Heterogeneity Analysis

The statistical measures are shown in Figure 2-16 including the results of “V&S”, slowness and velocity based statistical measures. In this section research focuses on the algorithms that do not require expensive data sorting. Only the above three are presented

and compared. For slowness measure, it consists with the results from SPE10 model that it gives a wide range of optimal candidates of 10 ~ 30 layers. On the contrary, velocity measure shows aggressive combinations with narrow band of the optimal ranges from 9 to 17. For “V&S” measure, it shows a layer range between those two measures of 12 ~ 19 layers. Three methods give a general agreement on optimal range of 10 ~ 20 layers in the final coarsened model. The heterogeneity analysis charts show that the curves remain linear until the models were aggressively combined with only few layers left, as seen in Figure 2-16. Comparing to the original fine scale layer number of 420, the coarsened models contain only a limited number of layers. The total cell number was reduced to around 2.5% to 5% of the fine scale model. Following the same procedures applied for SPE10 case, three different static measures are compared under Lorenz coefficient scale, as seen in Figure 2-17. “V&S” curve shows a better preservation of heterogeneity since it does not overestimate the effect from the high/low permeability contrast. Local slowness and velocity preserve the same amount of heterogeneity when the number of layers is above 30. There is no obvious difference shown in the normalized curve from Figure 2-17 at early stage (large layer number).

To compare all the field performances from different coarsened models in a systematic way, all the simulation results are plotted in the same chart and labeled with different color code, as seen in Figure 2-18. The reference curve showing the 420 layer fine scale model is labeled in black and it is overlapped with the blue lines which represent the coarse models having a layer number greater than 34. The blue curves show the models from velocity, slowness and “V&S” algorithms and the differences are not identifiable. The red curves show the results from the three algorithms but with number of layers from 10 to 17. Range of 10 to 17 is generally agreed to the optimal ranges from all those three static measures. Except one single curve from the local velocity was away from the reference curve, other red curves show good match of the oil production. The green curves represent the combinations with number of layers less than 9, from different static measures. Keeping only few layers preserved, the green curves spread out and are away

from the reference curve. Figure 2-19 presents the cumulative oil production from different models. Each dot in Figure 2-19 represents one simulation run with different number of layers preserved in the coarse model. With 17 layers preserved, “V&S” shows the best estimation of the oil production. “Velocity” presents the worst estimation among the three measures. Below the lower bound of 10 layers, all measures fail to reproduce the fine scale simulation performance.

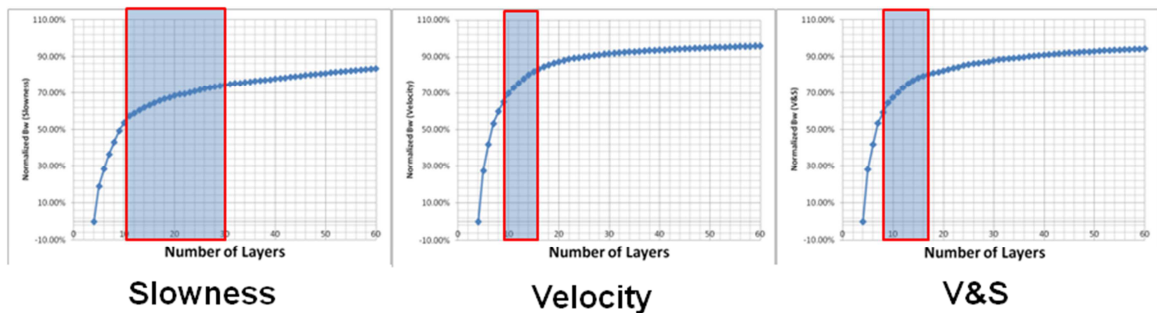


**Figure 2-16 Heterogeneity analysis of case2 (A) V&S (B) Slowness (C) Velocity**

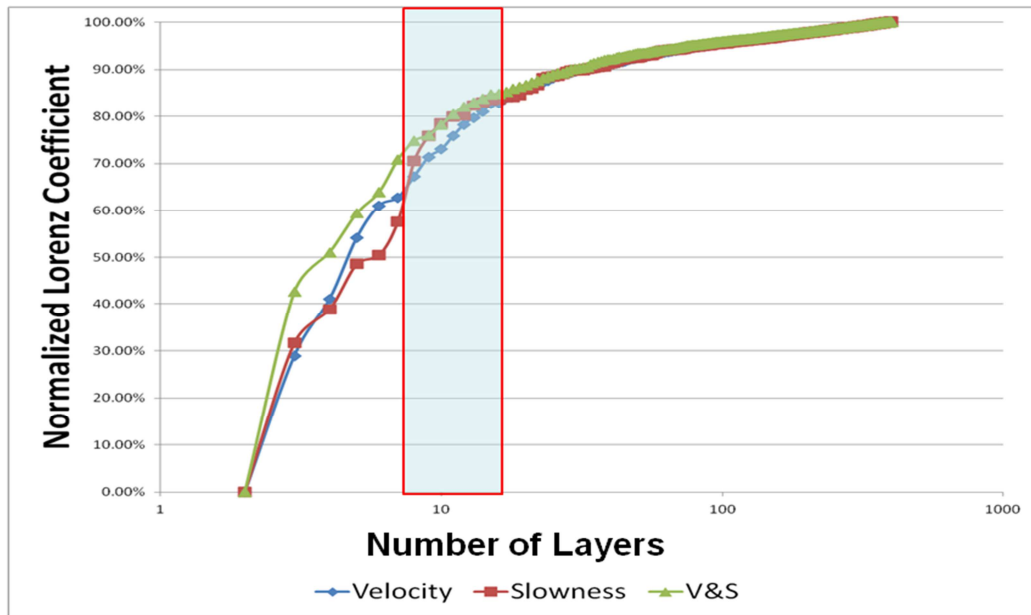


Figure 2-17 Heterogeneity under Lorenz coefficient scale

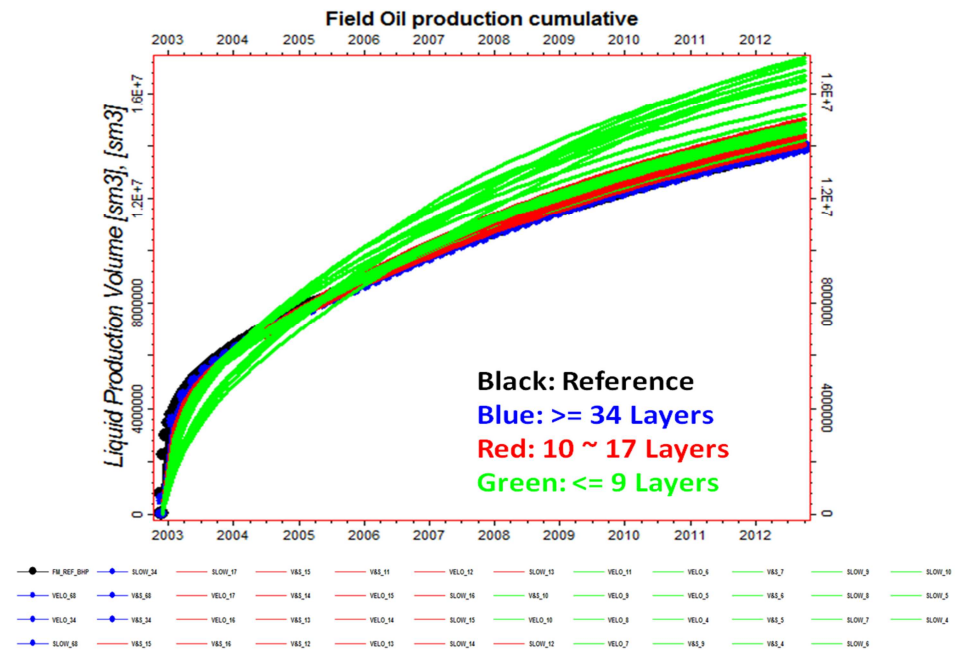
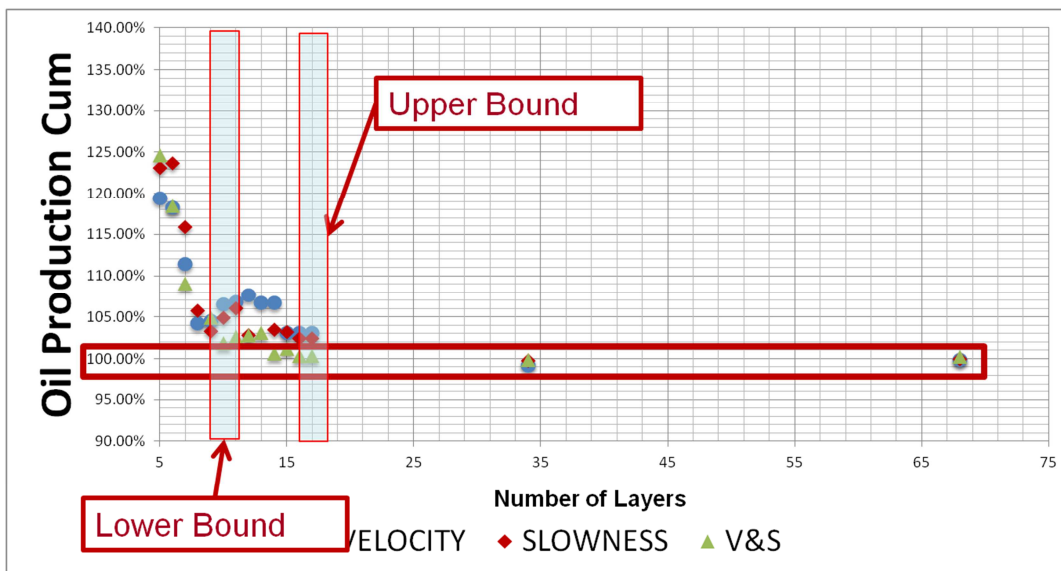


Figure 2-18 Field performance: oil production prediction with different layer combination





**Figure 2-19 Filed performance: cumulative oil production with different layer combination**

The CPU times for these same cases are shown in Figure 2-20. Different static measures present similar CPU cost. The CPU cost is essentially only a function of the number of coarse cells. With a cell ratio from 2.5% to 5%, the total simulation time is reduced to 1% to 3% of original CPU time.

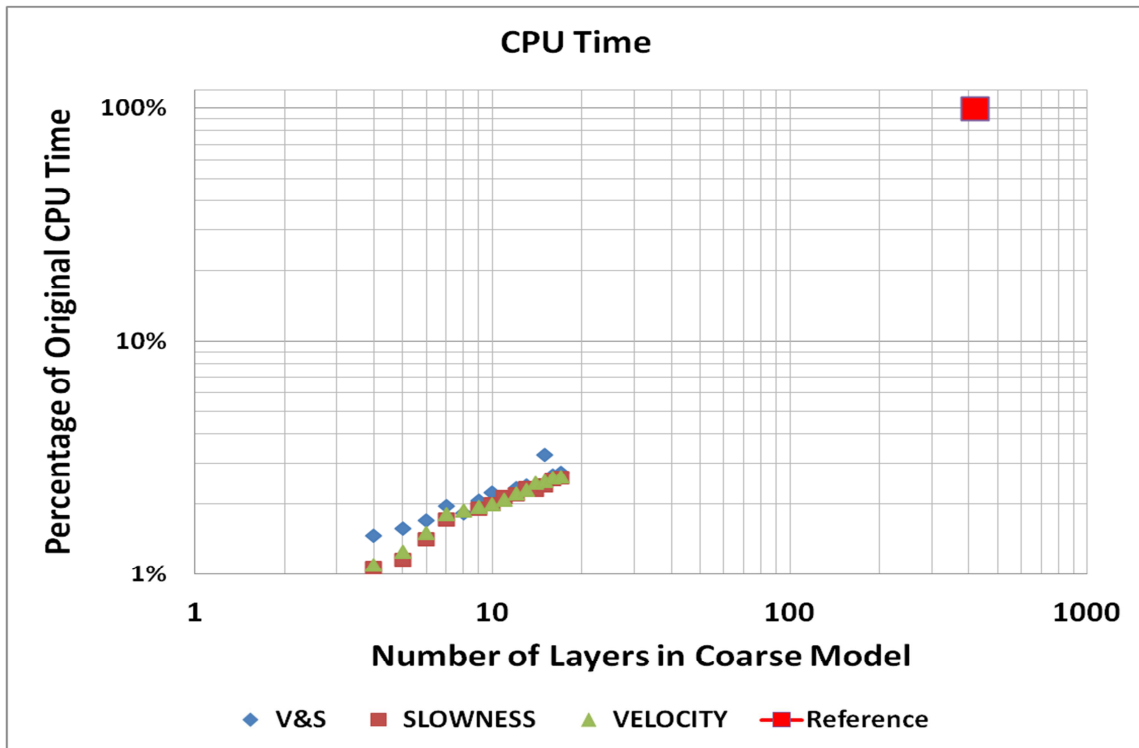


Figure 2-20 Comparison of the fine and coarse scale CPU time

## 2.5 Discussion

### 2.5.1 Gridding Design

Our layer design algorithm relies on the sequential layer grouping in such a way that the loss of the heterogeneity of a defined measure is minimized. In this research, we mainly focus on the vertical upgridding with respect to zonation boundaries and keep the areal model resolution as the original. When performing a  $1 \times 1 \times N$  upscaling calculation we impose pressure and/or no flow boundary conditions and calculate total flux per unit pressure drop to obtain the effective permeability. The statistical analysis assumes that the major error occurs at the multiphase flood front. However, this assumption may not be valid under different exceptional situations.

In heterogeneous reservoirs, the flow rate varies with permeability change and different flow regimes prevail in different locations of the reservoir. In this layer design algorithm, it is presumed the fluxes follow a dominating horizontal direction and are replaced by the average speed, as seen in Figure 2-4, and the vertical flow is relatively negligible. The assumption is true when water injections are planned for all layers. This assumption is also true when simulating an edge-water drive reservoir, as seen in Figure 2-21 (a). In such circumstances, water moves into the flanks of the reservoir as a result of hydrocarbon production and pressure drop at the reservoir–aquifer boundary. The flow is essentially radial with negligible flow in the vertical direction. However, let's consider a heterogeneous reservoir having an aquifer with large areal extent and a gentle dip, as seen in Figure 2-21 (b). The flow is essentially radial and, in contrast to the edge-water drive, the bottom water drive has significant vertical flow (Ahmed and McKinney 2004). If the reservoirs are vertical flow dominating, applying this sequential layer design may result in incorrect flow modeling on the large scale.

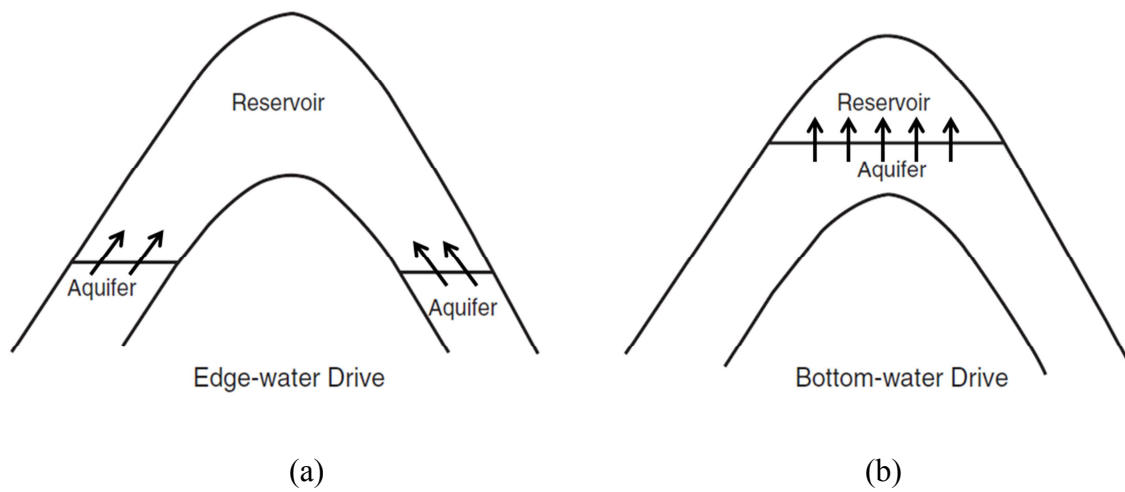


**Figure 2-21 Aquifer flow geometries**

If the SPE10 model is modified to have the injector perforated at the bottom 10 layers only and all producers remained the same, the oil recovery results are shown in Figure 2-22. Figure 2-22 presents the reference (fine scale) model and coarsened models using the Lorenz coefficient as the static measure. All the coarsened models underestimate the cumulative oil production. The mismatch from the coarsened model can reach up to 40%. In this modified SPE10 model, only perforation position of the injector is changed. The flow pathway and overall recovery are changed accordingly. The layer design algorithm fails to reproduce the fine scale simulation results because it assumes horizontal flow dominates.

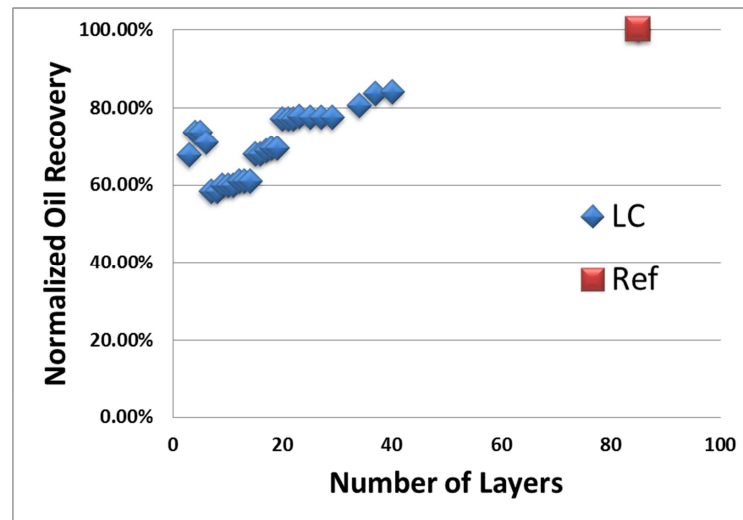


Figure 2-22 Oil recovery for modified SPE10 at 2000 days

In short, based on a heterogeneity analysis, the layer design is suitable to capture horizontal convective transport with low resolution model. However, high resolution grids may still need to be preserved for describing other physical and chemical processes. For example, the layering analysis is too coarse for modeling the near-well flow, horizontal wells and/or hydraulic fracture performance. First of all, in such cases, the dominant flow direction may be vertical, and a frontal advance analysis may not be sufficient. Second of all, different flow regimes near fractures present at different periods of time and may not be able to be captured by the coarsened gridblocks. Finally, the high resolution modeling in the near-well region may help provide the pressure and stress profiles, which are critical for the infill drilling programs.

Layer design algorithm shows its limitation on tight gas reservoir models. Tight gas reservoirs present unique structures showing the pay zones on a non-pay background and intermittent connectivity existing with the thin fluvial sands. The layer design algorithm tends to merge the pay and non-pay cells together, and permeability upscaling results in overestimation of the areal continuity. In short, the 1x1 optimal layering can still

preserve the heterogeneity contrast between the coarse layers, however, within a layer, the vertical communication has been underestimated, and the horizontal communication has been overestimated. Major errors of tight gas reservoir upscaling arise when the isolated pay cell in the fine scale model are incorrectly connected by applying layer coarsening. Pillar based upscaling for tight gas reservoirs can be the good alternative (Zhou and King 2011).

### 2.5.2 Modified V&S

Non-uniform upgridding of geologic models for simulation grid design has been studied by different authors, and is reviewed in the previous section. The results of the heterogeneity analysis of the original “V&S” by Hosseini and Kelkar (2008) and modified “V&S” are shown in Figure 2-23. The plots have been put into the Lorenz coefficient scale so that different “V&S” analyses can be presented on the same plot. The modified “V&S” shows a better preservation of heterogeneity as the number of layers is reduced. Though the modified “V&S” measure presents a similar formula to the original work, it includes the porosity influence and a correct use of bulk rock volume as the weighting factor. Figure 2-24 shows the grouping consequence based upon the original “V&S” measure. Compared with the previous grouping sequences, the original “V&S” preserves the bottom zone resolutions and the top geologic zone is combined into a trunk after 40 steps. This measure gives a relatively narrower and more conservative optimal layer range of 19 ~ 23. Figure 2-25 presents the additional comparison of the original “V&S” grouping vs. other static measure based grouping at 25 layers with QQ scatterplots. Comparing the three plots, the original “V&S” based grouping is closer to the modified “V&S” though obvious difference is observed at the layer range from 70 ~ 85. However, QQ plots are not able to identify which coarsened model performs better.

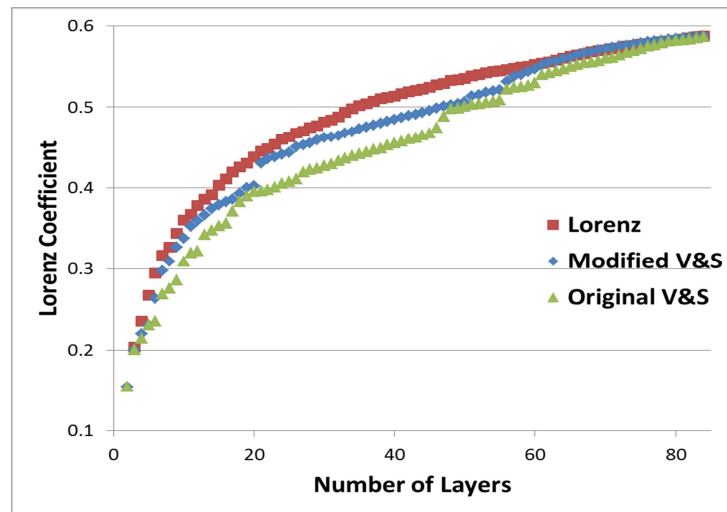


Figure 2-23 Between-variation heterogeneity analysis for the SPE10 case study

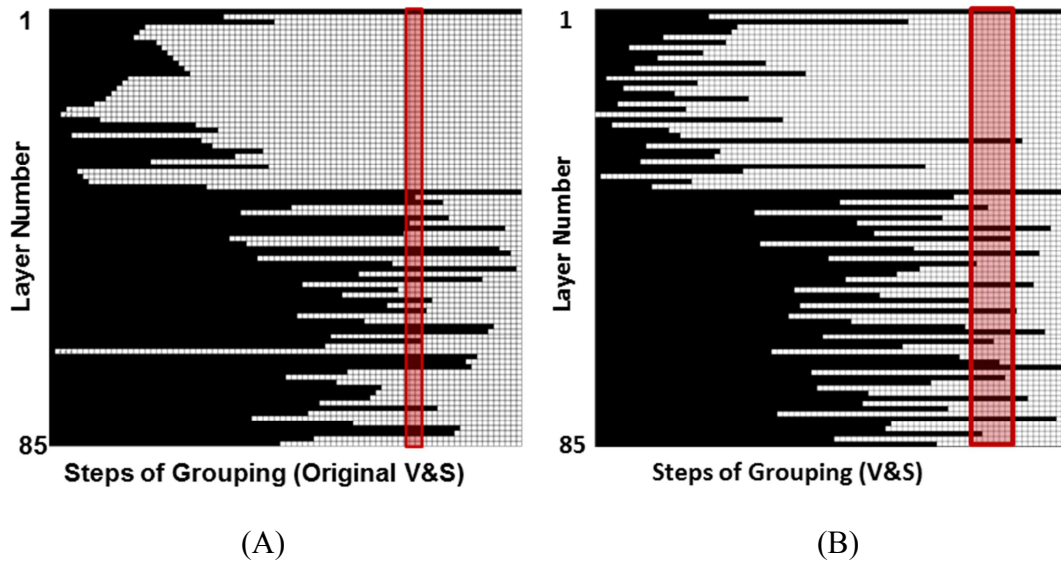
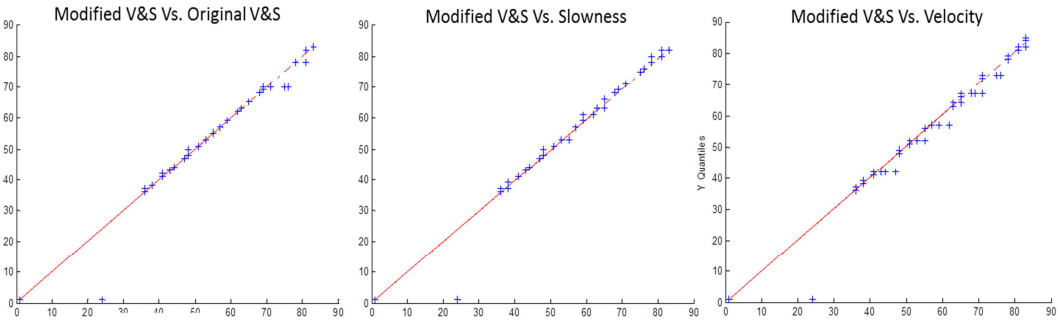


Figure 2-24 Grouping sequence for: (A) original “V&S” by Kelkar and (B) modified “V&S”



**Figure 2-25 QQ scatterplot of original “V&S” grouping vs. other static measure based grouping (25 layer model)**



## 2.6 Conclusions

In this chapter we have studied the impact of the layering scheme and upscaling approach when approximating the SPE10 and a deepwater Gulf of Mexico case. We introduce two novel heterogeneity measures, modified “V&S” and LC, which are able to predict optimal number of layers for convective dominated process. Our statistical analysis can be used to predict the strong break in terms of the dynamic field response.

We have demonstrated the importance of error analysis in designing the layering scheme. Both Dykstra-Parsons coefficient and Lorenz coefficient are traditional static measures ignoring correlations. Dykstra-Parsons coefficient concerns only the permeability distributions, is non-uniqueness and is influenced by the subjective element in drawing the “best-fit” line. Lorenz coefficient and coefficient of variation are applied in our layer design algorithm. Of the four measures (velocity, slowness, “V&S” and Lorenz coefficient), error analysis demonstrates that “V&S” and Lorenz coefficient are compatible useful error indicators and perform better than the velocity and slowness. The derivation of the “V&S” measure is similar to the previous work of Hosseini and Kelkar (2008) but includes the porosity influence and also correct use of weighting factor of bulk rock volume. Lorenz coefficient provides an evaluation of the model heterogeneity in a wide distribution, and it takes care of the flow capacity and the storage capacity at the same time.

The error analysis has been applied to the development of a reservoir layering scheme and has not yet been utilized for the design of the areal grid. However, previous experience with tight gas reservoir models (King 2006, Zhou and King 2011) may suggest that a combination of areal and 3D adaptive approaches may allow much better results, which, in the absence of an appropriate error analysis, shows only an increase in error with loss of resolution, without guidance on resolution. The analysis is driven by

the dominant error in multiphase frontal progression included when a heterogeneous reservoir model is replaced by a coarsened one.

Our algorithm does not require specific flow boundary conditions, the placement of hypothetical or test wells, assumptions on wells rates or the specification of characteristic times. Therefore the results from the layer design are generally applicable. However, we still follow the geological constrains of the zonation, and layers belonging to different zones are never merged.

To further reduce the CPU time, areal upscaling may be applied. Interestingly we have found that the dominant factor that controlled the accuracy of the upscaled result was the grid resolution and layering scheme, with only a secondary impact based upon the upscaling approach. Major limitations and restrictions of applying such a layer design algorithm are due to the flow geometries and paths.

### 3 PSEUDO FUNCTIONS AND THEIR APPLICATIONS

#### 3.1 Introduction

Accurate upgridding and upscaling of single-phase parameters is necessary. However, there is always a need for accuracy improvement of simulating coarse scale models, especially the aggressively coarsened ones. Therefore, the multiphase property upscaling must be brought into consideration to maintain the fine scale flow behaviors on a coarse model. In general, high degree of coarsening desires the introduction of the multiphase parameter modifications.

Although lots of work has been done in the past decades, effective relative permeability upscaling of highly heterogeneous reservoir models is still a challenging problem. The previous pseudoization methods often involves: 1) generation of one pseudo functions for each coarse grid block. 2) fine scale full field model simulation run is required. A new pseudoization algorithm is proposed in this chapter to conquer the problem mentioned.

In this chapter, we first review the previous work on multiphase upscaling and then introduce a novel multiphase upscaling algorithm, which integrates the classic JBN method for homogeneous core flood analysis with heterogeneous large scale sector models. This novel algorithm also presents the impact of total mobility upscaling. In the new algorithm, the effective fraction flow and total mobility are calculated at the outlet of a typical sector model. There is no need to run a fine scale full field simulation. For a highly heterogeneous model, we create a model calibration to eliminate the overestimated total mobility at lower saturation and to correct water breakthrough estimation. The case study using new pseudo relative permeability curves demonstrates the requirement of rescaling the overall permeability as part of the multiphase upscaling procedures. The simulation results also indicate the matches for the breakthrough time

and overall field performance are accurate and improved using the new pseudo relative permeability curves. We provide a simple parameterization to upscale rock curves to reservoir scale.

### 3.2 Literature Review

The original purpose of using pseudo functions in reservoir simulation was to switch a 3D reservoir model to a 2D model and to approximate the radial flow near wells (Aziz and Settari 1979). Generally, the pseudo functions are derived from simplified and analytical or numerical models. The rock relative permeability and capillary pressure relationships are going to be replaced. Therefore, the coarsened model is able to reveal the detailed flow information removed from the fine scale model.

Early in 1960s, analytical solutions of the pseudo functions were calculated based on the assumption of vertical equilibrium (Coats et al. 1971; Coats et al. 1967; Hearn 1971). The concept of dynamic pseudo relative permeabilities was proposed by Jacks et al. (1973). They calculated the pseudo functions based on the fine scale simulation results and applied the pseudo curves to the coarsened model. The procedures are similar to the flow-based upscaling methods. The pseudo functions and the flow-based upscaling share similar issues that are critical to the overall reservoir performance. The major issues include the selection of local domain and local boundary conditions. It is also critical to average the fine scale flow simulation results of flux, pressure and saturation. Different ways to average saturation and various methods of handling the numerical dispersion had brought interests in the past days.

Kyte and Berry (1975) proposed a method that had been widely applied for years. They introduced the correction for numerical dispersion in the generation of pseudo functions. Darcy's equation was applied to the coarsened model to calculate the effective (pseudo) relative permeabilities, based on the averaged pressure and fluxes in the coarsened cells.

The pressure and flux data were collected from fine scale simulation runs. The averaged flux was calculated at the boundary of a coarse block and associated with the volume-averaged saturation of the upstream block. Later this method was further improved as a “pore-volume-weighted” method that used different weighting factors for pressure calculation.

Another famous method was proposed by Stone (1991). He avoided using the averaged pressure gradient in the method of KYTE and BERRY (1975) and used the total mobility for pseudo function calculations. Major advantage of this method is that there are no negative or “infinite” pseudo relative permeabilities. On the other hand, Stone’s method of treating the total mobility was proved not suitable for the problems facing with significant variation in total mobility (Barker and Thibeau 1997). Many similar methods were proposed later with better averaging of total mobility.

It has been proposed that the dynamic pseudo functions depend upon both the original fine scale model solution and the coarse model scheme (Ekrann and Dale 1989; Ekrann and Mykkeltveit 1995). More review works has been provided by Barker and Thibeau (1997) and Barker and Dupouy (1999). Conditions like the selection of the number of coarse blocks, local fine scale simulation runs, and dependency of pseudo relative permeabilities can contribute the final solutions. Also, they pointed out that, if the well rates or positions are changed, the pseudos would have to be regenerated from the fine grid simulation runs which have the updated well rates and patterns.

Guzman et al. (1996) and Darman et al. (2002) finished similar studies for the different pseudoization algorithms on various conditions including viscosity to gravity ratios and capillary numbers. Christie et al. (1995) provided calculation of pseudo relative permeabilities based on saturations and flow rates which were averaged over the outlet edge of a coarse block. The model was upscaled in such a way that each block had its own set of directional pseudo-functions. Their calculation did not account for the

numerical dispersion because they considered Kyte and Berry's (1975) method overestimated such effects.

Hewett et al. (1998) presented an analytical approach for calculating the corrections for pseudo functions. The calculation was based on the Buckley-Leverett solution. They computed average saturation and total mobility on the coarse scale while maintaining the consistency with the coarse scale discretization. The calculated relative permeabilities were often non-monotonic with increase end point values.

Thibeau et al. (1995) and Thibeau (1996) combined global coarse scale grids with local grid refinement (LGR) to generate pseudo functions. The method was to maintain heterogeneity in both global and local scale and permitted the reproduction of the fine scale flow. Portella and Hewett (2000) developed a method to generate coarse grids based on streamtubes and isobars. The upscaled properties were accurately calculated using the properties of each streamtube that constituted the coarse block. The single-phase pressure distribution from a numerical solution of Laplace's equation was used to calculate the pressure distribution for a two-phase flow. The calculation was based on the mapping of the solution of the Buckley-Leverett equation onto the streamtubes derived from the single-phase solution. Injection tubes were introduced to connect the injection wellbores to all inlet faces thus capturing the flow behavior of a finely gridded model. The entire fine scale model was sequentially upscaled using injection tubes to determine the boundary conditions.

### 3.3 Methodology

It is important that the detailed heterogeneity of geologic models can be preserved so that the coarsened models are able to present the flow behaviors. In other words, the reproduction of fine scale model performance is greatly affected by the heterogeneity preservation.

The method presented here is a hybrid, with elements selected from various approaches to minimize the known artifacts. This method will focus on the total mobility and fractional water flow. The phase mobilities are defined as  $\lambda_w(S_w)$  and  $\lambda_o(S_w)$  for water and oil phase respectively. Total mobility is

$$\lambda(S_w) = \lambda_w(S_w) + \lambda_o(S_w) \quad 3-1$$

and a fractional water flow is

$$F_w(S_w) = \lambda_w(S_w) / \lambda(S_w) \quad 3-2$$

Effective fractional flows and total mobilities is determined separately by analyzing averaged saturation profiles obtained from fine scale simulation runs on a sector model. The fractional flow calculation is an extension of the JBN method (Johnson et al. 1959; King et al. 1998) which was used to provide water and oil relative permeability that can perfectly reproduce the laboratory experiments. The newly proposed multiphase upscaling method involves novel multiphase upscaling procedures, in which the absolute permeability upscaling impacts are considered.

Recall that the intention of using pseudo functions on the coarsened models is to avoid solving the full field (global) fine scale flow. Our rule of thumb is to address the local flow problems to approximate global flow behavior in the coarsened models. Our dynamic pseudo relative permeability curves are derived from a detailed 3D sector model. This sector model should represent the reservoir under conditions to be expected in the area or 3D simulation model. We try to avoid fine scale simulation on full field models. It is not profitable running the full field fine scale model to compute the pseudo functions.

As the effective relative permeabilities describe the physical displacement of fluids, the pseudo relative permeabilities should include the considerations of numerical dispersions

for areal coarsening. However, in our study, we consider the pseudoization for the models from layer design as described in Chapter 3. Since the models are coarsened only in the vertical direction, there is no need to compensate numerical dispersion in this study.

### 3.3.1 JBN Methodology

Our analysis is based upon the one dimensional Buckley-Leverett equations for incompressible fluids in a variable cross-section.

$$\phi \frac{\partial S_w}{\partial t} + \frac{Q}{A} \frac{\partial F_w}{\partial x} = 0 \quad 3-3$$

Define:

$$X = \int A \phi dx$$

$$T = \int Q dt$$

Simply we can have

$$X = T \frac{dF_w}{dS_w} = T \bullet F'_w(S_w) \quad 3-4$$

Define PV as the total pore volume:

$$PV = W_i \cdot F'_w(S_w^{Outlet}) \quad 3-5$$

Following the JBN approach, we calculate both fractional water flow and the water saturation at the outlet, based on the average water saturation and its time derivative.

$$\begin{aligned} PV \cdot \bar{S}_w &= \int_{X=0}^{PV} S_w dX = X \cdot S_w \Big|_{Inlet}^{Outlet} - \int_{Inlet}^{Outlet} X dS_w \\ &= PV \cdot S_w^{Outlet} - \int_{Inlet}^{Outlet} T dF_w \\ &= PV \cdot S_w^{Outlet} - (W_i \cdot F_w^{Outlet} - W_i) \\ &= PV \cdot S_w^{Outlet} + W_i \cdot (1 - F_w^{Outlet}) \end{aligned} \quad 3-6$$



From Equation 3-3, we can also have:

$$\begin{aligned}\partial F_w &= \frac{\partial S_w}{\partial T} \cdot \partial X \\ \Rightarrow 1 - F_w^{Outlet} &= \frac{\partial \bar{S}_w}{\partial T} \cdot PV = \frac{\partial \bar{S}_w}{\partial W_i} \cdot PV\end{aligned}\quad 3-7$$

Combining Equation 3-6 and 3-7:

$$\bar{S}_w = S_w^{out} + \frac{d\bar{S}_w}{dW_i} \cdot W_i \quad 3-8$$

Since we have:

$$\begin{aligned}\frac{d(\bar{S}_w / W_i)}{d(1/W_i)} &= \frac{d(\bar{S}_w / W_i)}{d(W_i)} \cdot \frac{d(W_i)}{d(1/W_i)} \\ &= -(W_i)^2 \left( \frac{d\bar{S}_w}{dW_i} / W_i + \frac{d(1/W_i)}{dW_i} \cdot \bar{S}_w \right) \\ &= \left( -W_i \cdot \frac{d\bar{S}_w}{dW_i} + \bar{S}_w \right)\end{aligned}\quad 3-9$$

Add Equation 3-8 to Equation 3-9, we have:

$$S_w^{out} = \frac{d(\bar{S}_w / W_i)}{d(1/W_i)} \quad 3-10$$

Here

$S_w^{Outlet}$  is the saturation at the outlet

$\bar{S}_w$  is the averaged saturation of entire model

$F_w^{Outlet}$  is fractional flow at the outlet

$W_i$  is cumulative of water injection

The pore volume becomes the equivalent of spatial positions and the volume of water injected is the equivalent of time.

A typical chart of a synthetic model is presented in Figure 3-1. It shows the cross-plot of the fraction flow and water saturation at the outlet in orange and the original fraction flow in blue. The effective fractional flow helps to reproduce the average waterflood performance.

At low saturation (equivalently, low fractional flow) level, the foot of the curve continues to steepen as the profile evolves. This is a gravity slump, the importance of which is increasing as the flood proceeds. At late times, the rate of recovery appears to be essentially independent of cell, i.e., independent of the viscous to gravity ratio. This is also why the effective fractional flow curve and the rock curve merge at late time. After calculating the effective relative permeability, the total mobility is updated with two different methods as described in the previous sections. In the finite difference simulator, the average saturation in a grid block is calculated from the fluxes that enter and leave the block. Then the question focuses on how the time averaged flux function is calculated from the block averaged saturations.

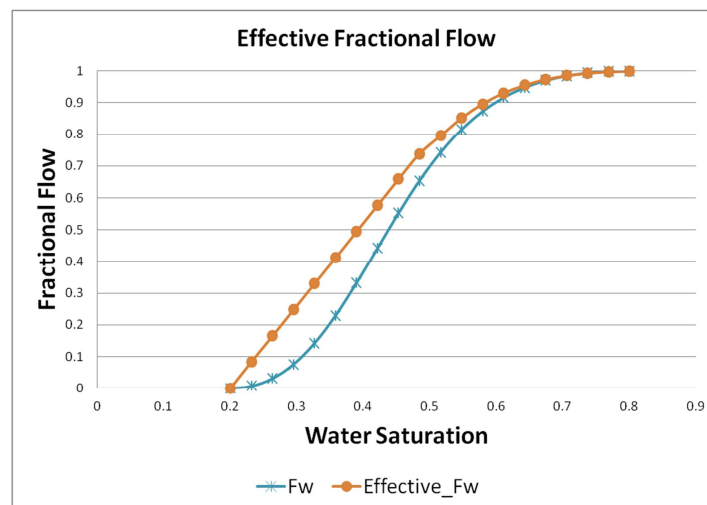


**Figure 3-1 Effective fractional flow illustration**

### 3.3.2 Effective Total Mobility

Literature has revealed different total mobility effect on the pseudos. However, the total mobility upscaling techniques are seldom robust. We propose a novel total mobility upscaling technique that involves the impacts of the total fluid segregation and global absolute permeability upscaling. Calculation of total mobility depends upon the knowledge of water and oil volumes as functions of time, regardless the pressure distribution.

In this section, we are going to introduce two different methods of estimating the effective total mobility, as in equation 3-11.

$$\lambda_{\text{total}} = \frac{k_{ro}}{\mu_o} + \frac{k_{rw}}{\mu_w} \quad 3-11$$

#### 3.3.2.1 Method 1

The extreme case is shown in Figure 3-2 that total fluid segregation is observed (A). It can be deduced that:

$$\lambda_{\text{total}} \propto \frac{k_{ro@Swir}}{\mu_o} \cdot (1 - S_w + S_{oir}) + \frac{k_{rw@Soir}}{\mu_w} \cdot (S_w - S_{oir}) \quad 3-12$$

$S_w$  is the only variable in Equation 3-13. It means when we have total fluid segregation, the total mobility curve is a straight line. In other words, this equation implies that the total mobility is a linear function of water saturation with the same end points as the rock curve. A total mobility chart of this synthetic case is shown in Figure 3-2 (B). The straight purple line represents the total segregation case and it also defines the upper bound of the total mobility. The lower bound is defined as the original rock curve. In other words, an intermittent curve between the straight line and the rock curve is expected for a coarsened model, without absolute permeability upscaling.

$$\lambda_{eff} = \omega \lambda_{linear} + (1 - \omega) \lambda_{rock}$$

3-13

$\lambda_{eff}$  is the effective total mobility

$\lambda_{linear}$  is the total mobility implying a total segregation of water and oil

$\lambda_{rock}$  is the original rock total mobility

$\omega$  is the weighting factor

Proper weighting factor will help to reproduce the fine scale reservoir performance with aggressively coarsened models. However, the sensitivity studies on sector models are required to evaluate the effectiveness of different weighting factors.

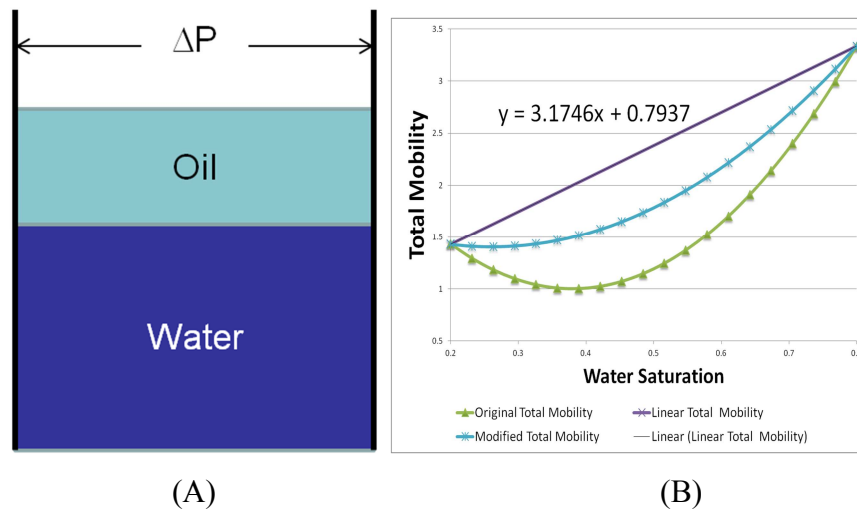


**Figure 3-2 Illustration of total fluid segregation**

### 3.3.2.2 Method 2

From the JBN analysis (Johnson et al, 1959) and its extension (King et al. 1998), know that: the pressure gradient is proportional to the inverse of the total mobility.

We start from:

$$\frac{Q}{A} = -\lambda_r \frac{k}{\mu} \frac{\partial P}{\partial x} \quad 3-14$$

and re-write the equation to have :

$$\begin{aligned} \Delta P &= \mu Q \int_{x=0}^L \lambda_r^{-1} \frac{1}{Ak} dx \\ &= \mu Q \int_{X=0}^{PV} \lambda_r^{-1} \frac{1}{A^2 \phi k} dX \\ &= \mu Q \int_{T=0}^{W_i} \lambda_r^{-1} \frac{1}{A^2 \phi k} \cdot F'(S_w) dT \end{aligned} \quad 3-15$$

To simplify the problem, we ignore the effect from the model geometry and permeability changes in the model. This impact is going to be calibrated using a fine scale sector model. Therefore, our equation is affected by the water injection and pore volume only.

Therefore, reorganize Equation 3-15 and calculate its derivative against T, we have

$$\frac{d}{dT} \left( \frac{\Delta P}{QT} \right) \propto \frac{1}{\lambda_r^{Outlet}} \frac{\partial (F'_w(S_w^{outlet}))}{\partial T} \quad 3-16$$

From Equation 3-5, we have:

$$\frac{\partial (F'_w(S_w^{outlet}))}{\partial T} = -\frac{1}{W_i^2} PV^{outlet} \quad 3-17$$

Combinint Equation 3-16 and 3-17

$$\begin{aligned} \frac{d}{dT} \left( \frac{\Delta P}{QT} \right) &\propto \frac{1}{\lambda_r^{Outlet}} \cdot \frac{1}{W_i^2} \\ &\Rightarrow \frac{1}{\lambda_r^{Outlet}} \propto \frac{d}{dT} \left( \frac{\Delta P}{QT} \right) \cdot W_i^2 \end{aligned}$$

Notice  $T = \int Q dt = W_i$ , we have

$$\frac{1}{\lambda_r^{Outlet}} \propto \frac{d}{dT} \left( \frac{\Delta P}{QT} \right) \cdot W_i^2 = \frac{d \left( \frac{\Delta P}{QW_i} \right)_i}{d(1/W_i)} \quad \text{3-18}$$

Equation 3-18 does not show the impact from the geometry or from the absolute permeability upscaling impact. We collect the pressure, flux, and injection data from the numerical simulation results of a sector model to evaluate the total mobility at the outlet. The global upscaling and geometry impacts have to be corrected by performing the calibration simulation runs on sector coarsened models. For coarse models with different layers preserved, various multipliers can be calculated to compensate the global permeability upscaling effect. Equation 3-18 has a simple format for the 1D model:

$$\frac{1}{\lambda_r^{Outlet}} = \frac{Ak}{LQ} \frac{d(\Delta P/QW_i)}{d(1/W_i)}$$

### 3.3.3 General Workflow

This section discusses the general workflow of the multiphase upscaling. This method requires initial fine scale simulation runs on a sector model and pseudo functions will be applied to the full field coarse models.

- 1) Run fine scale simulation on a sector model which contains typical geologic features from the full field model. In our case study, we test both a quarter of a five spot pattern and the line drive flow pattern.

- 2) Calculate the effective fractional flow at the outlet based on the averaged water saturation and flux. For each of the coarsened model, one fractional flow curve is calculated.
- 3) Calculate the effective total mobility at the outlet by extracting the fluid production rate, water injection rate, and pressure profiles from the fine scale sector model run.
- 4) Update the pseudo relative permeability functions with the effective fractional flow and total mobility curves.
- 5) Run simulation on the coarsened full field model with pseudo relative permeability.

As mentioned in the previous chapter of layer design, we are not considering the areal upgridding/upscaling. No numerical dispersion problem will be involved in this study.

## 3.4 Results and Discussions

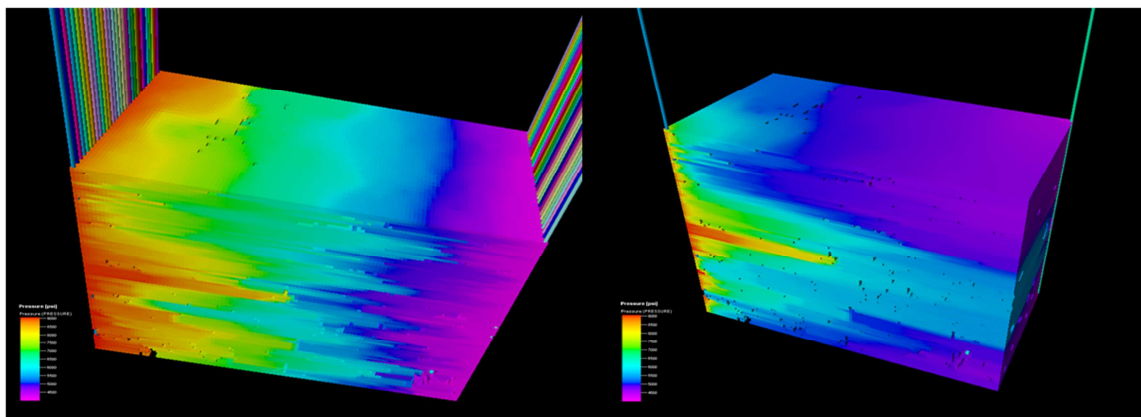
### 3.4.1 Model Description

In this section we are going to apply the pseudo functions to the SPE10, Model 2. This SPE10 model contains a dimension of 60x220x85. The upper unit is the Tarbert. The lower unit is the Upper Ness. It is channelized and there is a big contrast between channel/non-channel permeability values. Also these two geological units have different ranges of permeabilities, with higher permeabilities in the Upper Ness.

As mentioned in the previous section, the fundamental idea of using pseudo functions is to eliminate the need of full field simulation runs on the fine scale. Therefore, a quarter-model is selected from an original full field model and is used as the reference fine scale model to calculate the pseudo relative permeability functions. The quarter-model (Figure 3-3) contains 30x110x85 cells and preserves the two geologic zones. We are trying to

preserve the typical features from the original field with the reduced simulation time. The pseudo functions are applied to the full field coarse model with different injection schemes.

Two flow patterns are applied: line drive and quarter of a five spot (named as Q5 pattern). In the line drive pattern (Figure 3-3 A), 30 injectors and 30 producers are placed at each end of the sector model separately. This line drive model mimics the 1-D flow model on which the original JBN analysis (Johnson et al. 1959; King et al. 1998) was developed. For the Q5 pattern model, shown as Figure 3-3 (B), one injector is at the corner and one producer is placed at the far end corner. This arrangement is designed to evaluate the well performances at original locations. The original SPE10 model has a 5-spot pattern and we use the quarter model with the corresponding well locations. According to the reviews from Barker and Thibeau (1997) and Barker and Dupouy (1999), the pseudos depend upon well positions and rates. Sensitivity analysis is performed to evaluate such impacts from well conditions in the following sections.



(A) (B)  
**Figure 3-3 Quarter model (A) line drive pattern (B) Q5 pattern**



### 3.4.2 Results and Comparisons

In our studies, model geometry (flow patterns), vertical model resolution, injection control scenario, and averaging on outlet saturation are major concerns. This pseudoization study is a great support for the layer design algorithm presented in chapter 3. All test models presented in this chapter have limited vertical resolutions. In previous studies, injection wells were under rate control which made it easier to match the fine scale field performance. In our study, two different injection control modes are applied. We first use a total injection rate of 5000 bbl/day and later apply a BHP control of 6500 psi for the injectors.

#### 3.4.2.1 Calibration of Pseudo Function

The calculations of pseudo functions are calibrated with the fine scale sector models. This algorithm is based upon the calculation of averaged water saturation and effective fractional flow at the outlet. In the ideal case, if no upgridding/upscaling has been applied, the model should remain at the fine scale and the fractional flow curve should overlap on the rock curve, although it is impossible because the model is highly heterogeneous.

To calibrate the pseudo functions for the specific flow pattern chosen, we followed the steps:

- 1) Calculate effective fractional flow at the outlet for each fine scale layer, shown as blue curves in Figure 3-4.
- 2) Calculate the effective fraction flow and saturation at the outlet of entire model using the following equation:

$$a. \quad F_w = \frac{\sum_{i=1}^n Q_{it}^{outlet} f_{wi}}{Q_{total}^{outlet}}$$

$$\text{b. } S_w = \frac{\sum_1^n PV_i \cdot S_{wi}}{\sum_1^n PV_i}$$

- 3) Plot the  $F_w$  against  $S_w$ , as the green curve in Figure 3-4. This curve represents an effective performance curve based on the outlet flow behavior under a specific flow pattern and well planning. The red curve represents the original rock curve.
- 4) Plot the reference (rock) curve and measure the difference between the two.

Figure 3-4 shows an example of model calibration. Blue curves show the individual fractional flow for each of the fine scale layer. No coarsening is applied to this calibration model. Green curves show the averaged fractional flow, and the original (rock) curves are in red. The difference between the pseudo and the rock curves shows up at the low water saturation region of the Q5 pattern. Green and red curves are merged after water saturation reaches about 0.4. This difference is more obvious in the line drive pattern. This is a measure of the difference between the ideal rock curve we can have from lab experiments and the actual model behavior curve (in green). If there are enough layers in the original fine scale models, the green curves should be overlapped to the rock curves. In our study, the green curve is used as a base line for the future calculation.

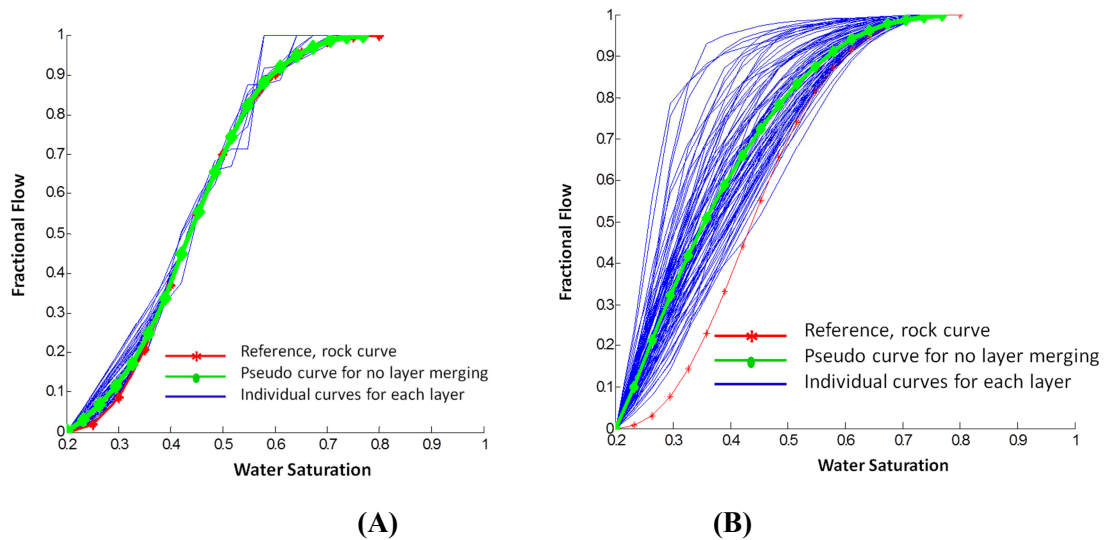


**Figure 3-4 Pseudo function bias and calibration: (A) Q5 pattern (B) line drive pattern**

### 3.4.2.2 Rate Control

#### 3.4.2.2.1 Line drive Pattern vs. Q5 Pattern

As described in the previous review work (Barker and Thibeau, 1997 and Barker and Dupouy, 1999), the pseudos depend upon well locations and rates. In this section, we present a quarter of a 5-spot pattern model and a line drive model and benchmark the overall field performances.

Under different patterns, the updated effective relative permeability and total mobility functions can be seen from Figure 3-5. Figure 3-5 (A) presents the cross-plot of the original (rock) fractional flow against the water saturation and a number of pseudo fractional flows calculated at the outlet. The solid and the dotted green lines represent the data acquired from the 2 and 5 layer coarse models with the line drive flow pattern.

Since the model has only two geological zones, the 2 layer model layers were grouped vertically in such a way that each geological zone has only one layer left. The overall coarsened model has a size of 60x220x2. The solid and dotted purple lines show the results of the 2 and 5 layer model with a quarter of a 5-spot flow pattern. The solid and dotted blue lines show the Coats method (Christie and Blunt 2001; Coats Engineering 2000) in which the water relative permeability exponent is adjusted for different coarse models. In this SPE10 case, water relative permeability exponents are set to 1.3 for the 2 layer model and 1.32 for the 5 layer model.

Generally, with more layers preserved in the coarse model, the pseudo fractional flow curve is closer to the reference (rock) curve. The Q5 pattern 5 layer curve almost overlaps the Coats curve. However, Coats method does not involve calculating the effective total mobility which is critical for field pressure match. Compared to the Q5 patterns, the line drive patterns tend to generate relative permeability curves that are close to the reference (rock) curve.

At low saturation (equivalently, low fractional flow) level, the gravity slump is clearly identified. This low saturation profile change shows great impact on the water breakthrough time match. As water saturation increases, different coarse models show a wide distribution of slopes. At late times, the effective fractional flow curve and the rock curve merge eventually, because the rate of recovery appears to be essentially independent of cell. After calculating the effective relative permeability, the total mobility is updated with two different methods, which were described in the previous sections.

Figure 3-5(B) shows the straight line (in brown) representing the total mobility for the extreme case of the absolute water and oil segregation. The red line represents the original total mobility curve from lab experiments. The upscaled curve keeps the same shape if it does not vary with facies or poro-fabric. The blue curves show the total

mobility from the Coats method, and the curves is in between of the reference (rock) curve and the total segregation curve (straight line). The green and purple lines show the total mobility from the coarse models with line drive flow pattern and Q5 spot flow pattern respectively. The calculated lines are shallower than the reference (rock) curve. The reduced total mobility shows an impact from the global absolute permeability upscaling. The coarsening of the grids and upscaling of the absolute permeability lead to a shallower shape of the effective total mobility.

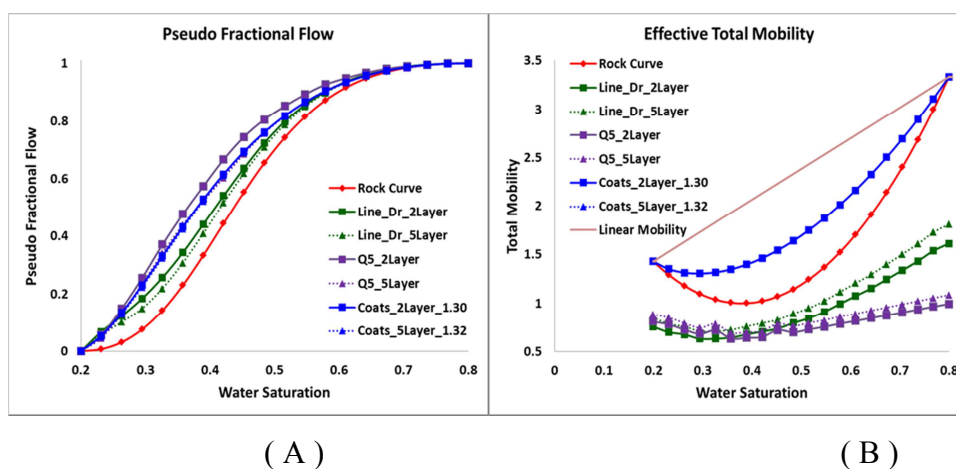
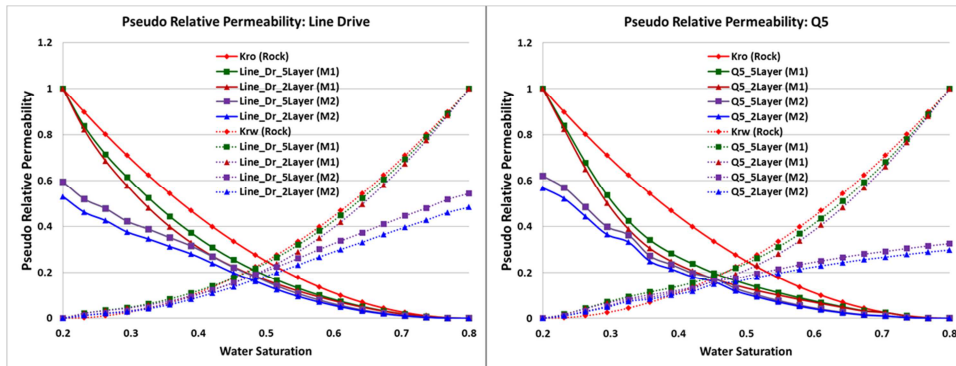


**Figure 3-5 Rate control: (A) pseudo fractional flow and (B) effective total mobility**

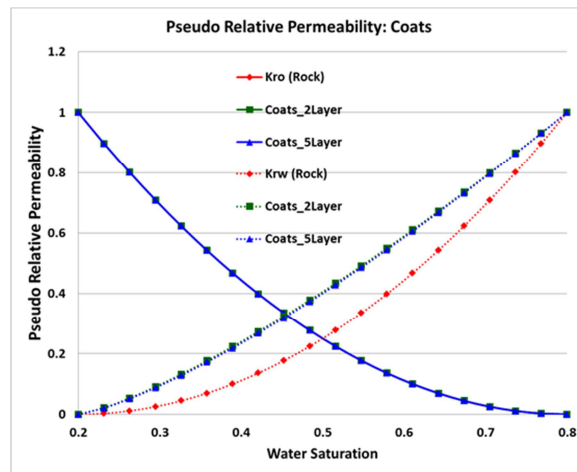
Figure 3-6 shows the pseudo relative permeability curves from a number of total mobility calculations. Figure 3-6 (A) and (B) show the rock relative permeability curves and pseudo curves from the line drive models and Q5 models with 2 and 5 layers, (C) presents the curve updates from Coats method. “M1” indicates the total mobility calculated using method 1 (weighting factor) and “M2” represents the method 2 in which the total mobility is calculated at the outlet of with respect to the single permeability

upscaling at the coarse scale. The oil relative permeability curves show a monotonic decreasing trend as water saturation increasing.



( A )

( B )



( C )

**Figure 3-6 Effective total mobility for (A) line drive models and (B) Q5 spot models (C) Coats models**

The method 1 relies on a proper selection of weighting factors. The green and maroon lines in Figure 3-6 show the results of using different weighting factors for different

models. The water and oil relative permeability curves have the same start and end points as the reference (rock) curves. This weighting factor is calibrated on the sector model and depends upon both the layer combination and the flow pattern. The weighting factor is 0.1 for the 2 layer model and 0.15 for the 5 layer model. The purple and blue curves represent the curves from the models using the calculated effective total mobility (M2). Method 2 results in a shallower shape of the relative permeability curve. The calculated total mobility curves no longer show the same start and end points as the reference (rock) curves. Both the oil and water relative permeabilities are reduced because of the absolute permeability impact. Lower water movability is expected at low water saturation, and lower oil movability is expected at high water saturation region. The effective relative permeability curves for the coarsened models are shifted to the left hand side of the original curves. For the same flow patterns, as the number of layers decreases, the overall relative permeability curves shift to the lower saturation (left) side. Comparing the two flow patterns, line drive and Q5, Q5 presents similar water relative permeability curves but shallower oil relative permeability curves. Coats method modifies the water relative permeability exponent only. In this case, we use 1.30 for the 2 layer model and 1.32 for the 5 layer model. The oil relative permeability curves are overlapped for the fine and coarse models.

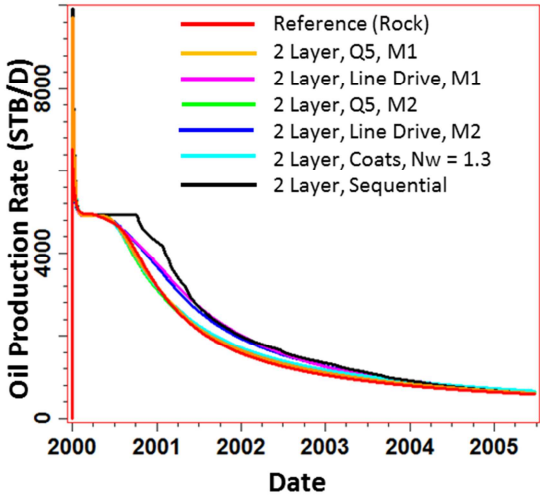
Figure 3-7 shows the results of fine scale simulation and a number of coarse scale simulation results. The figures show field oil production rate, cumulative oil production, field water cut, and field pressure. The cases on the left side of the figure show 2 layer models and the figures on the right side use 5 layer models with different relative permeability curves.

In Figure 3-7, each of the figures shows 7 different curves. Red lines represent the reference full field model containing cell number of 60x220x85. The yellow and purple lines show the model performances with relative permeabilities calculated from the Q5 spot and line drive pattern sector models respectively. The weighting factor is 0.1 for the

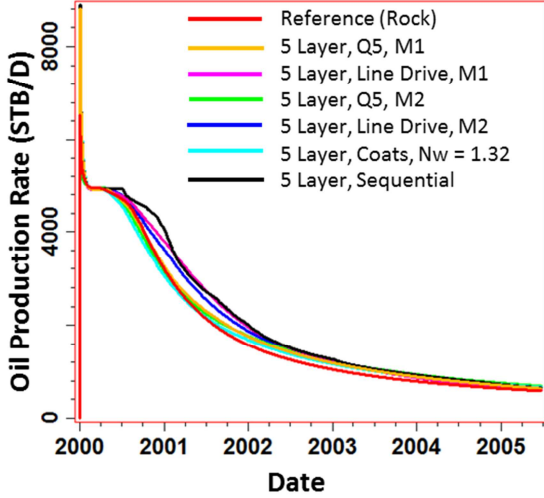
2 layer model and 0.15 for the 5 layer model. Sensitivity studies on the sector models are performed for weighting factor selection since no full field fine scale simulation run is required at this point. The green and blue curves present the models with pseudo relative permeabilities calculated using method 2. The cyan curves show results from the Coats method. The water relative permeability exponent is 1.30 for the 2 layer models and 1.32 for the 5 layer models. We use black curves to represent the coarse model performances in which the original rock curves are applied.

In general, all of the calculations with the pseudo permeability curves show better approximations to the fine scale result. With different number of layers preserved in the coarsened models, the best oil production predictions are from the Q5 flow pattern and Coats method. All of the line drive models slightly overestimate the oil production and underestimate the water-cut. The most sensitive indicator of the effectiveness of the pseudo function calculation is the field pressure response. Applying the method 2, we are able to reproduce the field pressure response with the coarse models. With either 2 or 5 layers preserved, method 2 generates the shallower relative permeability curves and preserves the field pressure behaviors. Though modifying the relative water permeability exponent (Coats method) or different weighting factors (method 1) are able to have a good match of the oil production, they fail to match the field pressure response. The line drive pattern shows acceptable oil production prediction but better field pressure reproductions in this specific case.

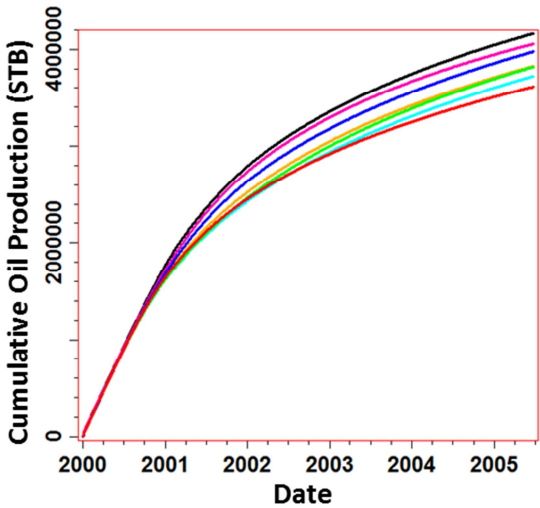




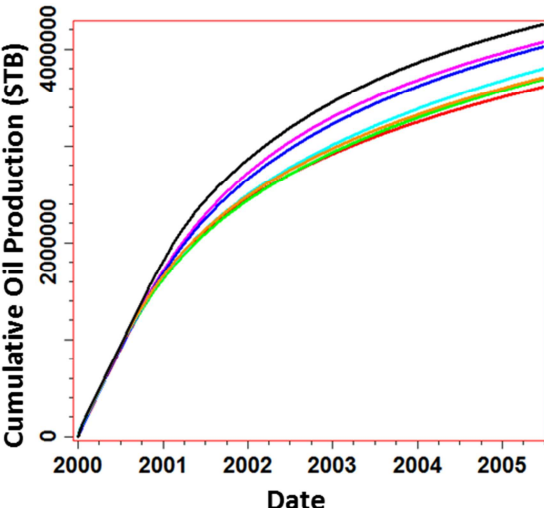
( A )



( B )

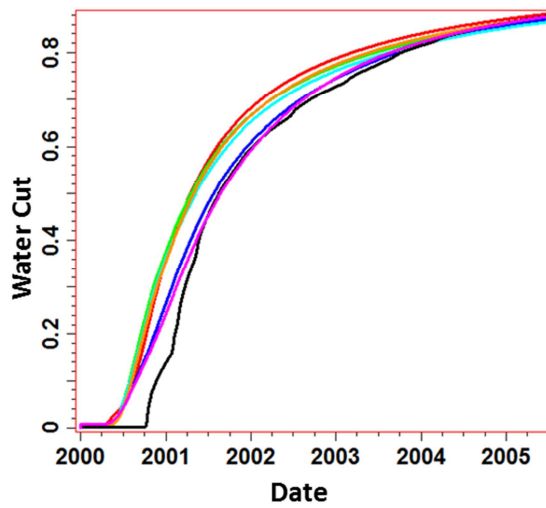


( C )

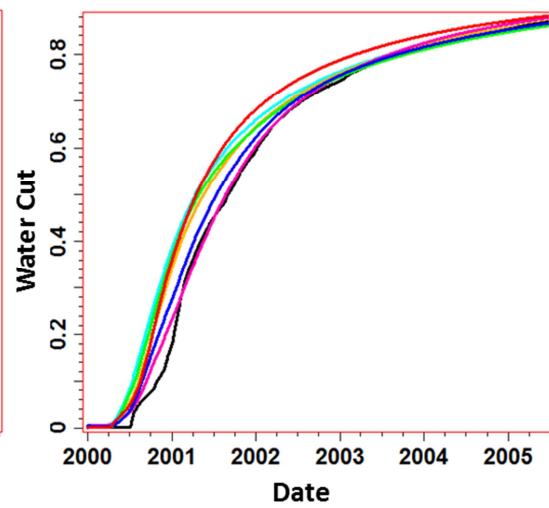


( D )

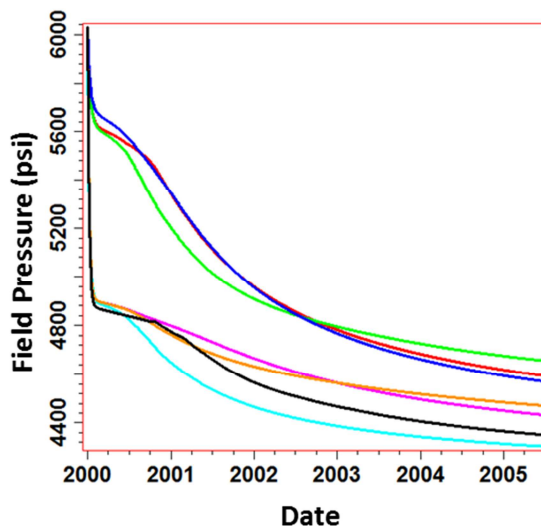
Figure 3-7 Rate control injection wells, field performance: (A, B) oil production rate (C, D) cumulative oil production (E, F) water cut (G, H) field pressure



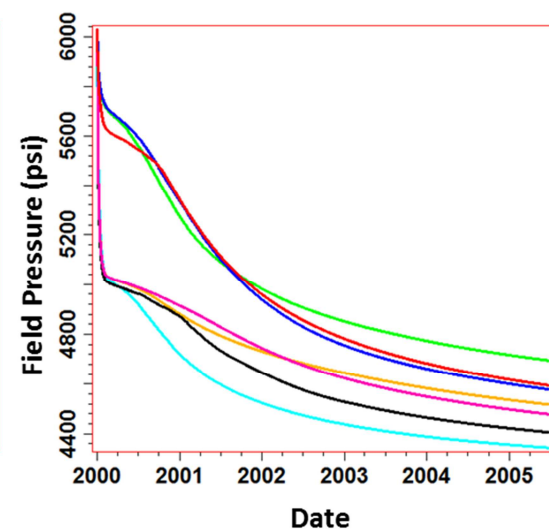
( E )



( F )



( G )



( H )

Figure 3-7 Continued

In this section, two coarsened models with different pseudo functions are presented. In each of the coarsened model, only one set of pseudo relative permeability curves are applied to the entire domain. Effective fractional flow curves obtained from different

patterns present slight differences at low water saturation range. The overall shapes of effective fractional flow curves are close to the concave envelope of the rock curve at low to intermittent saturation range. At high saturation region, the fractional flow curves are close to the rock curve eventually. Effective fractional flow dominates the overall reservoir performance while injection wells are under rate control. The total mobility curves dominate the average field pressure response. As described in the previous section, our novel total mobility upscaling (M2) involves the absolute permeability impacts. The method 2, with either line drive pattern or the Q5 pattern, generates better effective total mobility curves with which the aggressively coarsened models show improved field pressure match.

#### 3.4.2.3 Pressure Control

In this section, models with the same layer grouping but different injection control modes are presented. The injection pressure target is 6500 psi, and the field initial pressure is 6000 psi. The same algorithm and workflow are applied for the effective fractional flow and total mobility calculations. The upscaled relative permeability is applied to the full field model simulation for validation. Unlike the rate control models, when the injectors are under pressure control, coarsened models are more sensitive to the total mobility variations in terms of the oil production rate. With different flow patterns, the updated effective relative permeability and total mobility functions can be seen from Figure 3-8.

Figure 3-8 (A) presents the cross-plot of the original (rock) fractional flow fractional (in red) against the water saturation and a number of pseudo fractional flows at the outlet. All of the models presented in Figure 3-8 (A) have the same layer combinations as they are in the section 3.4.2.2 but with injectors under pressure control. Compared to the Q5 patterns, the line drive patterns tend to generate relative permeability curves that are closer to the reference (rock) curve. Compared to the rate control models in Figure 3-5,

the pseudo relative permeability curves for the pressure controlled model tend to be closer to the reference (rock) curve.

Figure 3-8 (B) shows the straight line (in brown) representing the total mobility for the extreme case of absolute water and oil segregation. The red line represents the original total mobility curve from lab experiments. The blue curves show the total mobility from the Coats method and the curves in the between of the reference (rock) curve and the total segregation curve (straight line). The green and purple lines show the total mobility from the coarse models with the line drive flow pattern and Q5 spot flow pattern respectively. The calculated lines are shallower than the reference (rock) curve. With pressure control, the coarsened models show similar total mobility from different coarsened models and patterns.

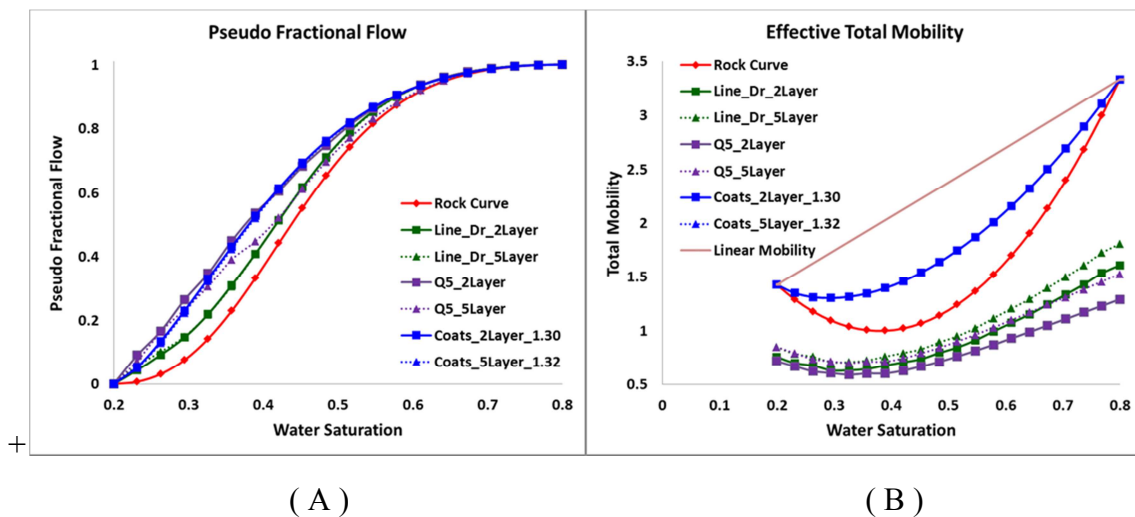
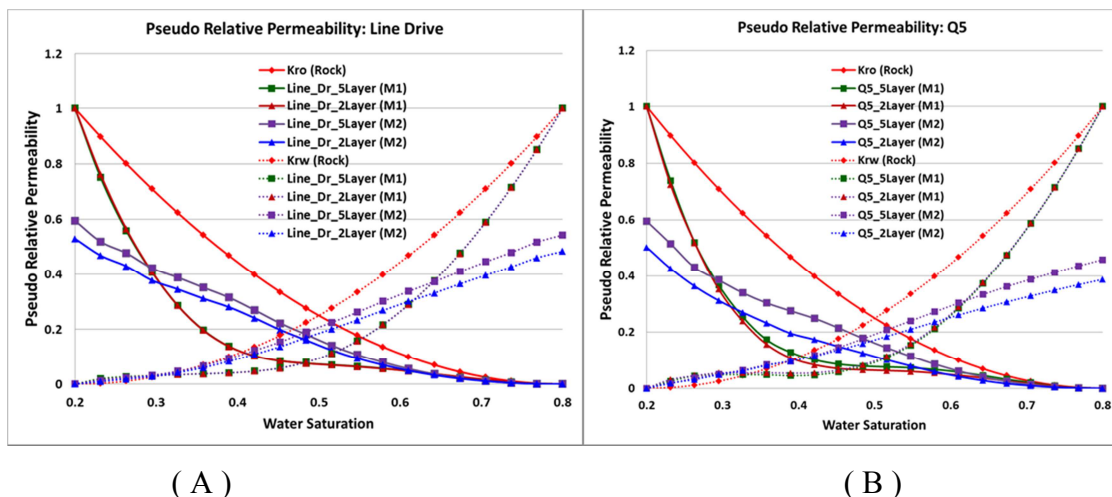


Figure 3-8 Pressure control: (A) Pseudo fractional flow and (B) effective total mobility

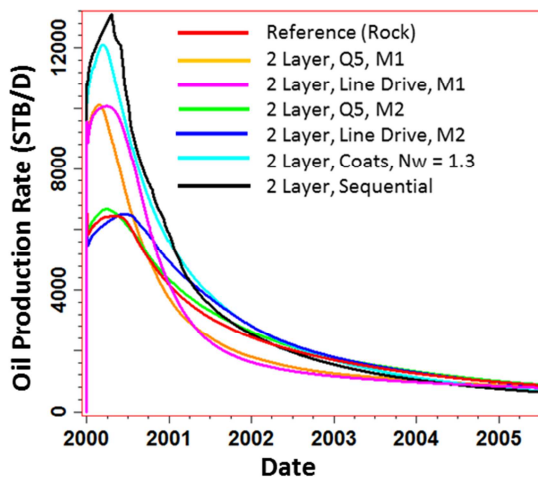
Figure 3-9 shows the pseudo relative permeability curves from a number of different models. Figure 3-9 (A) and (B) show the rock relative permeability curves and calculated results from the line drive models and Q5 models with 2 and 5 layers. “M1” indicates the total mobility calculated using method 1 (weighting factor) and “M2” represents the method 2 in which the total mobility is calculated at the outlet of the coarsened models. Compared to the pseudo permeability curves obtained from the rate control models, method 1 presents shallower shapes of the relative permeability curves. At low water saturation, the oil relative permeability curves rapidly decrease and, at high water saturation, the water relative permeability curves increase fast. Both the oil and water relative permeability curves maintain the same start and end points. With the effective total mobility calculated using the method 2, the line drive models provide similar relative permeability curves as seen in Figure 3-6 and Figure 3-9. Under pressure control, the Q5 models present shallower water relative permeability curves as shown in Figure 3-9 (B). The Coats method is performed with the same water relative permeability exponents that are applied in the previous rate control models.



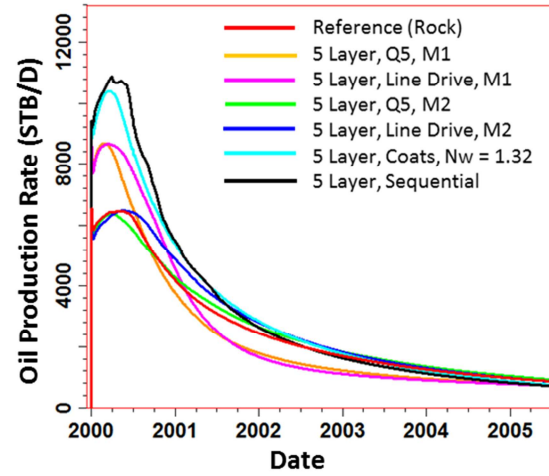
**Figure 3-9 Effective total mobility for (A) line drive models and (B) Q5 spot models (pressure control)**

Figure 3-10 shows the results of fine scale simulation and a number of coarse scale simulation results. All of the cases shown in Figure 3-10 have the injectors under pressure control. The figure A to H shows field oil production rate, cumulative oil production, field water cut, and field pressure. The cases on the left side of the figures show the results of the 2 layer models. The figures on the right side present the results of the 5 layer models having different relative permeability curves.

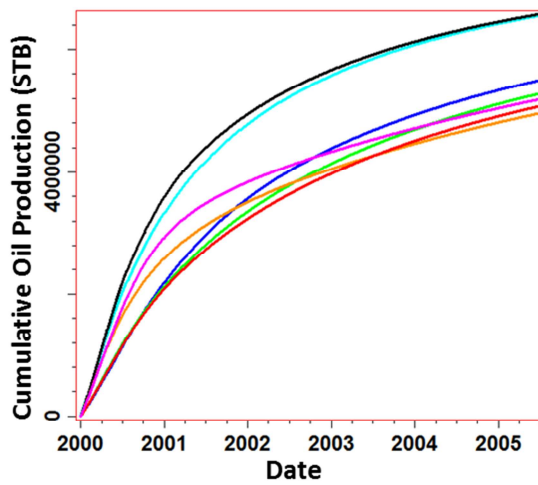
In Figure 3-10, each of the figures shows 7 different curves. Red lines represent the reference full filed model containing cell number of 60x220x85. The yellow and purple lines show the model performances with relative permeabilities calculated from the Q5 spot and line drive pattern sector models. The weighting factor is 0.65 for the 2 and 5 layer models. A weighting factor of 0.65 generates a monotonic function for both the oil and water relative permeability. The green and blue curves present the models with pseudo relative permeabilities calculated using method 2. The cyan curves show results from the Coats method. The water relative permeability exponent is 1.30 for the 2 layer models and 1.32 for the 5 layer models. We use black curves to represent the coarse model performances in which the original rock curves are applied.



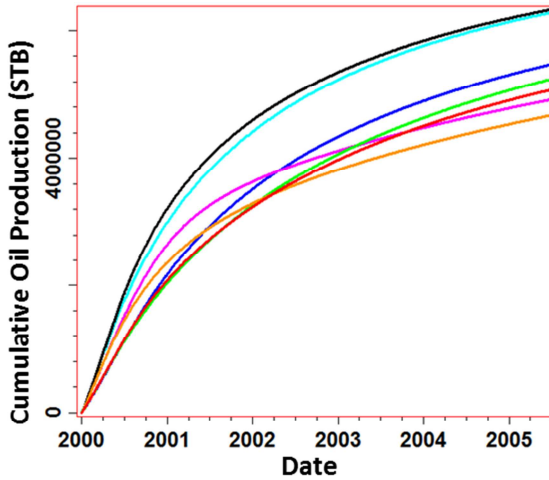
(A)



(B)

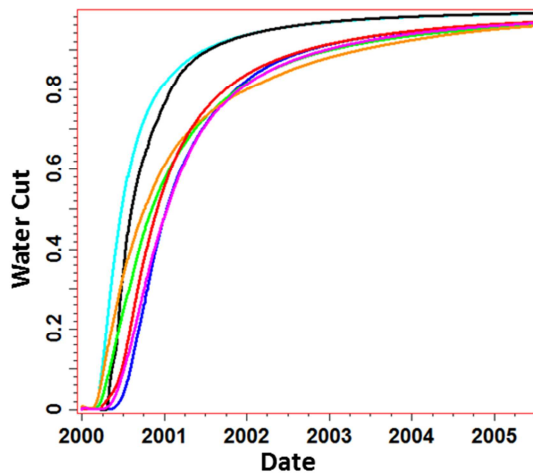


(C)

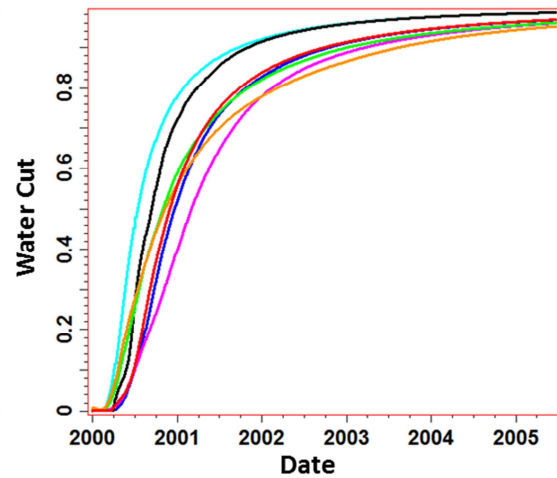


(D)

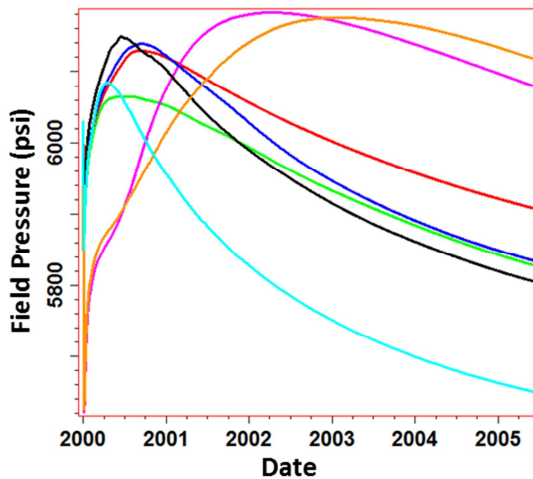
Figure 3-10 Pressure control injection wells, field performance: (A, B) oil production rate (C, D) cumulative oil production (E, F) water cut (G, H) field pressure



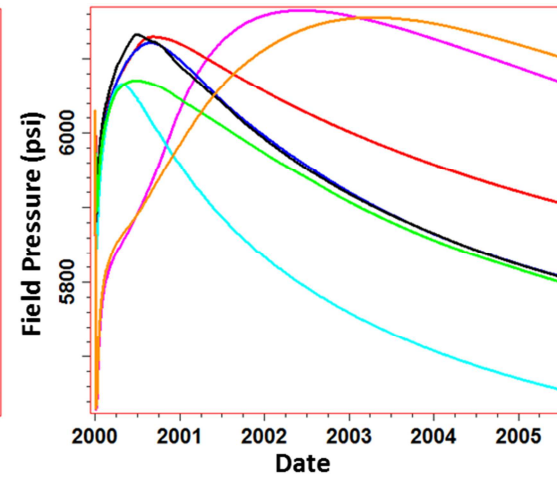
(E)



(F)



(G)



(H)

Figure 3-10 Continued

The oil rate curves (Figure 3-10 A and B) present a wide range of field responses from different models. Without using proper total mobility functions, the fine scale oil production performances cannot be reproduced. Coats method does not involve effective total mobility calculation. Therefore, the corresponding model simulations overestimate



the overall oil rates at the very beginning. The cyan curves are close to the black curves in Figure 3-10 (A-F). Compared to the coarse model, in which no multiphase upscaling is applied (shown as black curve), the Coats method shows very limited improvement. The overall oil production mismatch from the Coats method is around 30%. The Coats method also fails to provide a good estimation of the water cut and average field pressure. It shows an early breakthrough time and underestimates the overall field pressure (Figure 3-10 G and H).

Method 1 of calculating the effective relative permeability helps on improving the field oil production and field water cut responses. However, for either the Q5 or the line drive patterned models, they overestimate the oil production rate at the beginning and underestimate the oil production rate in the later simulation time, though the overall cumulative oil production in a range of 2000 days seems acceptable. Using method 1 will also lead to an early breakthrough as seen in Figure 3-10 (E & F). Using method 2 to calculate the effective total mobility provides the best oil production estimation. Both 2 and 5 layer models show significant field response improvements in terms of oil production rate. Compared with the line drive pattern, the Q5 pattern shows better oil production predictions but slightly earlier water breakthrough time estimation. Line drive models present the best water cut match and Coats method fails to reproduce the fine scale water cut behaviors, as seen in Figure 3-10 (E) and (F). Figure 3-10 (G) and (H) present the field pressure responses. Coats method totally underestimates the field pressure behaviors while the method 2 provides the best overall estimation.

In general, effective total mobility calculation provides better approximations to the fine scale simulation results. There is a basic trend that field responses are improved when more layer are preserved. Though the models applied the Coats method and the models with Q5 pattern have similar fractional flow curves (Figure 3-8 A), differences in effective total mobility lead to significant variations in field performances of both the 2 and 5 layer models. Applying the method 2 can help on reproducing the field responses

greatly. Compared with the rate control models, total mobility upscaling shows its importance and effectiveness on the reproduction of fine scale responses.

#### 3.4.2.4 Modified Well Control

Theoretically, if the pseudo functions are properly created, the coarse model should be able to reproduce the fine scale performance, even with the modified well control modes. Though previous review papers (Barker and Dupouy 1999; Barker and Thibeau 1997) suggested of using the similar flow patterns and well conditions. In this section, we use the relative permeability curves obtained from the previous pressure control models as seen in Figure 3-8. All of the injectors are restricted to 9000 psi and producers have applied rate control rules of 8000 bbl/day. The reservoir performances are presented in Figure 3-11, and the same color legend is applied as the one in Figure 3-10.

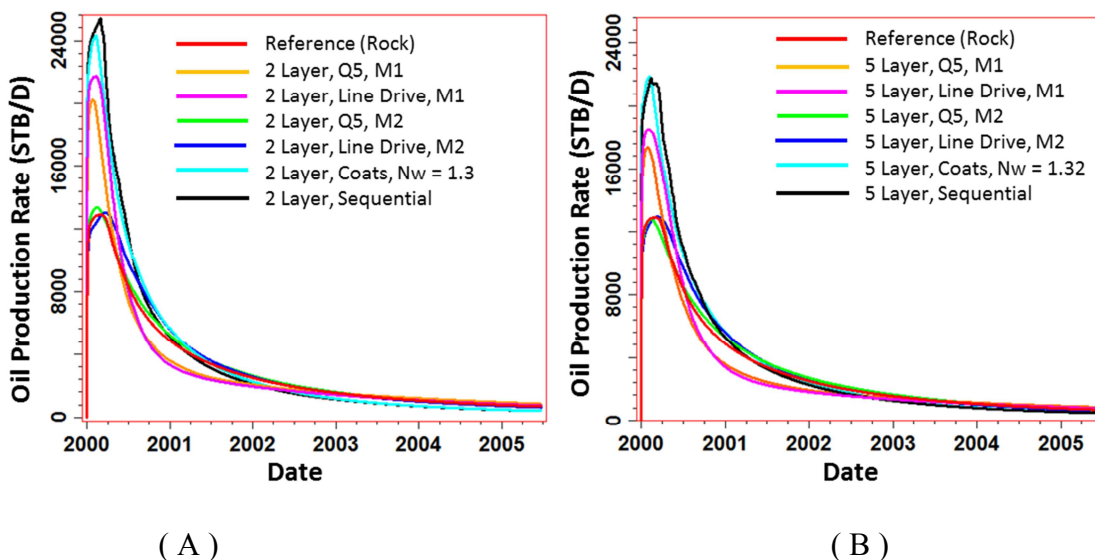
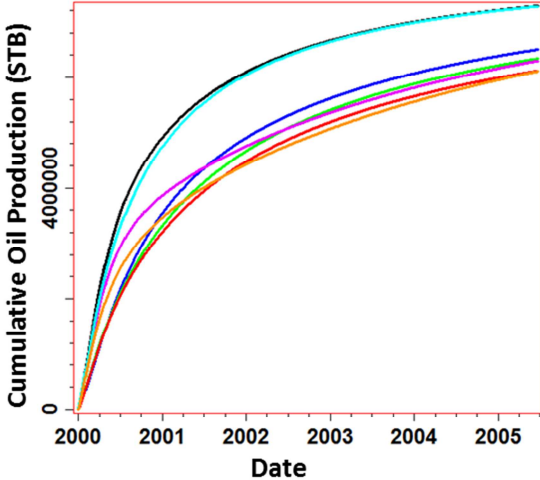
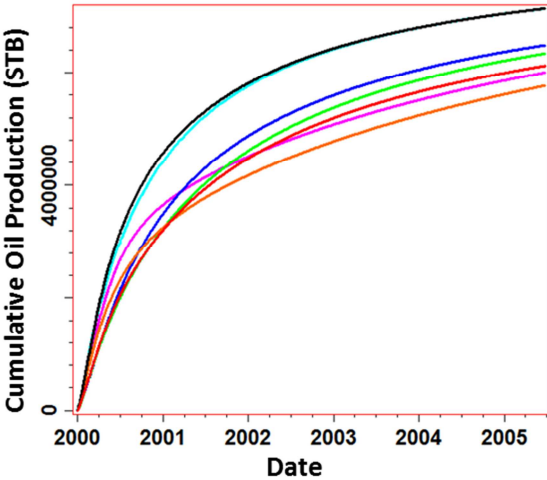


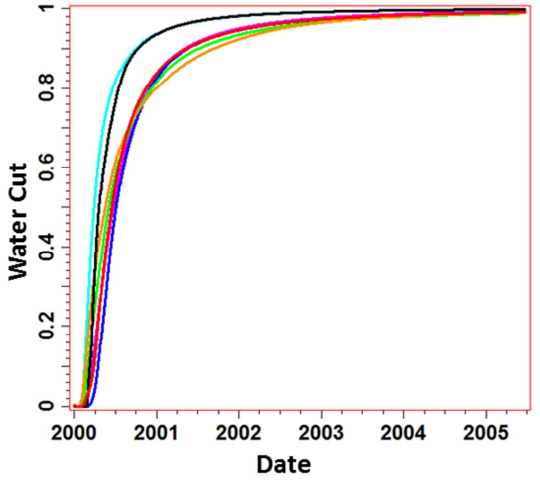
**Figure 3-11** Field performance when injectors are under pressure control and producers are under rate control: (A, B) oil production rate (C, D) cumulative oil production (E, F) water cut (G, H) field pressure



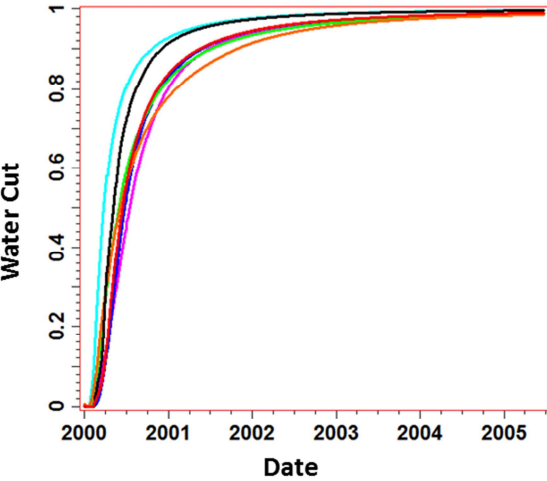
(C)



(D)



(E)



(F)

Figure 3-11 Continued

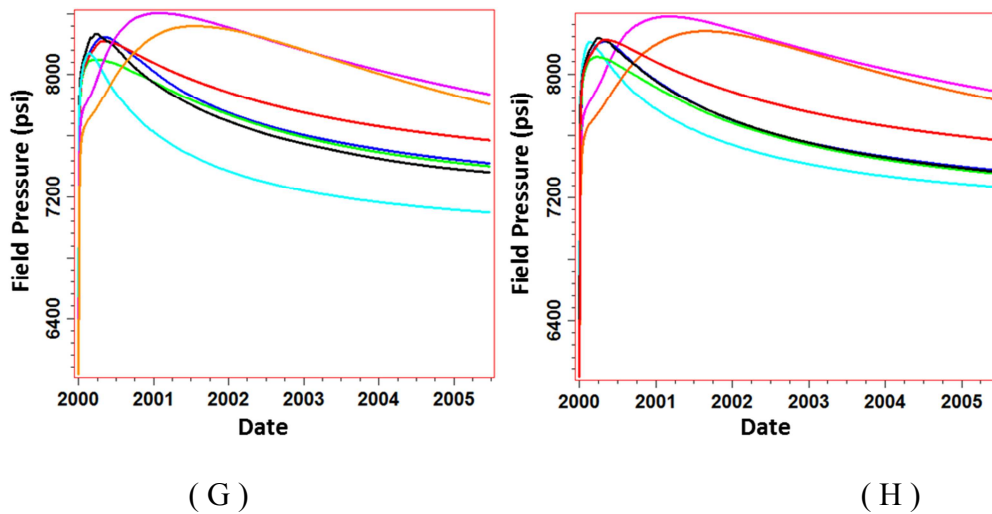


**Figure 3-11 Continued**

In general, applying the previous pseudo relative permeabilities acquired from the pressure (6500 psi) control model to the new models generates relative similar results as seen in Figure 3-10. The Q5 pattern model with the method 2 of calculating the effective total mobility provides best field oil production prediction and good water cut estimation. The effective total mobility calculated using method 1 (weighting factor method) cannot fully reproduce the fine scale performance. Method 1 leads to overestimation of the oil production rate at the beginning regardless the flow patterns or the number of layers preserved.

#### 3.4.2.5 Parameterization

In our total mobility upscaling procedures, there are two main parameters need to be taken care of. The first one is a factor for total fluid segregation, which is utilized in method 1. Using such a factor, the overall shape of the total mobility curve is flattened. The second factor is the multiplier used to correct the overall permeability upscaling

impact on the total mobility position. This multiplier is collected by performing calibrations runs on a typical sector model.

For the effective fractional flow calculation, we define a multiplier M as a function of the water saturation:

$$M = 1 + a(1 - S_{oir} - S_w)^4 \quad 3-19$$

and

$$F_w^{Outlet} = M \cdot F_w^{rock} \quad 3-20$$

Here

$S_{oir}$  is the irreducible oil saturation

$a$  is the factor controlling the saturation curve steepen at the low water saturation.

This “ $a$ ” factor shows a significant impact on the breakthrough match.

Figure 3-12 shows the effective fractional flow when “ $a$ ” is set to 25. Figure 3-13 presents the field performance for a two layer model. The overall field performance is improved, compared to the model without using pseudos. Water breakthrough time is significantly affected by the fraction flow steepening at low water saturation. However, the value of “ $a$ ” should be evaluated with the coarse sector models also. Field pressure match is improved because the total mobility upscaling concerns the overall permeability upscaling.

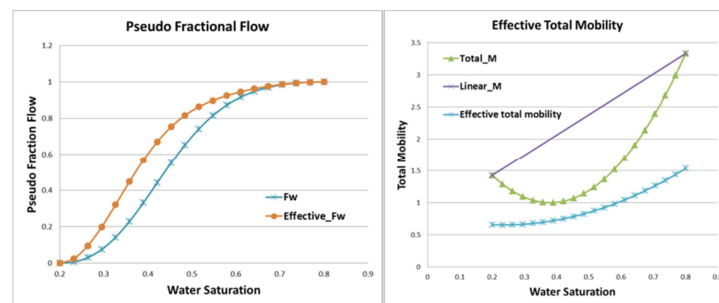
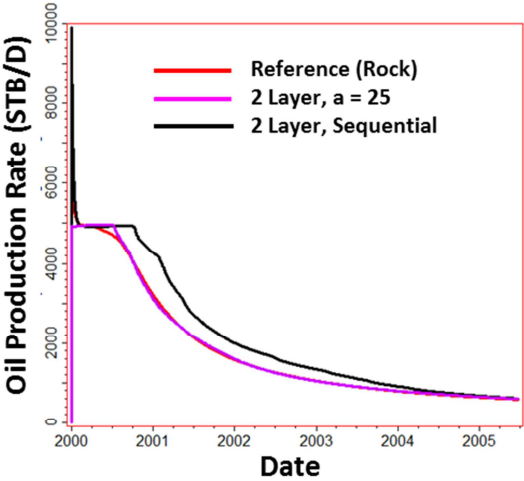
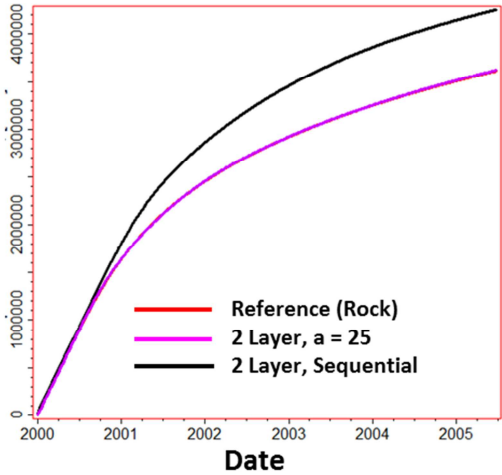


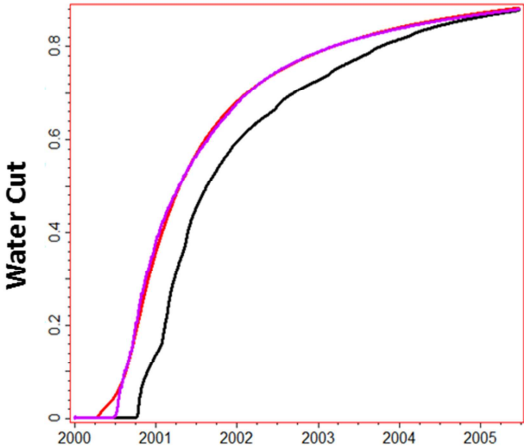
Figure 3-12 Effective fraction flow and total mobility:  $a = 2.5$



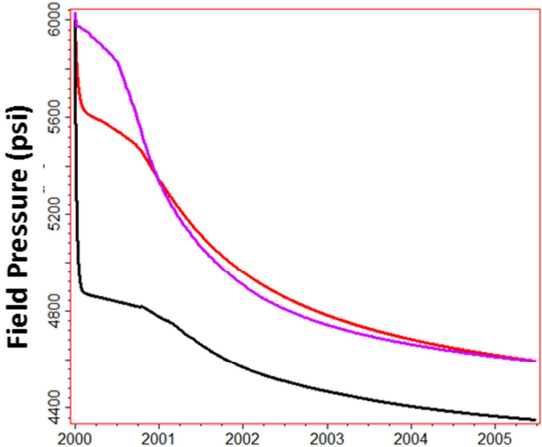
(A)



(B)



(C)



(D)

Figure 3-13 Field performance for a two layer model (A) oil production rate (B) cumulative oil production (C) water cut (D) field pressure

### 3.4.3 Discussions

In this chapter, we introduce a novel total mobility upscaling method which concerns the requirement of rescaling the global absolute permeability. The effective total mobility curves calculated from method 1 and 2 has similar flattened shape. However, M2 curves, which have shallower positions, always generate better field performance. It indicates the importance of accounting the global permeability upscaling. M1 method uses a single value as the weighting factor. It may also suggest that different weighting factors should be considered for different water saturations. The M1 method correctly processes the fluid segregation but ignores the global permeability rescaling. Our effective fractional flow calculation follows the classic JBN method but is extended to a 3D heterogeneous model. The steep curve of the effective fractional flow presents significant impact on the match of the breakthrough time. Time step should be small enough to provide sufficient resolution at low water saturation region. The novel pseudos are able to reproduce the results of fine scale field performance on a coarse grid.

#### 3.4.3.1 Selection of the Sector Fine Scale Simulations

We had a review on different dynamic pseudo functions, such as Kyte & Berry, pore volume weighted pseudos, Stone pseudos and etc. All of the pseudo functions are included in the Eclipse PSEUDO package (Schlumberger 2008). The first disadvantage of mentioned methods is that the full field fine scale simulation run must be performed and should cover sufficient time steps. Running simulation on the full field fine scale models is the foremost thing that should be avoided. If we have the ability to run the fine scale full field models, there may not be necessary to apply the pseudo functions at all. Secondly, for each of the coarsened grid block, a pseudo relative permeability table is generated. Take the SPE10 case as an example, if the model coarsened to a 2 layer model and areal resolution maintains the same, 26400 tables are generated. Applying more than 20 thousand individual pseudo relative permeability tables are impractical.

Therefore, a practical and useful pseudo functions should be able to reproduce the original fine scale simulation performance but without using individual curves for each coarsened gridblock. This method has been proven to be simple and effective with the case studies presented in the previous sections.

#### 3.4.3.2 Dependence on Well Conditions

In general, pseudos depend upon well locations and constrains. The Q5 pattern is similar to the fine scale well arrangement and the Q5 pattern pseudos presented slightly better oil production predictions compared to the line drives for both pressure and rate control of water injection wells. Line drive patterns, which mimic the 1-D flow, tend to overestimate the oil production rate with SPE10 model. According to the case study performed, we recommend of generating the pseudos from similar flow patterns and well constrains, which don't have to be exactly the same. The pseudos acquired at an injection pressure of 6500 psi can be used for the cases that have both pressure control for injectors and the rate control for the producers. This is consist with the previous statement that one can obtain acceptable results for similar production scenarios without renewing the pseudos (Thibeau et al. 1995). However, it is also noticed the pseudos from the pressure control and rate control models are different. Pseudo relative permeability curves need to be regenerated if flow conditions change a lot.

#### 3.4.3.3 Coats Method

Coats provided an aggressive coarsening of 10x20x10 results on the SPE10 model (Christie and Blunt 2001; Coats Engineering 2000). The model was uniformly coarsened with a water relative permeability exponent modified from 2 to 1.28. This method requires only one parameter (water relative permeability exponent) modification since there is only one rock type involved in this case. Of all the field response results, the greatest deviations from the fine scale were observed for field average pressure.



Landmark, Total, and Chevron obtained excellent matches of field average pressure. All had the advantage of knowing the fine-grid solution (Christie and Blunt 2001). If pressure behavior is known, it is a fairly simple matter to adjust the well PI's to match it. As reviewed in the previous section, our method shows very similar effective fractional flow curves for the coarsened models as the Coats method. However, Coats method does not involve the total mobility upscaling which is critical for improving the coarse field responses. Applying total mobility upscaling helps on matching the field pressure. Another critical issue is the well constraint. According to our sensitivity study on selecting proper weighing factor (method 1), the average field pressure is sensitive to the effective total mobility change when the injectors are under rate control, but not the oil production rate. When the injectors are under pressure control, oil production performance is greatly affected by both the fractional flow and the total mobility. Coats method fails to reproduce the fine scale simulation results for the models with the pressure controlled injectors. Another disadvantage of Coats method is that modifying the water relative permeability exponent requires a sensitivity study comparing the results against the fine scale full field model. In other words, Coats method does not have the prediction ability. If the full field data are not available, there is no way for the Coats method to choose a proper exponent at all. In short, Coats method fails providing any further guidance.

### 3.5 Conclusions

The idea of introducing pseudo relative permeability is to reproduce the fine scale model behaviors with the coarse scale model. The pseudo functions are usually computed by averaging fine scale flow solutions over local fine scale regions. We proposed and examined a method that required fine scale simulation runs on the sector models. Such simulations are affordable and are able to provide enough information for the calculation of effective fractional flow and total mobility at coarse scale.

The calculation of effective relative permeability at the outlet showed its effectiveness on representing the fine scale model behaviors. We follow the classic JBN analysis for fractional flow calculation but propose a novel total mobility upscaling which concerns the rescaling of the global absolute permeability values. However, for a highly heterogeneous model, calibration runs on sector models are necessary to eliminate the geologic structure or the absolute permeability upscaling impacts on the total mobility upscaling calculation.

Effectiveness of the pseudo functions is also affected by the flow patterns and well constraints. With rate control of injection wells, the effective fractional flow dominates the oil production behaviors and total mobility presents impacts on the field average pressure. Oil production performance is sensitive to the change of total mobility when the injection wells are under pressure control. With proper adjustment on the total mobility weighting factor, the generated monotonic relative permeability functions can be used as simulation input directly. The effective total mobility, considering both the fluid segregation and permeability scaling, helps reproduce the reservoir performance at coarse scale. Under different injection control mode, the impact from total mobility varies significantly. Injection wells under pressure control tend to be more sensitive to the total mobility changes.

## 4 TIGHT GAS RESERVOIR MANAGEMENT: MULTISCALE SIMULATION

### 4.1 Introduction

Tight gas reservoirs present interesting and important reservoir modeling challenges. Simulations on tight gas reservoir models are usually applied in order to: 1) design different completion options and estimate well performance and 2) evaluate infill potential by investigating well placement, spacing and economic benefits. In common with unconventional source rock plays, it is important to understand near well fracture characteristics, the coupling between well and reservoir, and local flow and pressure transients. However, as with conventional reservoirs, it is also necessary to understand the interaction between wells, their spacing, and large scale reservoir depletion.

To effectively model the fluid flow and predict reservoir performance, we have designed a complex multiscale simulation model that combines local grid refinement constructions for near well modeling, 3D adaptive grid coarsening away from wells and transmissibility upscaling to preserve reservoir heterogeneity. The multiscale simulation model has very high resolution near the fractures, high resolution for the interaction between a well, its fractures, and the reservoir, and progressively lower resolution between wells. The extreme low resolution is reached by using pillar-based adaptive gridding technique with transmissibility upscaling.

This model design is the first combination of using a novel unstructured coarsening algorithm, a traditional LGR structure and Nexus, the next generate “unstructured” simulator. Only by combining the new gridding design and effective workflow, can we achieve a performance success. We also reveal the facts that the simulation performance is disappointed when using the “structured” workflow but quite good when using “unstructured” input information. This reveals the opportunities for future performance improvements.

Tight gas reservoirs can be commercially profitable only when hydraulic fractures are applied. Previous full field studies on models integrated dynamic data have demonstrated that hydraulic fracture modeling is a key component for tight gas reservoir simulation (Frantz et al. 2005; Iwere et al. 2006). It is also crucial to couple the hydraulic fracture geometry and conductivity with the associated well for performance evaluation and further improvement (Cipolla et al. 2009; Mayerhofer et al. 2006; Vicente et al. 2002).

Existence of the hydraulic fractures in tight gas reservoirs brings numerical challenges and requires extra computational costs. Computational efficiency of simulating a hydraulically fractured tight gas reservoir model can be improved with pillar-based adaptive gridding technique (Zhou and King 2011), which can reduce the simulation cell count away from the wells while preserving reservoir connectivity. This adaptive upgridding method is designed to preserve high pay and non-pay contrast uniquely. It differs from our earlier studies of layer design algorithms. While the statistical layer design methods preserve the global heterogeneity of the reservoir models, they do not preserve local heterogeneity as does the pillar-based upgridding. Although the statistical approaches are superior to uniformly coarsened models, they are not as robust or as accurate as the current work constrained by local continuity for tight gas reservoirs. Pillar-based upgridding also utilizes an accurate property upscaling technique that simultaneously preserves the internal contrast of permeability within each sand, and the performance of wells within the model.

In this chapter, we first review the previous studies on tight gas reservoir simulation and then present the comparison of different methods representing the hydraulic fractures in tight gas reservoirs. After that, we review the fundamentals of the pillar based adaptive coarsening methodology. All of the approaches and workflows are demonstrated using a U.S. onshore tight gas sector model and a full field reservoir model. In this field

application, we compare well performance with different hydraulic fracture representation techniques, with or without pillar-based adaptive gridding techniques.

## 4.2 Literature Review

Holditch (2006) defines the tight gas sand as “a reservoir that cannot be produced at economic flow rates or recover economic volumes of natural gas unless the well is stimulated by a large hydraulic fracture treatment or produced by use of a horizontal wellbore or multilateral wellbores.” Tight gas reservoirs normally produce commercially at the very beginning and fall to low level later (Buchsteiner et al. 1993).

The overall challenges of tight gas reservoir modeling can be summarized as following:

- 1) The natural heterogeneity of tight sandstones determines that the flow properties are barely making the pay cut-offs. The pay and non-pay connections result in very poor gas productions from relatively large volumes of rock. From a modeling point of view, conventional upscaling and upgridding techniques may fail because they basically force too much reservoir volume connectivity.
- 2) Interactions between hydraulic fractures and natural fractures are complicated to represent and simulate. It is difficult to effectively representing hydraulic fractures for a large number of horizontal wells with large numbers of multistage fractures.
- 3) The well spacing becomes tighter as the infill drillings are performed. The increased well number in the full field simulation requires longer simulation time and extra computational expense. Hydraulic fracturing and infill drilling into a partially depleted reservoir is complex because the non-uniform stress state caused depletion.

### 4.2.1 Hydraulic Fracture Representation

Massive hydraulic fracturing brings lots of issues for numerical simulations of tight gas reservoir models. One challenging question is how to represent the fractures in the

simulations models so that the full field performance can be reproduced effectively. Different methods and techniques have been studied and compared in the past years for representing hydraulic fractures in a practical way.

One direct and simple representation of hydraulic fractures is to use the negative skin factor which was introduced in early 1980's (Cinco-Ley and Samaniego-V. 1981). It is based on the bilinear flow theory and finite conductivity fractures. This method treats the fractures as negative skin factors without taking care of fracture orientations or the interactions between different fractures. It was proved that the method works better if the fracture length is comparable to the simulation cell size. Curves showing the total effective wellbore radius (Chen and Raghavan 1997) were introduced and later further developed by Ozkan et al. (2011). The total effective wellbore radius can be used in the well productivity equation.

Combining the equation and the curves, Ozkan et al. (2011) pointed out that the optimization of fracture number can be successfully done, in long-term performances of multiple fractured horizontal wells, so long as the hydraulic fractures are small compared to the simulation cells size.

Well index (WI) modification based on the local (default) properties can be used. However, the transmissibility field should be updated based on the border region concept (Rai and Chaudhri 2009). This method has the advantage of preserving the local well productivity and the connectivity in an extended area. As with the use of skin, this is a steady state treatment and does not capture transients.

3D local grid refinement (LGR) is able to preserve the detailed flow behavior in the near-well region and to maintain the complex interactions between well-to-well, well-to-fracture, fracture-to-matrix and etc. However, LGRs bring extra cost for simulation runs because complicated gridding schemes are necessary to model fracture geometry. More

simulation grids are brought into the system, and cell size ratio is increased, especially at the fracture tips. Both of those problems result in numerical difficulties and increased simulation expense. Although hydraulic fractures are often treated as infinite conductivity fracture, the fracture conductivity is finite at in-situ reservoir conditions.

To avoid using LGRs in the full field model, single wells on sector models were studied with LGRs and then effective global model properties can be updated to perform the simulation without using LGRs (Iwere et al. 2006). Similarly (El-Ahmady and Wattenbarger 2004), enhanced (pseudo) permeability values are used for the grids occupied by the hydraulic fractures. Without using LGRs, hydraulic fractures can also be treated as an infinite conductivity line source (Abacioglu et al. 2009; Lefevre et al. 1993; Nghiem 1983). The fractures can be placed either at the centers of a series of grids or along the edges of the simulation grids. Each fractured cell will be given a Well Index (WI) to represent linear flow away from the fracture plane.

Unstructured grids with or without LGRs have more flexibility in representing complex fractures. High permeability cells in shapes of triangles, hexagons and other forms can be used for fractures. Major directions of cells can be adjusted according to the fracture orientation and the fracture length and geometry. Near wellbore and near fracture regions can also be realistically modeled. Local grid refinements may not be necessary for a carefully designed reservoir model. Unstructured grid generation (UGG) techniques generally entail three steps: grid point insertion, triangulation and construction of the simulation grids. PEBI grid is normally applied for complex but flexible numerical modeling. The unstructured perpendicular-bisector (PEBI) grids were developed by Heinemann (1994); Heinemann et al. (1991). This development is based on the success of structured flow-based gridding (Durlafsky et al. 1996; Verma and Aziz 1997), which aimed at preserving fine grid flow information in an unstructured coarse grid. PEBI gridding techniques can also link well testing with reservoir simulation and provide a more efficient workflow in modeling unconventional gas reservoirs with



multistage hydraulic fractures (Deng et al. 2011). Using 2.5D PEBI grids around the wells and fractures has several advantages: it allows sufficient resolutions between wells and fractures and avoids grid non-orthogonality issues by aligning the grid with the fracture geometry. A complex numerical model based on Computational Fluid Dynamics (CFD) was built by Belhaj and Mnejja (2011) to explicitly represent the fractures. Their discrete fracture model was implemented using a mixed finite element method. A flexible algorithm was introduced by Yadecuri & Mahani (2009) to generate the unstructured coarse grid on the fine background grid which stores grid point spacing parameter. The spacing is described by Poisson's equation, and local density of grid points is controlled by a variable source term. This source term is based on different grid point density indicators such as permeability variations, fluid velocity or their combination.

#### 4.2.2 Well Spacing Design and Infill Drilling Potentials

Unlike conventional reservoirs, both well scale and field scale contribute to the economic success in an unconventional reservoir. Traditionally the decisions on infill completions are made based on expensive trial and error procedures, and optimal well spacing and patterns are decided by statistical drilling approach. Optimization of drilling and completion design can be done with a single well model, ignoring the inter-well interference, and more complex geological model can be built to evaluate infill well locations, spacing and patterns and areal depletion plans (Gallego 2011).

In the past years, several statistical techniques have been developed to estimate the potential of an infill well. Cipolla and Wood (1996) presented an algorithm which uses a limited single-well reservoir model to predict infill-drilling potential in a tight gas reservoir. They developed a distribution of ultimate recovery and drainage areas to estimate incremental reserves. This technique was validated with the Ozona gas field. The statistical drainage area and estimated ultimate recovery data were combined to

estimate the potential reserve growth with 40-acre development. Guan et al. (2002) used a statistical moving window technique to evaluate infill candidates. The moving window method has been used in tight gas reservoirs to evaluate the infill well potential. This method can predict the infill well potential by using production data and comparing it with the result from reservoir simulation. According to their analysis, for individual wells, the results of moving window infill prediction can be off more than 50%, but it can accurately predict the combined production from a group of infill candidates. The accuracy of this technique increases with the number of wells in the analysis and decreases as reservoir becomes more heterogeneous. Gao and McVay (2004) further improved their method by using a new simulation-based inversion approach for rapid assessment of infill well potential. Instead of focusing on the small scale high resolution problems, they worked on large-scale coarse-resolution studies. In the application, well locations, production data and approximate reservoir description were used to evaluate the infill drilling potential locations quickly. The accuracy of this method increases with reservoir characterization effort. The new approach was demonstrated to be more accurate than the moving window statistical method. In general, the proposed methods use simulation as a basis, and do not rely only on production data. The methods may be more accurate but not very practical because most operators rarely use flow simulation to determine in fill potential.

Luo and Kelkar (2010) proposed a method that determines incremental versus accelerations by using the production data. They determine an appropriate time function to get linear relationship with cumulative production thus evaluating acceleration and incremental contributions for infill wells.

## 4.3 Hydraulic Fracture Representation

### 4.3.1 Introduction

To precisely model the gas flow in tight gas reservoirs which have hydraulically fractured wells, the fractures can be explicitly represented with global grid refinements. However, the explicit model increases the number of grid cells significantly and increases the CPU requirements. Therefore, it is impractical to use fine grids to simulate full field models, despite significant increase in the computer power in the past decades.

In this section, multiple methods of hydraulic fractures modeling are presented and compared. We first review the approaches of using effective permeability and modified transmissibilities, then introduce the infinite conductivity method and finally discuss the local grid refinement methods with pillar based upgridding techniques.

### 4.3.2 Effective Permeability

The original idea of using effective permeability was proposed by Elahmady and Wattenbarger (2006) and Iwere et al. (2006). Figure 4-1 shows an example of a hydraulic fracture passing through four original cells and is placed at the center of the cells. Equation 4-1 and 4-2 present the pseudo permeability in the x-direction (direction along the fracture) and in the y-direction (direction perpendicular to the fracture) respectively in the original scale.

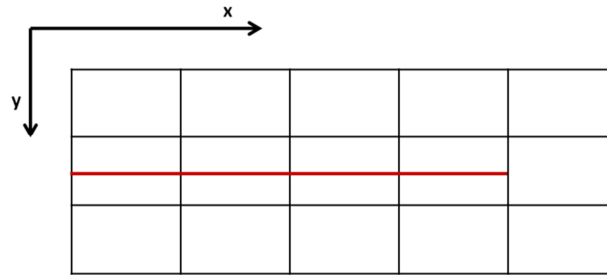


Figure 4-1 Illustration of hydraulic fracture through original simulation grids

$$\tilde{k}_x = \frac{k(\Delta y - w) + k_f w}{\Delta y} \approx k + \frac{k_f w}{\Delta y} \quad 4-1$$

$$\tilde{k}_y = \frac{\Delta y}{\left[ \frac{w}{k_f} + \frac{\Delta y}{k} - \frac{w}{k} \right]} \approx k \quad 4-2$$

$\tilde{k}_x$  is pseudo permeability in x direction

$\tilde{k}_y$  is pseudo permeability in y direction

$\Delta x$  is cell length in x direction

$\Delta y$  is cell width in y direction

$k$  is permeability

$k_f$  is fracture permeability

The calculated effective permeability (pseudo-permeability) is used to replace the original cell permeability in the geologic model. This method restricts the fracture penetrating the entire cell without any truncation.

#### 4.3.3 Enhanced Transmissibility

Similar to the effective permeability approximation, adjusted transmissibilities can be applied to the original or coarse model to represent the cells with hydraulic fractures. El-

Ahmady and Wattenbarger used the pseudo permeability values derived in the previous section to calculate the transmissibilities.

$$Transx = \frac{\tilde{k}_x}{k} \quad 4-3$$

They also derived the transmissibility for a cell in which the hydraulic fracture did not extend to the end of that cell, using the following equation.

$$Transx = \frac{\tilde{k}_x \Delta x}{k \left[ \frac{\Delta x}{2} + a \right] + \tilde{k}_x \left[ \frac{\Delta x}{2} - a \right]} \quad 4-4$$

Here,

$Transx$  is pseudo transmissibility in x direction

“a” is the distance that the hydraulic fracture extends in either direction from the edge of the cell, as seen in Figure 4-2.

The value of “a” can be either positive or negative.

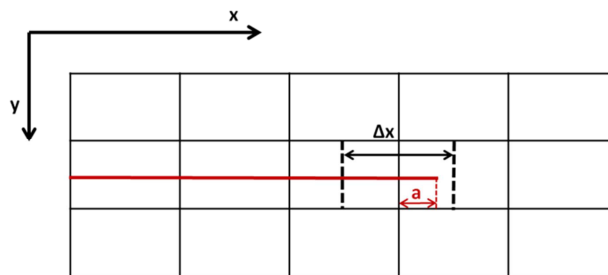


**Figure 4-2 Illustration of hydraulic fracture through partial cells**

The transmissibility modification should be applied to the direction that along the fractures only.

#### 4.3.4 Infinite Conductivity Model

Hydraulic fractures can be treated as an infinite-conductivity line source that happens to coincide with the center or edge of the simulation grids, as seen in Figure 4-3. This is the method used and described in our benchmarking studies.

The concept of infinite conductivity line source was presented by Nghiem (1983) and later extended (Abacioglu et al. 2009; Lefevre et al. 1993). Fractures are treated as infinite conductivity line source lying at the centers of the grid blocks. This will help to rebuild the elliptical drainage patterns corresponding to the hydraulic fractures. The pressure in the infinite-conductivity fracture is assumed to be uniform and equal to the bottomhole flowing pressure.

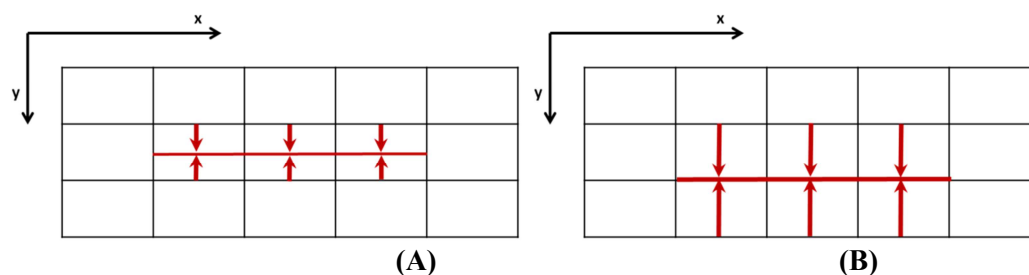


**Figure 4-3 Illustration of infinite-conductivity line source on (A) cell centers (B) cell edges**

To simplify the problem, the fracture length is considered to exclude partial penetration of cells. In other words, the fracture covers only a series of connected cells. Each of the

simulation cell attached to the fractures is treated as a perforated cell. A simulation WI will be assigned to each such cell. As shown in Figure 4-3, we assume linear flow represents the fracture flow. Therefore, as described by Abacioglu et al. (2009), the vertical wells are not treated as a well with a unique location but as a combination of individually perforated cells. Similarly, the horizontal wells with multistage of fractures were treated as several groups of perforated cells at different locations.

The modifications needed to model linear flow in the well blocks were made to the Peaceman equation for radial inflow. Equation 4-5 and Equation 4-6 show the radial flow and linear flow in a single layer from the center of a single cell to the edge of the grid block.

$$q = 0.00708 \frac{kh(P_b - P_{wf})}{\mu B \ln\left(\frac{r_b}{r_w}\right) + s} \quad 4-5$$

$$q = 0.001127 \frac{kh\Delta x(P_b - P_{wf})}{\mu B \left(\frac{\Delta x}{2}\right)} \quad 4-6$$

Here:

k is average of the directional  $k_x$  and  $k_y$  permeability values in the well block

b is the “equivalent radius” or “Peaceman radius” of the well block

s is the skin factor

$\Delta x$  is the grid block length along the direction of the fracture

$\Delta y$  is the grid block length in the direction perpendicular to the fracture

From equation 4-6, the well index (WI) can be easily calculated and imported to the simulator, for multiple cells intersected by the fractures.

#### 4.3.5 Local Grid Refinement

To reveal the detailed flow behavior in the narrow fracture regions and to show the interactions between fractures and matrix, 3D local grid refinements can be applied to the relatively coarse cell models. Near fracture regions are refined with smaller cells, hydraulic fracture orientations are taken into consideration, and cell properties are also modified corresponding to the fracture information.

Figure 4-4 shows a typical LGR distribution of a horizontal well with 8 stages of hydraulic fractures. Fractures are reconstructed with LGRs but not the wellbore. The general idea is that the major production for a typical tight gas reservoir comes from the fractures only. Therefore, there is no need to model the wellbore with extra grid blocks. Logarithmic distributions of the grids can relatively reduce the cell number, compared to the uniform distribution. However, the simulation cell width is usually bigger than the actual fracture width and the fracture permeability needs to be recalculated to have the correct fracture conductivity.

It is well known that LGR brings extra cost of simulation time because complex gridding schemes are necessary to model the fracture geometry. Increased model grid number and cell size contrasts at the fracture regions will result in numerical difficulties and extended simulation expense. In the next section, we will discuss the method of improving the simulation efficiency of the reservoir models with LGR by introducing a multiscale simulation model. The multiscale simulation model has very high resolution near the fractures, high resolution for the interaction between a well, its fractures, and the reservoir, and progressively lower resolution between wells. Combining with the unique pillar-based upgridding techniques, the multiscale simulation model has considerably improved computational efficiency.

Different static and dynamic LGR methods were investigated to keep a balance of the gridding efficiency and capability of capturing the detailed flow behaviors through the



run times. In our discussion, the topic will be restricted to static LGR for structured simulation grids.

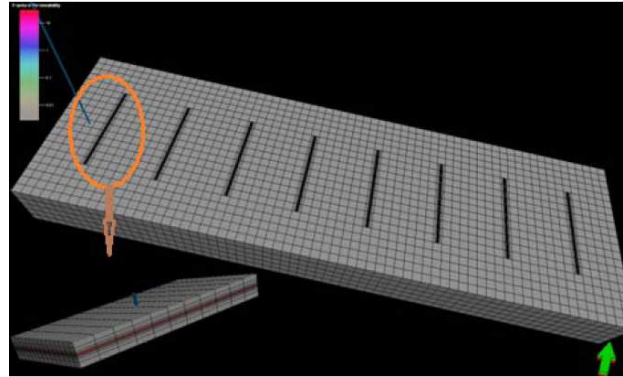


**Figure 4-4 Sample of local grid refinement**

However, the actual fractures show much more complicated structures. Those structures include both vertical and horizontal wells with multiple-stages of fractures. The interactions between fractures should be taken care of. Figure 4-5 shows a typical sector model containing three wells with fractures. This sector model has a size of 10x10x329. Well (A) is a vertical well with hydraulic fractures covering four cells which penetrate the entire reservoir model. Well (B) is a horizontal well with three stages of fractures and partially through the model from 1 to 85 layer. The third well (C) is also a vertical well penetrating the entire reservoir and it is overlapped with the second stage of the fracture of the well (C). A nested fracture is used to represent the interference from well (B) and (C). Only carefully designed LGR is able to handle such a complex geometric structure and correctly model the flow behaviors at different scales.

All of the grids shown have been developed for this project. LGRs are placed according to the well trajectories and fracture spacing. Fracture extent is specified by the user, and typically constrained to fully fracture one or more geologic units. The initial grid is

typically fairly, regular. The grid and properties are obtained directly from a 3D geologic model.

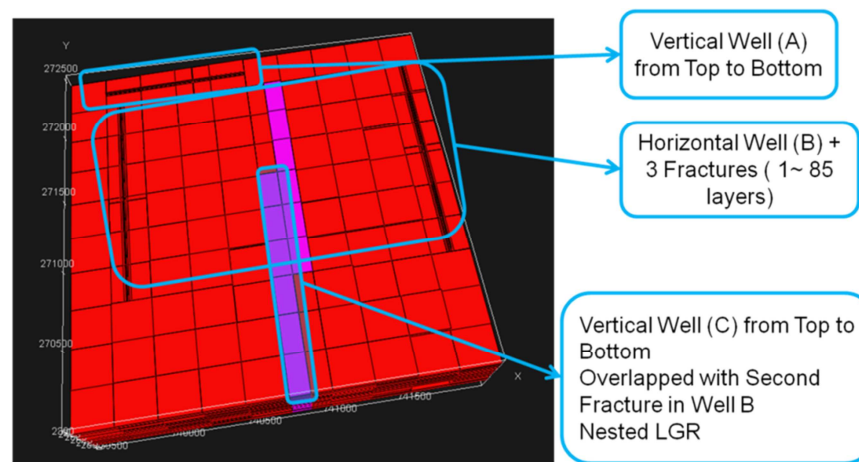


**Figure 4-5 Typical hydraulic fracture distribution**

## 4.4 Pillar Based Upscaling

### 4.4.1 Introduction

For a conventional reservoir, the entire reservoir can be replaced by a single coarse cell at the end of an upgridding calculation. We may have large scale pressure equilibrium, and at late times we can build simplified reservoir models based solely upon mass balance.

However, the tight gas reservoirs have extremely low permeability and the pressure transient period of time is dominant during the majority of reservoir production. Pressure transient studies can help to determine the duration of various flow regimes imposed by fractures and shows the elongated transient flow may lead to accelerated production. The drainage area maybe limited to the near well regions, and the reservoir boundary may never be reached during the production periods. Or, there may be sufficient permeability that the pressure equilibrium can be reached after months or years, but by passing undepleted sands.

Different from the conventional gas reservoir, tight gas reservoirs have complex non-pay structures which present more restrictions for commercial production. It is very often that hydraulic fractures are required so that the well can produce with commercial benefit. A tight gas reservoir may have intermittent thin sand continuity, with distinctive flow behaviors at different simulation scales.

Similar to the layer design algorithm, the ultimate goal of the adaptive pillar-based gridding approach is to preserve the necessary heterogeneity of the fine scale model while improving the computational efficiency at the same time. Therefore, in this research, error analysis is crucial to identify the key error source thus helping build up reliable coarse simulation grid which minimizes residual errors. The upscaling technique

applied in our algorithm is distinctive. The approach was originally designed by Zhou and King (2011), is an extension of that presented by King et al. (1998) and King (2007). There is no need for upscaled permeability to show at the same time in the process of the different transport coefficient calculations, such as well index, transmissibility and fault connection transmissibilities. Unlike other unstructured gridding algorithms, the pillar-based upscaling is immediately applicable to any existing structured model for any further coarsening, well performance prediction and infill potential evaluation.

The following section focuses on the explanation of the pillar based upscaling and error analysis with a sector model demonstration. The field application will be presented at the end of this chapter.

#### 4.4.2 Methodology

##### 4.4.2.1 Pillar Based Upgridding

Tight gas reservoirs present unique structures showing the pay zone on a non-pay background and intermittent connectivity existing within the thin fluvial sands. This section presents the fundamental ideas of the  $1 \times 1 \times N$  pillar-based upgridding technique, which is suitable for tight gas reservoirs.

This upgridding is distinct from the earlier layer design algorithms because it never merges pay and non-pay cells together. For tight gas reservoirs, if the pay and non-pay cells are merged, it is possible to amalgamate two distinct thin fluvial channels, in which the pressure equilibrium may not be reached during reservoir production. Figure 4-6 presents a clear illustration of pillar based ( $1 \times 1 \times N$ ) upgridding. The original cross-section contains 16 pay cells, shown in white, and 6 inactive cells colored in gray. After coarsening the pay and non-pay cells separately, this model has only 6 active coarse cells left. This algorithm reduces the total active cell count but also creates non-neighbor connections for the merged pay cells.

This 1x1xN upgridding results in a different number of “N” reservoir and in different locations. For any channel structures, this “N” should be restricted within the channels, resulting in coarsened structures that follow the local geology. More aggressive combinations could result in one coarse cell penetrating the entire geologic model. The current method is conservative in that district channels are not merged vertically. After applying the pillar based upgridding, the simulation grids are regenerated without preserving a layer, and structure should be treated as an unstructured numerical problem.

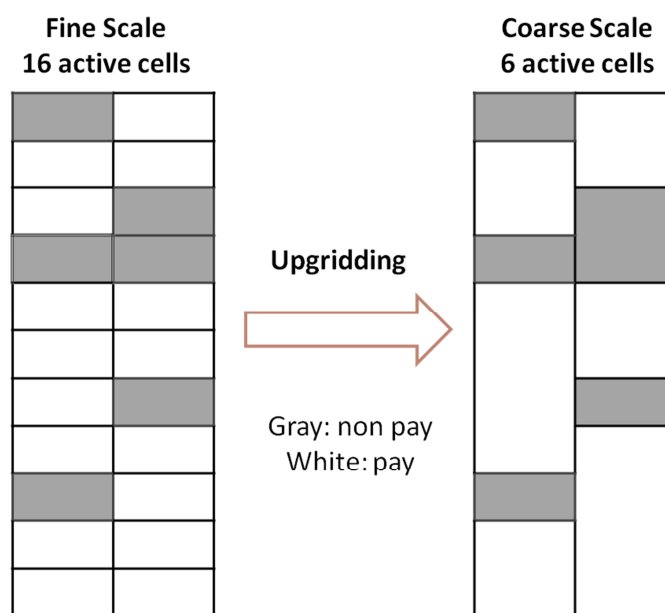


**Figure 4-6 Illustration of pillar based upgridding**

The fundamental assumption of the upgridding approach is that pressure equilibrium can be reached within a coarsened cell in a period that less than, or at least comparable to the simulation time step. However, the coarsened cells cannot always reach the pressure equilibrium fast enough. Therefore, in actuality, some of the “pay” cells should be redefined as “barrier” cells. Pressure transient diffusive time can be used to the pay cells,

as seen in Equation 4-7 for the horizontal direction and Equation 4-8 for the vertical direction. The histogram of the diffusive time can be seen in Figure 4-7. The aspect ratio effect dominates: most pressure equilibrium can be reached in about 5 hours in the vertical direction but will take up to several years ( $10^5$  hours) in the horizontal direction. The major source of error in tight gas reservoir upgridding is the disconnected pay within the coarse cell that cannot reach equilibrium. Pillar based upgridding focuses on the vertical combination in which direction the pressure equilibrium is reached within one simulation time step.

$$dt_x = \frac{1896\phi\mu c_t}{k_x} \cdot DX^2 (\text{hours}) \quad 4-7$$

$$dt_z = \frac{1896\phi\mu c_t}{k_z} \cdot DZ^2 (\text{hours}) \quad 4-8$$

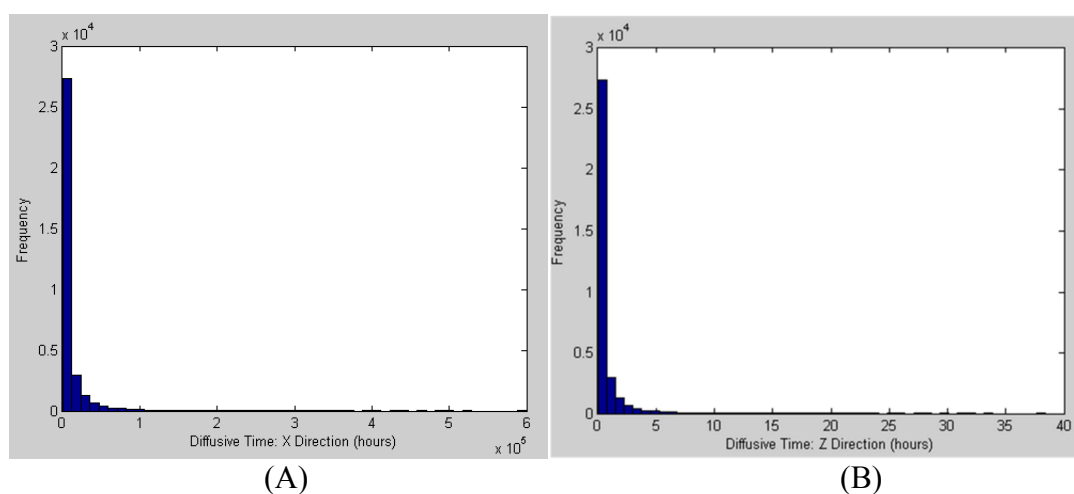


**Figure 4-7 Diffusive time in (A) horizontal direction (B) Vertical direction.**

In our workflow, the initial full field reservoir model is provided in RMS<sup>TM</sup> (Reservoir Modeling System) 2011. The RMS Internal Programming Language (IPL) program is used to extract fine scale properties and calculate inter-cell transmissibilities and well indices. The IPL upscaling code then creates coarse versions of these same properties.

The simulation files required by the Nexus simulator (Nexus 5000.4.1, 2010) are exported for the coarse simulation runs. Nexus shows its advantage of handling the non-neighbor transmissibilities compared to other commercial simulators. Along with the fine scale grid, the “COARSEN” matrix defines the coarsened grids in the simulator and “FTRANS” provides the transmissibility multipliers. For 1x1xN upscaling, horizontal permeabilities are upscaled using an arithmetic average. Transmissibilities are then calculated from the harmonic average, reproducing the upper bound of Cardwell and Parsons (1945). Detailed discussion why we use transmissibility upscaling instead of permeability upscaling will be reviewed in the next section. Specific issues on the use of Nexus, Landmark’s next generation unstructured reservoir simulator, will also be discussed.

In short, the local continuity of the reservoir sands in the geologic model is preserved in a 1x1xN coarsened grid. The number “N” varies depending upon the local sand thickness. The heterogeneity within each sand is preserved through the use of transmissibility upscaling. Case studies on a sector model and a full field model are reviewed at the end of this section.

#### 4.4.2.2 Error Analysis and Upscaling

In this section, we briefly discuss the error and biases introduced while upscaling (Christie et al. 1995; Durlofsky 1991; Farmer 2002; Renard and de Marsily 1997) and explore the reasons why we use transmissibility upscaling for tight gas reservoir.

The permeability upscaling and transmissibility upscaling have totally different ways of handling the cell connections. The horizontal permeabilities will be the net rock volume weighted arithmetic averages of the fine scale permeability within each column. The summation of the total flux between any two columns depends upon the summation of the inter-cell transmissibilities which are calculated by the harmonic average of the cell permeabilities. The transmissibility upscaling is the arithmetic average of the harmonic

average of the fine permeabilities. As proven by Cardwell and Parsons (1945), this is a rigorous upper bound on the effective permeability of the original system. Here, we describe a synthetic example, shown as Figure 4-8, to demonstrate how the conventional permeability upscaling systematically overestimate horizontal flow capacity of a heterogeneous system, leading to too much lateral connectivity within an upscaled model.

The permeability shown in red represents a permeability of 100 md and the purple cells have a permeability of 0 md. Performing a 2x4 permeability upscaling will have a 50 md permeability in each coarsened cell. The inter-cell transmissibility would not be 0. However, if we perform the transmissibility upscaling, we will calculate the flow between the cell centers, which should be 0, except at the fault regions. It is clear that the transmissibility upscaling does a better job of preserving the lateral heterogeneity. Although this is an extreme case, it does demonstrate a systematic bias that is introduced when permeability upscaling is used.

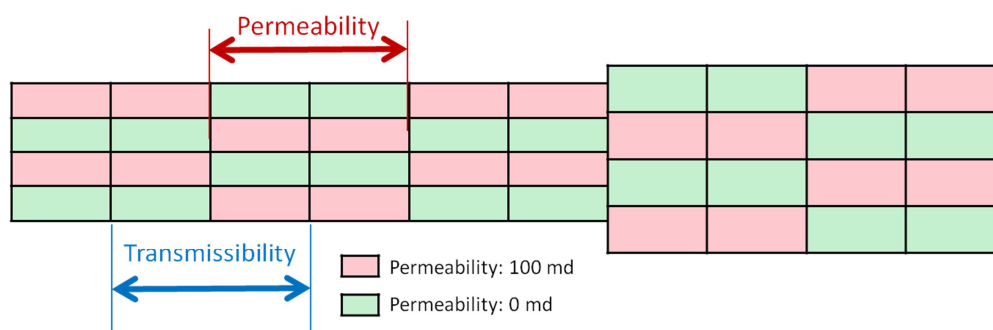


**Figure 4-8 2x4 Upscaling: Transmissibility vs. Permeability**



## 4.5 Tight Gas Reservoir Description

The field case is a high resolution 3D geologic model of a U.S. offshore tight gas reservoir. The matrix net-to-gross ratio is shown in Figure 4-9(A), and the permeability distribution is presented in Figure 4-9(B). This model contains five geologic units to represent stratigraphic variations in thin fluvial channel dimensions and sand properties. The model size is 100x100x329, and it contains 3,290,000 cells in total. The cells are roughly 250 feet in width and length and are approximately 2 feet in thickness. The areal grid is uniform while the vertical grid is stratigraphic. The model has been built with proportional layering within each zone, and it has no faults. Neither pinch-out nor non-standard connections on the fine scale need to be considered in this study.

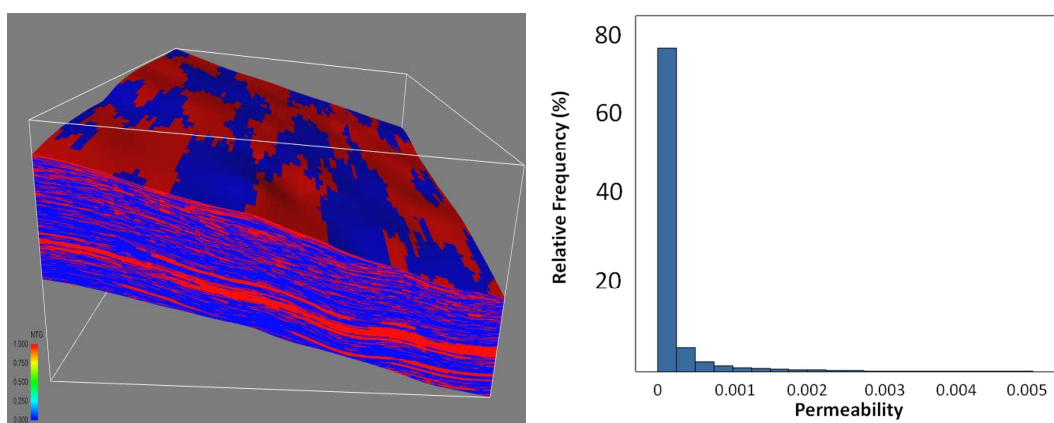


**Figure 4-9 Geologic model for Wamsutter tight gas reservoir (A) NTG (B) permeability distribution**

### 4.5.1 Multiscale Modeling Results

One of the objectives is to validate the multiscale simulation modeling which combines LGRs and pillar based upscaling. This simulation model was built with 11 wells, including both vertical and horizontal wells with multistage hydraulic fractures. The

reservoir grid and distribution of the fractures are presented in Figure 4-10. Vertical fractures penetrate the whole geologic model and the horizontal wells are restricted within certain zones. Figure 4-11 shows a cross-sectional view of the pore volume of the hydraulic fractures in the multiscale reservoir model. The fractured wells are represented with non-uniformly distributed LGRs in both the x and y directions. The near fracture regions are preserved as transition zones in the original resolution of the grid. For all other cells away from the fracture locations, pillar based coarsening algorithm is applied. Various cell pore volumes for the coarsened cells can be observed in Figure 4-11. Except in the near fracture region, there are no layers left in the model. Pay and non-pay cells are connected separately to preserve the vertical continuity and transmissibility upscaling is applied to the coarsened model.

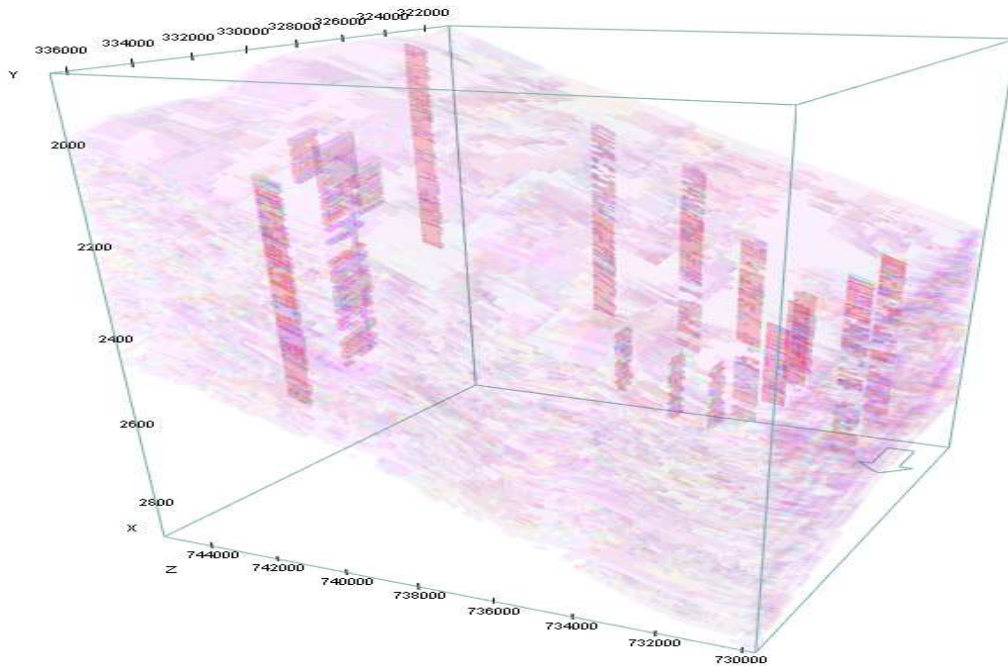


**Figure 4-10 Fracture distributions and cross-section of upscaled models**

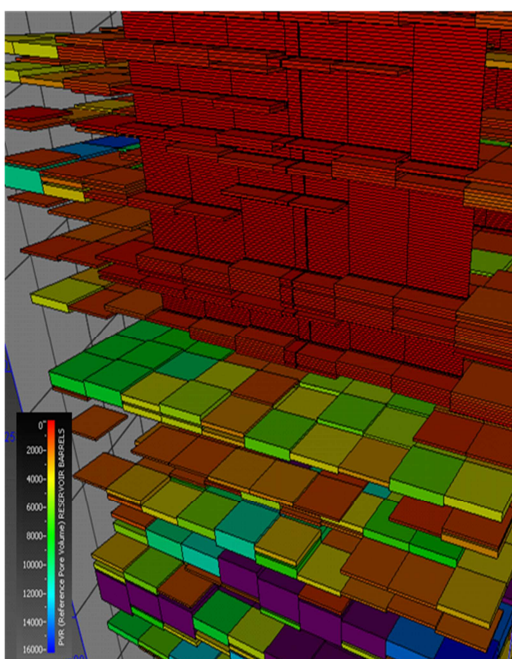


**Figure 4-11 Cross-section view of the fracture representation in a multiscale model**

The simulation results are presented in Figure 4-12. It benchmarks the results from different hydraulic fracture representations, e.g., enhanced permeability, infinite line-source with well index adjustment and the LGRs with pillar coarsening with/without transmissibility multiplier. The reference model is defined as the one utilizing LGR to represent the fractures but no application of any coarsening/upscaling techniques. All simulation runs are performed by Nexus, which is an unstructured simulator. In Figure 4-12, red columns represent the cumulative of the gas production in a range of 8000 days. The reference simulation is labeled as “LGR”. “LGR+Coarse” represents the case applying LGR and pillar based upgridding without transmissibility upscaling. “LGR+Coarse+FTRANS” shows the case including transmissibility. The transmissibility upscaling is processed by submitting the “FTRANS” keyword to Nexus in the RECURRENT section. The “FTRANS” keyword provides transmissibility values for all the non-neighbor connected coarse cells. This keyword can also be used in the GRID section, and the simulation result is labeled as “LGR+Coarse+FTRANS @grid”. The pseudo permeability method is chosen for comparison and is labeled as “Pseudo K”.

“Pseudo K+Coarse” and the “Pseudo K+Coarse+FTRANS” cases apply pillar based upgridding with and without transmissibility upscaling in the RECURRENT section. The line source method is chosen for comparison and is labeled as “LS”. “LS+Coarse” and “LS+Coarse+FTRANS” label cases applying pillar based upgridding with and without transmissibility upscaling in the RECURRENT section. Blue columns represent the computational time for each simulation run. Green columns show the peak gas production rates which occur at the beginning of the production period.

The multiscale modeling with transmissibility upscaling showed the best production match. The mismatch is only 0.9% after 8000 days. Without using the transmissibility upscaling, “LGR+Coarse” shows an increased mismatch of 8.5%, which is similar to the results from the model applying transmissibility upscaling at grid definition section. Transmissibility upscaling provides more accurate simulation results but also requires extra computer costs. It also implies that the “FTRANS” keyword did not affect the simulation runs when it is applied in the GRID section. Both pseudo permeability and line source methods show a higher degree of mismatch in terms of gas production. The pseudo permeability method provides better prediction than the Linear Source (LS) treatment in this specific case study. LS method results in up to 22.8% mismatch when coarsening is applied. Applying the pillar based upgridding method reduces the computational time but also leads to extra simulation errors. Transmissibility upscaling compensates the errors introduced by the property upscaling within the simulation, although it demands more simulation time.

The simulation cost for each case is also presented in Figure 4-12 as the blue columns. Without applying the transmissibility upscaling, the coarse model has a production performance that is close to the reference and shows a large reduction of computer time (~42.9%). Applying transmissibility modifications requires more simulation time. One reason is that the pillar-based upscaling breaks the traditional layers and regenerates lots of non-neighbor connections. Nexus calculates transmissibilities for the coarsened grid

cells first and then calculates the permeabilities. The simulator takes relatively longer time processing the transmissibility multipliers assigned for those unstructured grids. Another possible reason for such a situation is a known issue of the Nexus simulator that it cannot process the “FTRANS” keyword correctly in the GRID section. The evidence can be found in the Figure 4-12 that the multiscale model with transmissibility upscaling keyword processed in the “GRID” section does not provide any corrections on simulations. The transmissibility multipliers provided in the RECURRENT section will be processed each time step and therefore leads to increased simulation time.

The peak gas production of each case is presented as green columns in Figure 4-12. The peak production of the reference case can be reproduced with local grid refinements only, though the peak rate decreases rapidly. As expected, the effective permeability and line source treatments fail to model the flow behaviors accurately at the beginning. They show less than 1% of the peak gas production, although the long term production prediction is close to the reference.

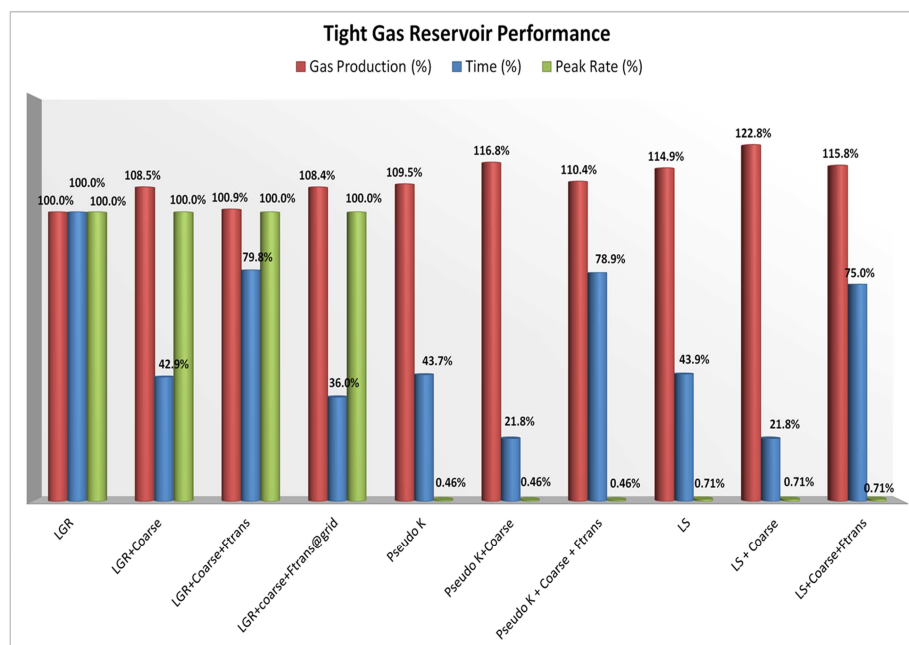


**Figure 4-12 Benchmarking of model simulation prediction from different algorithms**

In the long term simulation of 8000 days, the pseudo methods show a close match to the overall oil production prediction. The initial peak rate has only a limited effect since it lasts only short period of time. Figure 4-13 shows the gas production at 10 years for the same well arrangements. The transient behavior now shows a significantly greater effect. Only with LGR and transmissibility multipliers, can the coarsened model reproduce the fine scale simulation results with a small mismatch. All other simulation runs with pseudo methods overestimate production compared to the simulations at 8000 days. The pseudo methods fail to mimic the transient behaviors but show acceptable overall reservoir performance for a 22 year (8000 days) field life.

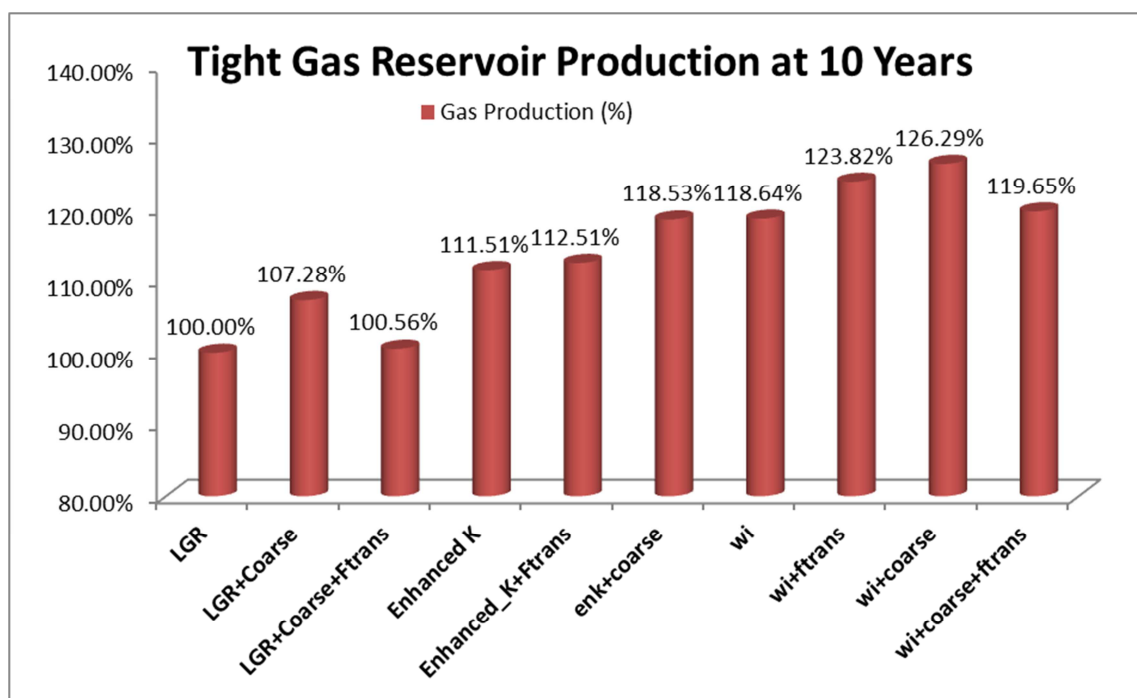


**Figure 4-13 Benchmarking of model simulation prediction from different algorithms at 10 years**

To verify the algorithm effectiveness, we benchmarked simulation results (Figure 4-14) with Eclipse runs, which have the same well arrangement. Figure 4-14 presents the gas production rate and the cumulative gas production in a range of 8000 days for both the reference model and the coarse model. The coarse model contains LGR and pillar-based upgridding grids. However, no transmissibility multipliers are applied in the coarsened model, indicating that Eclipse is performing transmissibility based upscaling internally. The benchmarking presents improved production match using Eclipse. However, the overall simulation time was largely increased. Nexus finished fine scale simulation in around 4 hours, and Eclipse took 18 hours for the same model. Although the coarse model saved 40% of the CPU time, Eclipse run still took more than 11 hours to finish.

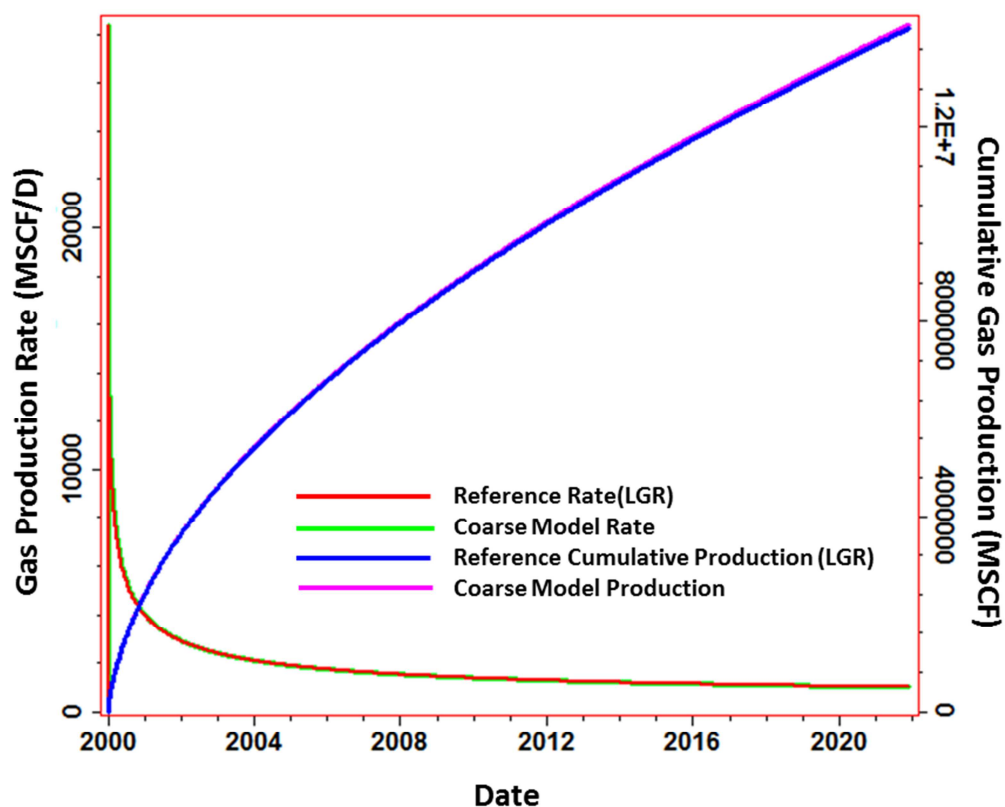


**Figure 4-14 Benchmarking of model simulation prediction using ECLIPSE**

The tight gas reservoir model is modified in such a way that all the LGRs are removed, and we use the modified tight gas model to test the simulator performance. Figure 4-15 shows the field prediction performance from different simulators. Nexus, as next generation simulator, has two different workflows: structured and unstructured. We use the unstructured workflow as the reference to compare the simulation production and the CPU time for the tight gas reservoir model performance. All the fine scale runs from Nexus and Eclipse have an agreement on the cumulative gas production. However, using Eclipse takes more than 4 times of the Nexus runs. Interestingly, using structured workflow in Nexus on the fine scale model also leads to extra 10.7% of the CPU time. Comparing the coarse model performances, Eclipse provides the best estimation. The coarse scale simulation on Eclipse is more computationally expensive compared to the



fine scale Nexus runs. Unstructured Nexus coarse model presents the fastest simulation run, which is 25.9% of the reference time. The Nexus simulator is clearly optimized for unstructured simulations. However, Nexus does not support LGRs in an unstructured workflow. Therefore, the application of the unstructured simulator is limited.

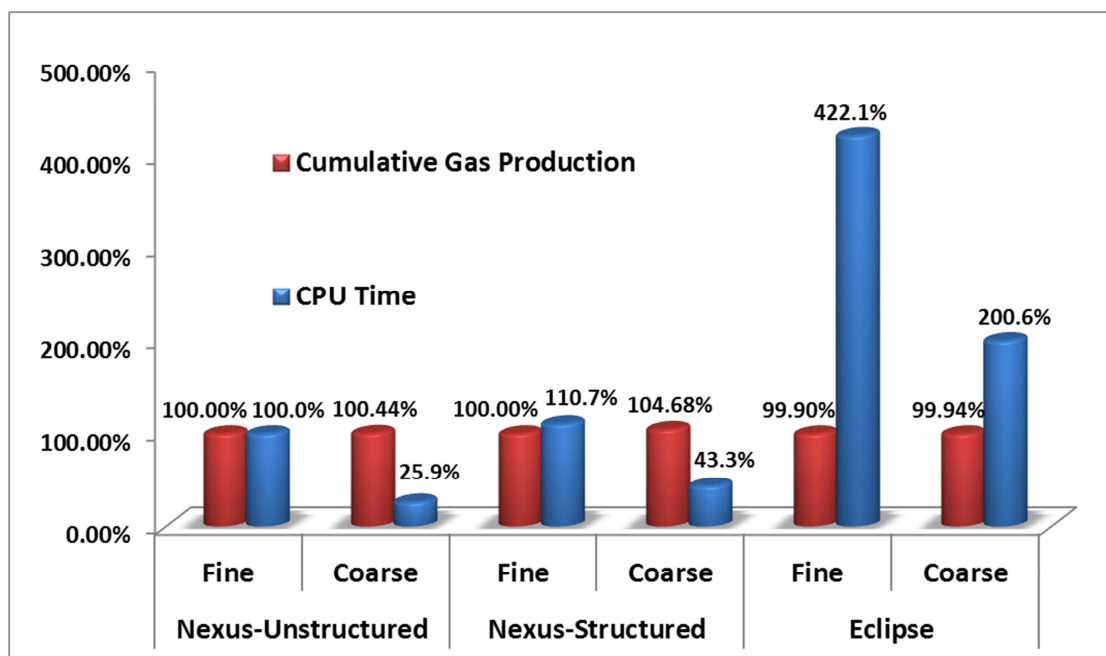


Figure 4-15 Benchmarking of different simulator performance

#### 4.5.2 Discussions

Tight gas reservoir models present lots of numerical challenges because of their unique pay and non-pay structures, complicated well management scenarios and existence of the hydraulic fractures. Explicit modeling of the hydraulic fractures with local grid refinements for the full field models were considered as an effective but computationally expensive method. Many methods had been proposed to improve the simulation accuracy while maintaining the computational efficiency.

#### 4.5.2.1 Hydraulic Fractures

Different implicit hydraulic fracture representation methods have been tested and are proven to be effective for long term production prediction. Using the implicit modeling methods has one substantial advantage that it does not require a large amount of simulation cells. Therefore, the simulation time is reduced, compared to the explicit modeling of the fractures, especially for a field model with a large number of wells. For a model showing a short period of the transient time, those implicit methods are able to reproduce the overall reservoir productions in a long term. However, none of the pseudo methods are able to capture the transient behaviors. The drainage patterns may also be misrepresented. Explicitly modeling of fractures with LGRs can reveal the detailed flow behaviors, though the subdividing of the grids demands extra computational time. To reduce the overall simulation grids and the total simulation time, we applied grid coarsening methods in the non-fracturing regions. Combining both the pillar-based upgridding and LGRs, a multiscale simulation model can reproduce the fine scale simulation runs perfectly. This method requires a transmissibility upscaling for further accuracy improvements. A combination of pillar based coarsening and transmissibility upscaling was proven to be effective in the tight gas reservoir simulation, especially when lots of non-standard connections are created during the coarsening procedures.

#### 4.5.2.2 Transmissibility Upscaling

By Nexus simulator default, the half transmissibilities of the coarse block are calculated from those of the constituent fine blocks, but the internal upscaling algorithms do not utilize intercell transmissibility. The average coarse block permeabilities that are used for calculating well, influx properties, and for other uses by Nexus are calculated from the averaged coarse block properties. As a result, the transmissibility calculation in the simulation will not preserve the non-standard connections between coarsened cells. We can improve the accuracy by preserving such non-neighbor transmissibility values. The

field response on the full field models have proven the effectiveness of transmissibility upscaling on tight gas reservoir models. However, the overriding of the transmissibility values usually takes extra computational costs.

#### 4.6 Conclusions

Tight gas reservoirs provide significant challenges due to their unique geologic descriptions (e.g., low permeability and poor connections). Massive hydraulic fractures, which are required for commercial production rates, result in considerable numerical difficulties. Local grid refinement (LGR) has proven to be the most accurate way of representing the hydraulic fractures but increases the simulation time.

We have shown how to design a complex multiscale simulation model that combines local grid refinement constructions for near well modeling, 3D adaptive grid regeneration and transmissibility upscaling for improving computational efficiency. Such a model provides as accurate a prediction of the reservoir performance as the fine scale models. As the near-well flow behavior is preserved using the LGR, the progressively lower resolution between wells can be reached using the pillar-based coarsening. The multiscale simulation model, designed specifically for tight gas reservoir, effectively reproduces the original fine scale reservoir performance.

Pillar-based adaptive coarsening can be used for compensating the extra computational costs from introducing the LGRs. It also promises with the minimum cell count and at the same time preserving internal reservoir heterogeneity. Pillar-based coarsening breaks the concept of “layer” and generates coarsened cells preserving the internal contrast of permeability within each sand. The diffusive time analysis provides support for the pillar-based coarsening since the vertical equilibrium can be reached easily comparing the horizontal equilibrium. The extremely long diffusive time of flight in the horizontal direction also implies the limitation of areal coarsening; areal coarsening may

not be feasible in tight gas reservoir. The statistical layer design algorithm studied earlier in this thesis is not suitable for tight gas reservoir because of the overestimation of the horizontal connectivity. The overestimated continuity leads to mismatch in gas production and overall reservoir performance.

## 5 CONCLUSIONS AND FUTURE WORK

This work studies the upgridding techniques for effective layer design, multiphase pseudoization and multiscale near-well modeling in heterogeneous reservoirs. It emphasizes scale manipulation from geostatistical modeling to flow simulation. This work is important because there is always a need to preserve critical heterogeneity information and flow behaviors at different scales while maintaining high computational efficiency.

### 5.1 Summary and Conclusions

In this work, we first investigated and improved layer design algorithm based on static heterogeneity error analysis.

- 1) Sequential upgridding based on minimizing the loss of heterogeneity is used for effective layer design. Different measures of heterogeneity have different emphases on preserving the model details. The specific statistical measures provide the capability of predicting the degree of coarsening that can be performed before “damage” is done to the underlying reservoir description. Effective layer design, as a statistical analysis, provides an indicator of the strong break in the field response. This strong break indicates an upgridding limit beyond which the coarse simulation model cannot reproduce the fine scale performance without applying multiphase upscaling. “Optimal” number of the preserved layers can be estimated to better reproduce the fine scale performance and also to reduce the computational costs largely.
- 2) Lorenz coefficient provides an evaluation of the model heterogeneity in a wide distribution, and it takes care of the flow capacity and the storage capacity at the same time. Both Dykstra-Parsons coefficient and Lorenz

coefficient are traditional static measures ignoring correlations. Dykstra-Parsons coefficient concerns only the permeability distributions, is non-uniqueness and is influenced by the subjective element in drawing the “best-fit” line.

- 3) The modified “V&S” measure provides a better reservoir heterogeneity evaluation, compared to the previously developed “slowness” and “velocity” measures. It emphasizes on the time of flight and breakthrough response at the same time. “V&S” shows almost the same level of accuracy of predicting the reservoir performance as Lorenz coefficient does. Optimal layer numbers are similar for those two measures, although the combinations may vary. However, “V&S” measure has its own advantage of not sorting data and provides a fast and accurate estimation.
- 4) Compared to the flow-based upscaling algorithms, the layer design algorithm does not require any fine scale simulation run. The whole upgridding procedures can finish in tens of seconds for a reservoir model containing up to 1 million cells. The overall workflow efficiency is remarkable.
- 5) Effective layer design algorithm does not require the knowledge of typical well locations, rates or well spacing. Therefore, this method is applicable early in the appraisal process when the depletion plan is still under development.
- 6) A Petrel plug-in for effective layer design is developed as a part of the technology transfer program. This plug-in, called SWIFT, is able to build the coarse 3D model based on the high resolution model with respect to the geological markers and horizons. This plug-in utilizes the novel static measures of “V&S”.

As discussed in our study of pseudoization, there are advantages in recalibrating global permeability once a well plan has been specified. We developed novel pseudoization methods for the use of aggressively coarsened reservoir models.

- 1) The first part of the pseudoization method involves calculation of the effective fractional flow. This calculation is based on the extension of the JBN 1D analysis to 3D full field models. We introduced a model calibration method generating a base line for the complex model to eliminate the geologic structure effects on the calculation of the flows. The resulting pseudo curves appear monotonic and can be used for coarse model simulations.
- 2) The second part involves a novel total mobility upscaling which shows the global absolute permeability upscaling impact. Our effective total mobility calculation is based upon the pressure change against invers of the total water injection and its time derivative. This effective total mobility used in the coarse model shows two major impacts: 1) total segregation of water and oil and 2) the global permeability upscaling. For injection wells under rate control, the total mobility variation shows very limited effect on the oil production but a significant impact on the field pressure performance. For reservoirs under pressure control, combination of the total mobility and the relative permeability dominates the coarse scale reservoir performance. A sensitivity study on the sector model should be performed as part of the model calibration.
- 3) This pseudoization algorithm has the prediction ability because it does not require the fine scale simulations on the full field model, but only on the sector models. The sector model should contain the typical geological

structures presented in the full field model. Only one set of the pseudo relative permeability curves is used in a coarsened model. This algorithm does not provide individual curves for each of the coarsened cells. Our pseudoization method is a strong support for the layer design algorithm, especially for those models which has very limited layer numbers preserved.

In our last study, we investigated the challenges of tight gas reservoir performance predictions.

- 1) Tight gas reservoirs present unique requirements due to pay zones on a non-pay background with intermittent connectivity. A key issue of accurately simulating tight gas reservoir models is how to model the flux in the hydraulic fractures and their nearby regions successfully. Different ways have been developed to represent the hydraulic fractures with limited cells. The most accurate way utilizes LGR which largely increases the computational cost. Pillar-based structure upgridding with transmissibility upscaling shows its effectiveness on both saving the computer time and maintaining the production performance in the tight gas reservoir modeling. It is a unique coarsening algorithm which combines pay and non-pay cells separately. The cell-by-cell pressure equilibrium check guarantees the effectiveness of the pillar-base coarsening.
- 2) We have designed a complex multiscale simulation grid design that combines local grid refinement constructions for near well modeling, 3D adaptive grid regeneration for improving computational efficiency and transmissibility upscaling for preserving accuracy. The multiscale simulation model has very high resolution near the fractures, high resolution for the interaction between a well, its fractures, and the reservoir, and progressively lower resolution between wells. The multiscale model provides accurate reproduction of the



fine scale reservoir performance and improves the computational efficiency at the same time.

- 3) Different workflows can impact the simulator performance, especially for Nexus, the next generation simulators. Nexus is optimized for unstructured input workflow and can precisely reproduce the fine scale performance with considerable time saving on the coarse scale models. Nexus with the structured workflow takes extra computational cost and needs transmissibility modifications on the coarse scale models.
- 4) An Internal Programming Language (IPL) based multiscale tight gas reservoir modeling script is developed as part of the technology transfer program. This script, cooperating with Reservoir Management Systems (RMS), can be applied to any existing tight gas reservoir models directly to generate the necessary model coarsening files for Nexus. The next generation simulator, Nexus, utilizes those files for model coarsening.

## 5.2 Suggestions for Future Work

The effective layer design algorithm has focused on the development of a vertical coarsening method with no areal upscaling. Gridding and upscaling are two complimentary components in accurate coarse flow modeling. It is possible to apply areal upscaling techniques to further improve simulator efficiency and to generate further simplified simulation grids. The selection of the optimal number of layers is based on a specific heterogeneity measure. More sophisticated methods may be considered based on solving certain objective functions, which depend upon dominant flow directions (vertical or horizontal) or on reservoir processes, e.g., gas over-ride.

A novel approach to multiphase upscaling has been introduced. However, since the multiphase upscaling algorithm is a support of the effective layer design, no areal upscaling is considered. Also, no numerical dispersion effect has been discussed. The numerical dispersion problem will be of great importance when areal upscaling applies. We provide two different methods for calculating the effective total mobility. The optimal weighting factor selection requires a serial of calibration runs on the coarse scale sector models. Similar calibration simulation runs on the sector models are also necessary for selecting the permeability values at the outlet. Absolute permeability upscaling at the outlet shows significant impact on the overall coarse model performance. This algorithm utilizes data acquired from the fine scale sector model simulations for pseudo relative permeability calculations. It then applies the pseudo functions to the full field model, trying to avoid the fine scale simulation runs on the full field models. This sector model should contain enough typical geologic structures. In this study, a quarter of the fine scale model is selected. However, how to determine the optimal representative model size and where to pick such a model are still critical questions to be answered. It is also worth of expanding on use of simple parameterization for uncertainty studies, e.g., to upscale an ensemble of models.

In the tight gas reservoir study, the complex multiscale model preserves the necessary details of flow behaviors at different scales while maintaining high computational efficiency. The overall efficiency is restricted to the coarsening degree and transmissibility upscaling. Further extension of the pillar-based  $1 \times 1 \times N$  upgridding to a true 3-D adaptive upscaling will substantially reduce the computational costs. The transmissibility upscaling is taken care of by providing transmissibility multipliers to the simulator. It important to understand the workflows for specific simulators, especially as next generation simulators enter the commercial market.

## REFERENCES

- Abacioglu, Y., Sebastian, H.M., and Oluwa, J.B. 2009. Advancing Reservoir Simulation Capabilities for Tight Gas Reservoirs. Paper presented at the SPE Rocky Mountain Petroleum Technology Conference, Denver, Colorado. Society of Petroleum Engineers SPE-122793-MS. DOI: 10.2118/122793-ms.
- Ahmed, T.H. and McKinney, P.D. 2004. *Advanced Reservoir Engineering*: Publisher: Elsevier/Gulf Professional Pub. Burlington, MA, ISBN 9780750677332.
- Aziz, K. and Settari, A. 1979. *Petroleum Reservoir Simulation*. Applied Science Publishers. London. ISBN 9780853347873.
- Ballin, P.R., Journel, A.G., and Aziz, K. 1992. Prediction of Uncertainty in Reservoir Performance Forecast. *Journal of Canadian Petroleum Technology* **31** (4). DOI: 10.2118/92-04-05
- Ballin, P.R., Solano, R., Hird, K.B. et al. 2002. New Reservoir Dynamic Connectivity Measurement for Efficient Well Placement Strategy Analysis under Depletion. Paper presented at the SPE Annual Technical Conference and Exhibition, San Antonio, Texas. Copyright 2002, Society of Petroleum Engineers Inc. 00077375. DOI: 10.2118/77375-ms.
- Barker, J.W. and Dupouy, P. 1999. An Analysis of Dynamic Pseudo-Relative Permeability Methods for Oil-Water Flows. *Petroleum Geoscience* **5** (4): 385-394. DOI: 10.1144/petgeo.5.4.385
- Barker, J.W. and Thibeau, S. 1997. A Critical Review of the Use of Pseudorelative Permeabilities for Upscaling. *SPE Reservoir Engineering* **12** (2): 138-143. DOI:

10.2118/35491-pa

Belhaj, H.A. and Mnejja, M. 2011. Hydraulic Fracture Simulation of Two-Phase Flow: Discrete Fracture Modelling/Mixed Finite Element Approach. Paper presented at the SPE Reservoir Characterisation and Simulation Conference and Exhibition, Abu Dhabi, UAE. Society of Petroleum Engineers SPE-147028-MS. DOI: 10.2118/147028-ms.

Buchsteiner, H., Warpinski, N.R., and Economides, M.J. 1993. Stress-Induced Permeability Reduction in Fissured Reservoirs. Paper presented at the SPE Annual Technical Conference and Exhibition, Houston, Texas. 1993 Copyright 1993, Society of Petroleum Engineers, Inc. 00026513. DOI: 10.2118/26513-ms.

Cardwell, W.T. and Parsons, R.L. 1945. Average Permeabilities of Heterogeneous Oil Sands Transactions of the AIME, Vol. 160, 34-42

Chen, C.-C. and Raghavan, R. 1997. Computing Pressure Distributions in Wedges. *SPE Journal* **2** (1): 24-32. DOI: 10.2118/30555-pa

Chen, Y. and Durlofsky, L.J. 2007. An Ensemble Level Upscaling Approach for Efficient Estimation of Fine-Scale Production Statistics Using Coarse-Scale Simulations. Paper presented at the SPE Reservoir Simulation Symposium, Houston, Texas, U.S.A. Society of Petroleum Engineers SPE-106086-MS. DOI: 10.2118/106086-ms.

Chen, Y., Durlofsky, L.J., Gerritsen, M. et al. 2003. A Coupled Local–Global Upscaling Approach for Simulating Flow in Highly Heterogeneous Formations. *Advances in Water Resources* **26** (10): 1041-1060. DOI: 10.1016/s0309-1708(03)00101-5

- Christie, M.A. and Blunt, M.J. 2001. Tenth Spe Comparative Solution Project: A Comparison of Upscaling Techniques. *SPE Reservoir Evaluation & Engineering* **4** (4): 308-317. DOI: 10.2118/72469-pa
- Christie, M.A., Mansfield, M., King, P.R. et al. 1995. A Renormalisation-Based Upscaling Technique for Wag Floods in Heterogeneous Reservoirs. Paper presented at the SPE Reservoir Simulation Symposium, San Antonio, Texas. 1995 Copyright 1995, Society of Petroleum Engineers, Inc. 00029127. DOI: 10.2118/29127-ms.
- Cinco-Ley, H. and Samaniego-V., F. 1981. Transient Pressure Analysis for Fractured Wells. *SPE Journal of Petroleum Technology* **33** (9): 1749-1766. DOI: 10.2118/7490-pa
- Cipolla, C.L., Lolon, E., Mayerhofer, M.J. et al. 2009. Fracture Design Considerations in Horizontal Wells Drilled in Unconventional Gas Reservoirs. Paper presented at the SPE Hydraulic Fracturing Technology Conference, The Woodlands, Texas. Society of Petroleum Engineers SPE-119366-MS. DOI: 10.2118/119366-ms.
- Cipolla, C.L. and Wood, M.C. 1996. A Statistical Approach to Infill-Drilling Studies: Case History of the Ozona Canyon Sands. *SPE Reservoir Engineering* **11** (3): 196-202. DOI: 10.2118/35628-pa
- Coats Engineering, I. Spe10 and Upscaling. Accessed date: 2001.  
<http://www.coatsengineering.com/spe10.htm>.
- Coats, K.H., Dempsey, J.R., and Henderson, J.H. 1971. The Use of Vertical Equilibrium in Two-Dimensional Simulation of Three-Dimensional Reservoir Performance.

- Society of Petroleum Engineers Journal* **11** (1): 63-71. DOI: 10.2118/2797-pa
- Darman, N.H., Pickup, G.E., and Sorbie, K.S. 2002. A Comparison of Two-Phase Dynamic Upscaling Methods Based on Fluid Potentials. *Computational Geosciences* **6** (1): 5-27. DOI: 10.1023/a:1016572911992
- Datta-Gupta, A. and King, M.J. 2007. *Streamline Simulation: Theory and Practice*: Society of Petroleum Engineers. Original edition. Publisher: Society of Petroleum, USA, ISBN: 1555631118
- Deng, H., Leguizamon, J., and Aguilera, R. 2011. Petrophysics of Triple Porosity Tight Gas Reservoirs with a Link to Gas Productivity. Paper presented at the SPE Western North American Region Meeting, Anchorage, Alaska, USA. Society of Petroleum Engineers SPE-144590-MS. DOI: 10.2118/144590-ms.
- Deutsch, C.V. and Srinivasan, S. 1996. Improved Reservoir Management through Ranking Stochastic Reservoir Models. Paper presented at the SPE/DOE Improved Oil Recovery Symposium, Tulsa, Oklahoma. 1996 Copyright 1996, Society of Petroleum Engineers, Inc. 00035411. DOI: 10.2118/35411-ms.
- Durlofsky, L.J. 1991. Numerical Calculation of Equivalent Grid Block Permeability Tensors for Heterogeneous Porous Media. *Water Resour. Res.* **27** (5): 699-708. DOI: 10.1029/91wr00107
- Durlofsky, L.J., Behrens, R.A., Jones, R.C. et al. 1996. Scale up of Heterogeneous Three Dimensional Reservoir Descriptions. *SPE Journal* **1** (3): 313-326. DOI: 10.2118/30709-pa
- Dykstra, H. and Parsons, R.L. 1950. The Prediction of Oil Recovery by Water Flood. In

*Secondary Recovery of Oil in the United States*:160-174. New York: American Institute.

Efendiev, Y.R. and Durlofsky, L.J. 2003. Accurate Subgrid Models for Two-Phase Flow in Heterogeneous Reservoirs. Paper presented at the SPE Reservoir Simulation Symposium, Houston, Texas. Copyright 2003, Society of Petroleum Engineers Inc. 00079680. DOI: 10.2118/79680-ms.

Ekrann, S. and Dale, M. 1989. Averaging of Relative Permeability in Heterogeneous Reservoirs. Paper presented at the 1st European Conference on the Mathematics of Oil Recovery.

Ekrann, S. and Mykkeltveit, J. 1995. Dynamic Pseudos: How Accurate Outside Their Parent Case? Paper presented at the SPE Reservoir Simulation Symposium, San Antonio, Texas. 1995 Copyright 1995, Society of Petroleum Engineers, Inc. 00029138. DOI: 10.2118/29138-ms.

El-Ahmady, M.H. and Wattenbarger, R.A. 2004. Coarse Scale Simulation in Tight Gas Reservoirs. Paper presented at the Canadian International Petroleum Conference, Calgary, Alberta. Petroleum Society of Canada PETSOC-2004-181. DOI: 10.2118/2004-181.

Elahmady, M. and Wattenbarger, R.A. 2006. Coarse Scale Simulation in Tight Gas Reservoirs. *Journal of Canadian Petroleum Technology* **45** (12). DOI: 10.2118/06-12-03

Farmer, C.L. 2002. Upscaling: A Review. *International journal for numerical methods in fluids* **40** (1-2): 63-78.

- Frantz, J.H., Sawyer, W.K., MacDonald, R.J. et al. 2005. Evaluating Barnett Shale Production Performance Using an Integrated Approach. Paper presented at the SPE Annual Technical Conference and Exhibition, Dallas, Texas. Society of Petroleum Engineers SPE-96917-MS. DOI: 10.2118/96917-ms.
- Gallego, F. 2011. Tight Gas Modeling Frameworks for Improved Reservoir Management and Its Application to the Moxa Development Area. Paper presented at the SPE Middle East Unconventional Gas Conference and Exhibition, Muscat, Oman. Society of Petroleum Engineers SPE-142822-MS. DOI: 10.2118/142822-ms.
- Gao, H. and McVay, D.A. 2004. Gas Infill Well Selection Using Rapid Inversion Methods. Paper presented at the SPE Annual Technical Conference and Exhibition, Houston, Texas. Society of Petroleum Engineers 00090545. DOI: 10.2118/90545-ms.
- Guan, L., McVay, D.A., Jensen, J.L. et al. 2002. Evaluation of a Statistical Infill Candidate Selection Technique. Paper presented at the SPE Gas Technology Symposium, Calgary, Alberta, Canada. Copyright 2002, Society of Petroleum Engineers Inc. 00075718. DOI: 10.2118/75718-ms.
- Gunter, G.W., Finneran, J.M., Hartmann, D.J. et al. 1997. Early Determination of Reservoir Flow Units Using an Integrated Petrophysical Method. Paper presented at the SPE Annual Technical Conference and Exhibition, San Antonio, Texas. 1997 Copyright 1997, Society of Petroleum Engineers, Inc. 00038679. DOI: 10.2118/38679-ms.



- Guzman, R.E., Giordano, D., Fayers, F.J. et al. 1996. Evaluation of Dynamic Pseudo Functions for Reservoir Simulation. Paper presented at the SPE Annual Technical Conference and Exhibition, Denver, Colorado. 1996 Copyright 1996, Society of Petroleum Engineers, Inc. 00035157. DOI: 10.2118/35157-ms.
- Hearn, C.L. 1971. Simulation of Stratified Waterflooding by Pseudo Relative Permeability Curves. *SPE Journal of Petroleum Technology* **23** (7): 805-813. DOI: 10.2118/2929-pa
- Heinemann, Z.E. 1994. Interactive Generation of Irregular Simulation Grids and Its Practical Applications. Paper presented at the University of Tulsa Centennial Petroleum Engineering Symposium, Tulsa, Oklahoma. 1994 Society of Petroleum Engineers 00027998. DOI: 10.2118/27998-ms.
- Heinemann, Z.E., Brand, C.W., Munka, M. et al. 1991. Modeling Reservoir Geometry with Irregular Grids. *SPE Reservoir Engineering* **6** (2): 225-232. DOI: 10.2118/18412-pa
- Hewett, T.A., Suzuki, K., and Christie, M.A. 1998. Analytical Calculation of Coarse-Grid Corrections for Use in Pseudofunctions. *SPE Journal* **3** (3): 293-304. DOI: 10.2118/51269-pa
- Hird, K.B. and Dubrule, O. 1998. Quantification of Reservoir Connectivity for Reservoir Description Applications. *SPE Reservoir Evaluation & Engineering* **1** (1): 12-17. DOI: 10.2118/30571-pa
- Holditch, S.A. 2006. Tight Gas Sands. *SPE Journal of Petroleum Technology* **58** (6): 86-93. DOI: 10.2118/103356-ms

- Hosseini, S.A. and Kelkar, M. 2010. Analytical Upgridding Method to Preserve Dynamic Flow Behavior. *SPE Reservoir Evaluation & Engineering* **13** (3): pp. 473-484. DOI: 10.2118/116113-pa
- Hosseini, S.A. and Kelkar, M.G. 2008. Analytical Upgridding Method to Preserve Dynamic Flow Behavior. Paper presented at the SPE Annual Technical Conference and Exhibition, Denver, Colorado, USA. Society of Petroleum Engineers SPE-116113-MS. DOI: 10.2118/116113-ms.
- Iwere, F.O., Moreno, J.E., and Apaydin, O.G. 2006. Numerical Simulation of Thick, Tight Fluvial Sands. *SPE Reservoir Evaluation & Engineering* **9** (4): pp. 374-381. DOI: 10.2118/90630-pa
- Jacks, H.H., Smith, O.J.E., and Mattax, C.C. 1973. The Modeling of a Three-Dimensional Reservoir with a Two-Dimensional Reservoir Simulator-the Use of Dynamic Pseudo Functions. *Society of Petroleum Engineers Journal* **13** (3): 175-185. DOI: 10.2118/4071-pa
- Jensen, J.L. and Lake, L.W. 1988. The Influence of Sample Size and Permeability Distribution on Heterogeneity Measures. *SPE Reservoir Engineering* **3** (2): 629-637. DOI: 10.2118/15434-pa
- Johnson, E.F., Bossler, D.P., and Naumann, V.O. 1959. Calculation of Relative Permeability from Displacement Experiments, *Petroleum Transactions, AIME*, Vol. 216, 370-372
- Kelkar, M.G. and Atiq, M. 2010. Upgridding Method for Tight Gas Reservoirs. Paper presented at the SPE Annual Technical Conference and Exhibition, Florence,

- Italy. Society of Petroleum Engineers SPE-133301-MS. DOI: 10.2118/133301-ms.
- Kim, J.U. and Datta-Gupta, A. 2009. A Dual Scale Approach to Production Data Integration into High Resolution Geologic Models. Paper presented at the SPE Reservoir Simulation Symposium, The Woodlands, Texas. Society of Petroleum Engineers SPE-118950-MS. DOI: 10.2118/118950-ms.
- King, M.J. 2007. *Upgridding and Upscaling: Current Trends and Future Directions*, SPE-112810, SPE Distinguished Lecture
- King, M.J., Burn, K.S., Wang, P. et al. 2005. Optimal Coarsening of 3d Reservoir Models for Flow Simulation. Paper presented at the SPE Annual Technical Conference and Exhibition, Dallas, Texas. Society of Petroleum Engineers SPE-95759-MS. DOI: 10.2118/95759-ms.
- King, M.J., Burn, K.S., Wang, P. et al. 2006. Optimal Coarsening of 3d Reservoir Models for Flow Simulation. *SPE Reservoir Evaluation & Engineering* **9** (4): pp. 317-334. DOI: 10.2118/95759-pa
- King, M.J., MacDonald, D.G., Todd, S.P. et al. 1998. Application of Novel Upscaling Approaches to the Magnus and Andrew Reservoirs. Paper presented at the European Petroleum Conference, The Hague, Netherlands. 1998 Copyright 1998, Society of Petroleum Engineers Inc. 00050643. DOI: 10.2118/50643-ms.
- Lake, L.W. 1989. *Enhanced Oil Recovery*: Prentice Hall. Original edition. The University of California, CA, ISBN 9780132816014.
- Lake, L.W. and Jensen, J.L. 1989. A Review of Heterogeneity Measures Used in

Reservoir Characterization. Society of Petroleum Engineers, 00020156.

Lefevre, D., Pellissier, G., and Sabathier, J.-C. 1993. A New Reservoir Simulation System for a Better Reservoir Management. Paper presented at the Middle East Oil Show, Bahrain. 1993 Copyright 1993, Society of Petroleum Engineers, Inc. 00025604. DOI: 10.2118/25604-ms.

Li, D. and Beckner, B. 1999. A Practical and Efficient Uplayering Method for Scale-up of Multimillion-Cell Geologic Models. Paper presented at the SPE Asia Pacific Improved Oil Recovery Conference, Kuala Lumpur, Malaysia. Copyright 1999, Society of Petroleum Engineers Inc. 00057273. DOI: 10.2118/57273-ms.

Li, D. and Beckner, B. 2000. Optimal Uplayering for Scaleup of Multimillion-Cell Geologic Models. Paper presented at the SPE Annual Technical Conference and Exhibition, Dallas, Texas. Copyright 2000, Society of Petroleum Engineers Inc. 00062927. DOI: 10.2118/62927-ms.

Li, D. and Lake, L.W. 1995. Scaling Fluid Flow through Heterogeneous Permeable Media. *SPE Advanced Technology Series* **3** (1): 188-197. DOI: 10.2118/26648-pa

Luo, S. and Kelkar, M.G. 2010. Infill Drilling Potential in Tight Gas Reservoirs. Paper presented at the SPE Annual Technical Conference and Exhibition, Florence, Italy. Society of Petroleum Engineers SPE-134249-MS. DOI: 10.2118/134249-ms.

Mayerhofer, M.J., Stutz, H.L., Davis, E.J. et al. 2006. Optimizing Fracture Stimulation Using Treatment-Well Tiltmeters and Integrated Fracture Modeling. *SPE*

- Production & Operations* **21** (2): pp. 222-229. DOI: 10.2118/84490-pa
- Nghiem, L.X. 1983. Modeling Infinite-Conductivity Vertical Fractures with Source and Sink Terms. *Society of Petroleum Engineers Journal* **23** (4): 633-644. DOI: 10.2118/10507-pa
- Ozkan, E., Brown, M.L., Raghavan, R. et al. 2011. Comparison of Fractured-Horizontal-Well Performance in Tight Sand and Shale Reservoirs. *SPE Reservoir Evaluation & Engineering* **14** (2): pp. 248-259. DOI: 10.2118/121290-pa
- Peters, E.J. 2012. *Advanced Petrophysics: Volume 1* Original edition. Publisher: Live Oak Book Company, Austin, TX, ISBN 9781936909445.
- Portella, R.C.M. and Hewett, T.A. 2000. Upscaling, Gridding, and Simulating Using Streamtubes. *SPE Journal* **5** (3): 315-323. DOI: 10.2118/65684-pa
- Rai, H. and Chaudhri, M. 2009. Development and Real Field Application of Two Novel Upscaling Methodologies for Simulating Flow in Heterogeneous Reservoirs. Paper presented at the SPE Annual Technical Conference and Exhibition, New Orleans, Louisiana. Society of Petroleum Engineers SPE-124648-MS. DOI: 10.2118/124648-ms.
- Renard, P. and de Marsily, G. 1997. Calculating Equivalent Permeability: A Review. *Advances in Water Resources* **20** (5–6): 253-278. DOI: 10.1016/s0309-1708(96)00050-4
- Schlumberger. 2008. Pseudo Reference Manual. Houston, TX.
- Schmalz, J.P. and Rahhme, H.D. 1950. The Variation of Waterflood Performance with Variation in Permeability Profile. *Prod. Monthly* **15** (9): 9-12.

- Shook, G.M. and Mitchell, K.M. 2009. A Robust Measure of Heterogeneity for Ranking Earth Models: The F-Phi Curve and Dynamic Lorenz Coefficient. Paper presented at the SPE Annual Technical Conference and Exhibition, New Orleans, Louisiana. Society of Petroleum Engineers SPE-124625-MS. DOI: 10.2118/124625-ms.
- Stern, D. and Dawson, A.G. 1999. A Technique for Generating Reservoir Simulation Grids to Preserve Geologic Heterogeneity. Paper presented at the SPE Reservoir Simulation Symposium, Houston, Texas. Copyright 1999, Society of Petroleum Engineers, Inc. 00051942. DOI: 10.2118/51942-ms.
- Stone, H.L. 1991. Rigorous Black Oil Pseudo Functions. Paper presented at the SPE Symposium on Reservoir Simulation, Anaheim, California. 1991 00021207. DOI: 10.2118/21207-ms.
- Tang, H. and Liu, N. 2008. Static Connectivity and Heterogeneity (Sch) Analysis and Dynamic Uncertainty Estimation. Paper presented at the International Petroleum Technology Conference, Kuala Lumpur, Malaysia. International Petroleum Technology Conference IPTC-12877-MS. DOI: 10.2523/12877-ms.
- Testerman, J.D. 1962. A Statistical Reservoir-Zonation Technique, SPE Journal of Petroleum Technology 14 (8) DOI: 10.2118/286-PA
- Thibeau, S. 1996. Dual Scale Simulations: A Tool for Pseudoisation. Paper presented at the European Petroleum Conference, Milan, Italy. 1996 Copyright 1996, Society of Petroleum Engineers, Inc. 00036929. DOI: 10.2118/36929-ms.
- Thibeau, S., Barker, J.W., and Souillard, P. 1995. Dynamical Upscaling Techniques

- Applied to Compositional Flows. Paper presented at the SPE Reservoir Simulation Symposium, San Antonio, Texas. 1995 Copyright 1995, Society of Petroleum Engineers, Inc. 00029128. DOI: 10.2118/29128-ms.
- Verma, S. and Aziz, K. 1997. A Control Volume Scheme for Flexible Grids in Reservoir Simulation. Paper presented at the SPE Reservoir Simulation Symposium, Dallas, Texas. 1997 Copyright 1997, Society of Petroleum Engineers, Inc. 00037999. DOI: 10.2118/37999-ms.
- Vicente, R., Sarica, C., and Ertekin, T. 2002. A Numerical Model Coupling Reservoir and Horizontal Well-Flow Dynamics: Transient Behavior of Single-Phase Liquid and Gas Flow. *SPE Journal* 7 (1): 70-77. DOI: 10.2118/77096-pa
- White, C.D. and Horne, R.N. 1987. Computing Absolute Transmissibility in the Presence of Fine-Scale Heterogeneity. Paper presented at the SPE Symposium on Reservoir Simulation, San Antonio, Texas. 1987 Copyright 1987, Society of Petroleum Engineers 00016011. DOI: 10.2118/16011-ms.
- Wu, X.-H., Stone, M., Parashkevov, R. et al. 2007. Reservoir Modeling with Global Scaleup. Paper presented at the SPE Middle East Oil and Gas Show and Conference, Kingdom of Bahrain. Society of Petroleum Engineers SPE-105237-MS. DOI: 10.2118/105237-ms.
- Yadecuri, M. and Mahani, H. 2009. Unstructured Coarse Grid Generation for Reservoir Flow Simulation Using Background Grid Approach. Paper presented at the SPE Middle East Oil and Gas Show and Conference, Bahrain, Bahrain. Society of Petroleum Engineers SPE-120170-MS. DOI: 10.2118/120170-ms.

Zhang, P., Pickup, G.E., and Christie, M.A. 2006. A New Method for Accurate and Practical Upscaling in Highly Heterogeneous Reservoir Models. Paper presented at the International Oil & Gas Conference and Exhibition in China, Beijing, China. Society of Petroleum Engineers SPE-103760-MS. DOI: 10.2118/103760-ms.

Zhou, Y. and King, M.J. 2011. Improved Upscaling for Flow Simulation of Tight Gas Reservoir Models. Paper presented at the SPE Annual Technical Conference and Exhibition, Denver, Colorado, USA. Society of Petroleum Engineers SPE-147355-MS. DOI: 10.2118/147355-ms.



## APPENDIX A: COMBINATION OF VELOCITY AND SLOWNESS

For a given structured model, consider only the two adjacent fine scale cells that are going to be combined in the next step.

Using local slowness:

$$\bar{k} = \frac{k_{(i,j,k)}v_{(i,j,k)} + k_{(i,j,k+1)}v_{(i,j,k+1)}}{v_{(i,j,k)} + v_{(i,j,k+1)}} \quad (\text{B-1})$$

$$\bar{\phi} = \frac{\phi_{(i,j,k)}v_{(i,j,k)} + \phi_{(i,j,k+1)}v_{(i,j,k+1)}}{v_{(i,j,k)} + v_{(i,j,k+1)}} \quad (\text{B-2})$$

$$\begin{aligned} Error_s &= v_{(i,j,k)} \left[ \frac{\phi_{(i,j,k)}}{k_{(i,j,k)}} - \frac{\phi_{(i,j,k)}v_{(i,j,k)} + \phi_{(i,j,k+1)}v_{(i,j,k+1)}}{k_{(i,j,k)}v_{(i,j,k)} + k_{(i,j,k+1)}v_{(i,j,k+1)}} \right]^2 \\ &+ v_{(i,j,k+1)} \left[ \frac{\phi_{(i,j,k+1)}}{k_{(i,j,k+1)}} - \frac{\phi_{(i,j,k)}v_{(i,j,k)} + \phi_{(i,j,k+1)}v_{(i,j,k+1)}}{k_{(i,j,k)}v_{(i,j,k)} + k_{(i,j,k+1)}v_{(i,j,k+1)}} \right]^2 \\ &= v_{(i,j,k)} \times \left( \frac{k_{(i,j,k+1)}v_{(i,j,k+1)}\phi_{(i,j,k)} - k_{(i,j,k)}v_{(i,j,k+1)}\phi_{(i,j,k+1)}}{k_{(i,j,k)}(k_{(i,j,k)}v_{(i,j,k)} + k_{(i,j,k+1)}v_{(i,j,k+1)})} \right)^2 \\ &+ v_{(i,j,k+1)} \times \left( \frac{k_{(i,j,k)}v_{(i,j,k)}\phi_{(i,j,k+1)} - k_{(i,j,k+1)}v_{(i,j,k)}\phi_{(i,j,k)}}{k_{(i,j,k+1)}(k_{(i,j,k)}v_{(i,j,k)} + k_{(i,j,k+1)}v_{(i,j,k+1)})} \right)^2 \end{aligned} \quad (\text{B-3})$$

Using local velocity:

$$\bar{k} = \frac{k_{(i,j,k)}v_{(i,j,k)} + k_{(i,j,k+1)}v_{(i,j,k+1)}}{v_{(i,j,k)} + v_{(i,j,k+1)}} \quad (\text{B-4})$$

$$\bar{\phi} = \frac{\phi_{(i,j,k)}v_{(i,j,k)} + \phi_{(i,j,k+1)}v_{(i,j,k+1)}}{v_{(i,j,k)} + v_{(i,j,k+1)}} \quad (\text{B-5})$$

$$\begin{aligned}
Error_v &= v_{(i,j,k)} \left[ \frac{k_{(i,j,k)} - k_{(i,j,k)} v_{(i,j,k)} + k_{(i,j,k+1)} v_{(i,j,k+1)}}{\phi_{(i,j,k)} - \phi_{(i,j,k)} v_{(i,j,k)} + \phi_{(i,j,k+1)} v_{(i,j,k+1)}} \right]^2 \\
&+ v_{(i,j,k+1)} \left[ \frac{\phi_{(i,j,k+1)} - k_{(i,j,k)} v_{(i,j,k)} + k_{(i,j,k+1)} v_{(i,j,k+1)}}{\phi_{(i,j,k+1)} - \phi_{(i,j,k)} v_{(i,j,k)} + \phi_{(i,j,k+1)} v_{(i,j,k+1)}} \right]^2 \\
&= v_{(i,j,k)} \times \left( \frac{\phi_{(i,j,k+1)} v_{(i,j,k+1)} k_{(i,j,k)} - \phi_{(i,j,k)} v_{(i,j,k+1)} k_{(i,j,k+1)}}{\phi_{(i,j,k)} (\phi_{(i,j,k)} v_{(i,j,k)} + \phi_{(i,j,k+1)} v_{(i,j,k+1)})} \right)^2 \\
&+ v_{(i,j,k+1)} \times \left( \frac{\phi_{(i,j,k)} v_{(i,j,k)} k_{(i,j,k+1)} - \phi_{(i,j,k+1)} v_{(i,j,k)} k_{(i,j,k)}}{\phi_{(i,j,k+1)} (\phi_{(i,j,k)} v_{(i,j,k)} + \phi_{(i,j,k+1)} v_{(i,j,k+1)})} \right)^2
\end{aligned} \tag{B-6}$$

$$\begin{aligned}
Error_{v\&s} &= \sqrt{Error_v \times Error_s} \\
&= \sqrt{\frac{(v_{(i,j,k)} v_{(i,j,k+1)})^2 (\phi_{(i,j,k)} k_{(i,j,k+1)} - k_{(i,j,k)} \phi_{(i,j,k+1)})^4}{(k_{(i,j,k)} k_{(i,j,k+1)})^2 (\phi_{(i,j,k)} \phi_{(i,j,k+1)})^2}} \\
&\times \sqrt{\frac{(k^2_{(i,j,k+1)} v_{(i,j,k+1)} + k^2_{(i,j,k)} v_{(i,j,k)}) (\phi^2_{(i,j,k+1)} v_{(i,j,k+1)} + \phi^2_{(i,j,k)} v_{(i,j,k)})}{(v_{(i,j,k)} k_{(i,j,k)} + k_{(i,j,k+1)} v_{(i,j,k+1)})^2 (v_{(i,j,k)} \phi_{(i,j,k)} + \phi_{(i,j,k+1)} v_{(i,j,k+1)})^2}}
\end{aligned} \tag{B-7}$$

In our calculations, we consider the new upgridded properties first and then calculated the error based on the new slowness and velocity static measure ( $\frac{\bar{k}}{\phi}$  and  $\frac{\bar{\phi}}{k}$ ).

Here we provided a more generalized form of the error evaluation using equation

$$\begin{aligned}
Error_{v\&s} &= \sqrt{Error_v \times Error_s} \\
&= \sqrt{\frac{(v_{(i,j,k)} v_{(i,j,k+1)})^2 (\phi_{(i,j,k)} k_{(i,j,k+1)} - k_{(i,j,k)} \phi_{(i,j,k+1)})^4}{(k_{(i,j,k)} k_{(i,j,k+1)})^2 (\phi_{(i,j,k)} \phi_{(i,j,k+1)})^2}} \\
&\times \sqrt{\frac{(k^2_{(i,j,k+1)} v_{(i,j,k+1)} + k^2_{(i,j,k)} v_{(i,j,k)}) (\phi^2_{(i,j,k+1)} v_{(i,j,k+1)} + \phi^2_{(i,j,k)} v_{(i,j,k)})}{(v_{(i,j,k)} k_{(i,j,k)} + k_{(i,j,k+1)} v_{(i,j,k+1)})^2 (v_{(i,j,k)} \phi_{(i,j,k)} + \phi_{(i,j,k+1)} v_{(i,j,k+1)})^2}}
\end{aligned}$$

In Hosseini et.al (2008) paper, the final error for combining two layers (k and k+1 layer) will be given as:

$$\sum_{i,j} \sqrt{\frac{(K^2_{(i,j,k)} \times H^2_{(i,j,k)}) + (K^2_{(i,j,k+1)} \times H^2_{(i,j,k+1)})}{((K_{(i,j,k)} \times H_{(i,j,k)}) + (K_{(i,j,k+1)} \times H_{(i,j,k+1)}))^2}} \times \frac{(K_{(i,j,k)} - K_{(i,j,k+1)})^4}{(K_{(i,j,k)} \times K_{(i,j,k+1)})^2}$$

## APPENDIX B: SWIFT

### Introduction

The use of detailed three dimensional finely gridded geological models have become commonplace for reservoir description and subsurface uncertainty assessment, and as aides for reservoir appraisal, development, management and optimization. Reservoir simulation and performance prediction based upon these models remain a challenge which is resolved through the development of approximate upscaled reservoir models.

When done well, upscaled models preserve key aspects of the underlying reservoir description. When done poorly, upscaled models can be too homogeneous, with typically late fluid breakthrough and unrealistically high recovery estimates. The intent and scope of SWIFT is to provide high resolution upscaled simulation models. The simulation grid design or “upgridding” portion of SWIFT uses a priori upscaling error estimates to design an optimal grid, with the best compromise between having a minimum number of simulation cells and preservation of the reservoir heterogeneity. The property upscaling is based upon transmissibility for cell-cell transport and well index based property upscaling for the well-cell coupling.

The currently released version of SWIFT does not yet include property upscaling, but instead utilizes a statistical error analysis for the design of the coarsened simulation layering scheme based upon the layering of the high resolution geologic model. In our experience this is the most useful statistical problem to be solved in simulation grid design since areal coarsening is more typically constrained by well spacing and simulation cell count, and is not a statistical issue.

The SWIFT design is based upon an estimate of the impact of heterogeneity on multiphase flow frontal motion. Although no multiphase upscaling algorithms have yet been developed for SWIFT, our experience is that the layering schemes designed by SWIFT minimize the need for multiphase upscaling.

SWIFT is delivered as an executable with a text “SIP” SWIFT input file. This executable may be invoked from the command line to support uncertainty workflows or to support non-Petrel users. However, we expect the majority of users to access SWIFT as a Petrel plug-in, where the plug-in will prepare input data and the input file for SWIFT and then invoke the application.

#### Installation and getting started

The installation package consists of two files named “setup.exe” and “SWIFT\_install.msi”, as shown in Figure B-1, below. The names of the msi files will vary to indicate the version of Petrel and the operating system or hardware. Users can easily install the SWIFT plug-in for Petrel with just a few clicks on “setup.exe”. For successful installation, users need installation authority on that machine and an existing installation of Petrel. SWIFT updates will be available for downloading from our MCERI website (<http://www.pe.tamu.edu/mceri/>) with member’s log-in. If your specific version of Petrel or operating system and hardware is not available, you can ask us to make a new plug-in for your use.



**Figure B- 1 Installation Packages**

This installed plug-in is shown within the Petrel “Process Window” as indicated in Figure C-2. Users can start SWIFT by double clicking the swiftProcess icon. Note that Petrel allows just one process window at a time to prevent conflicts in the manipulation of the project data.

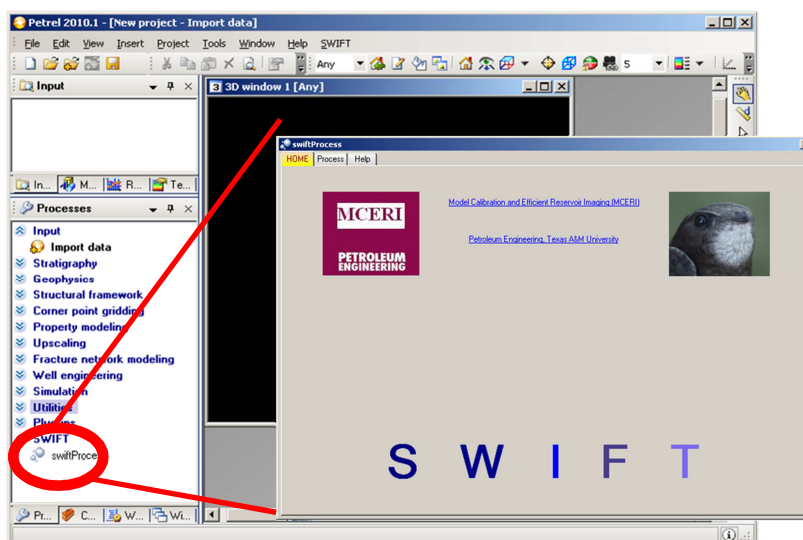


Figure B- 2 SWIFT shown in THE “ProcessES” Window

## User Interface

When SWIFT starts up, a “HOME” board, as shown in Figure 3, will provide the welcome message page. Technical support is provided by the MCERI JIP at Texas A&M University. After displaying the welcoming information, the Main Window will be launched to lead users through the use of SWIFT.



Figure B- 3 Home Page of SWIFT

The main window is created when the process is started and will lead users to the main process window as shown in Figure 4. At this version of SWIFT, all of the functionality may be accessed from this single window.

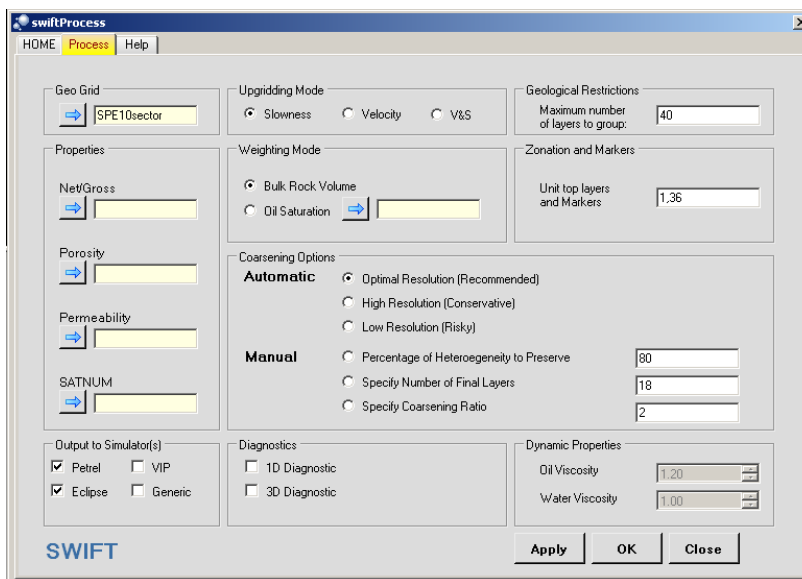


**Figure B- 4 SWIFT Process Page**

SWIFT will obtain its input from a Petrel grid model and properties. Depending upon the choice of output, it will provide the layer design either as simulator input (Eclipse, VIP or generic formats) or as files that may be used within Petrel to construct an upgridded geologic model before simulation. Figure 5 gives a simple illustration.

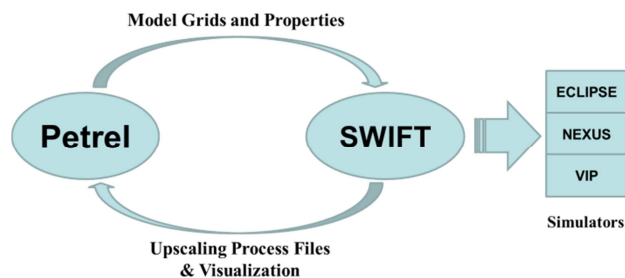


**Figure B- 5 SWIFT Combination**

The image shows a software interface for defining a grid and its properties. It is divided into two main sections: 'Geo Grid' and 'Properties'. In the 'Geo Grid' section, there is a blue arrow button pointing to a text box that contains the file name 'SPE10.EGRID'. The 'Properties' section contains four rows, each with a blue arrow button pointing to an empty text box. The rows are labeled 'Net/Gross', 'Porosity', 'Permeability', and 'SATNUM'.

**Figure B- 6 Grid and Property Definition**

Ensure that the coarse grid is active when you open the **SWIFT** process and drop the fine grid into the **Geo grid** box. The process will extract the grid geometry information from the selected fine grid; any existing zonation in the grid will be removed.

The second step is to drag and drop the reservoir properties for optimal coarsening to the corresponding boxes. The minimum required properties are the **Porosity** and **Permeability** for the currently selected geological model. If only the porosity and permeability are provided, the **Net/Gross** and **SATNUM** will be set to default values.

The image shows a software interface for selecting upgridding and weighting modes. It is divided into two sections: 'Upgridding Mode' and 'Weighting Mode'. In the 'Upgridding Mode' section, there are three radio buttons: 'Slowness' (which is selected), 'Velocity', and 'V&S'. In the 'Weighting Mode' section, there are two radio buttons: 'Bulk Rock Volume' (which is selected) and 'Oil Saturation'. Next to the 'Oil Saturation' radio button is a blue arrow button pointing to an empty text box.

**Figure B- 7 Upgridding mode and Weighting Modes**



In our current scope, we provide three different static measures of heterogeneity. The upgridding calculation will be performed based on the minimal loss of heterogeneity for the selected measure. Velocity is the most sensitive to high permeability streaks. Slowness is a better indicator of overall reservoir performance. The velocity and slowness mode (V&S) combines these two measures to preserve overall performance but with increased sensitivity to high permeability streaks. The bulk rock volume is the default weighting mode is calculated internally. Oil saturation is an alternative weighting mode which emphasizes those portions of the geologic model within the oil column.

Geological Restrictions	
Maximum number of layers to group:	22
Zonation and Markers	
Unit top layers and Markers	1, 36

**Figure B- 8 Upgridding Restrictions**

Figure B-8 shows the upgridding restrictions that help users specify upgridding constraints. **Maximum number of layers to group** will set the maximum number of fine layers which are allowed to be grouped into a coarsened layer. The geologic marker constraint is very important to preserve reservoir zonation. For different zones, top layer of each zone is asked for in the **Unit top layers and Markers** section. A comma is used to separate multiple entries. No grid amalgamation will occur across the boundary/marker.

Coarsening Options

**Automatic**

- Optimal Resolution (Recommended)
- High Resolution (Conservative)
- Low Resolution (Risky)

**Manual**

- Percentage of Heterogeneity to Preserve
- Specify Number of Final Layers
- Specify Coarsening Ratio

**Figure B- 9 Coarsening Setting**

Figure B-9 shows the automatic and manual coarsening options. **Optimal Resolution** provides the recommended layer design based on the specified heterogeneity measure. **High Resolution** and **Low Resolution** give relatively conservative and aggressive grouping combinations. Manual input is provided as an alternative. **Percentage of Heterogeneity to Preserve** will preserve that fraction of the total reservoir heterogeneity. If **Specify Number of Final Layers** is checked, the best layering scheme with that number of layers will be calculated. If **Specify Coarsening Ratio** is checked, the user must specify this ratio and uniform layer coarsening will be applied to the model.

Output to Simulator(s)

- Petrel  VIP
- Eclipse  Generic

Diagnostics

- 1D Diagnostic
- 3D Diagnostic

Dynamic Properties

Oil Viscosity

Water Viscosity

**Figure B- 10 Dynamic Property and Output panel**

**Dynamic Properties** panel is used to obtain the oil and water viscosity if the SATNUM variable is used when determining the Buckley-Leverett frontal speed for each relative permeability table. In the **Diagnostics** section, if the **1D Diagnostic** is checked, heterogeneity measured within each layer will be calculated and exported to the **1D**

**diagnostic** file. If **3D Diagnostic** is checked, the “Within-Cell” heterogeneity will be calculated for each cell and exported to the **3D diagnostic** file. **Output to Simulator(s)** section controls all the output files to different simulators. Files containing “**COARSEN**” keywords for certain simulators will be generated for simulation use. For simulation purposes, these files are the include files to be included with the fine scale model to instruct the simulator to create a coarsened simulation model following the designed layering scheme. Currently we support 3 difference simulators: Eclipse, VIP and Nexus. VIP and Nexus share the same file formats. A generic output format is also provided to support other simulators.

### A Step by Step Tutorial

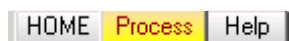
This section will give a step by step tutorial in using SWIFT. The model loaded in this tutorial is called “SPE10\_Sector”

### How to run SWIFT

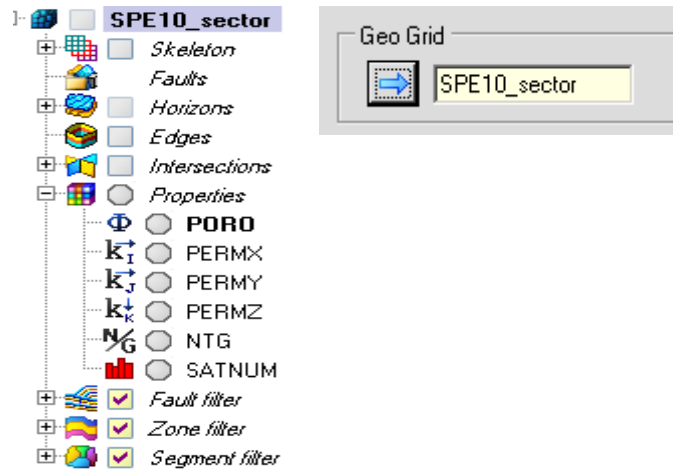
1. In the **Processes** panel, double click the **swiftProcess** icon to launch SWIFT.



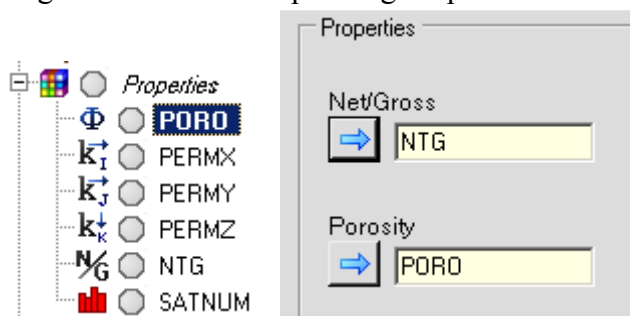
2. Click the **Process** tab at the top section.



3. Highlight the **SPE10\_sector** first and then drag/drop the grid to the **Geo Grid** box. Only “Grid” types can be accepted.



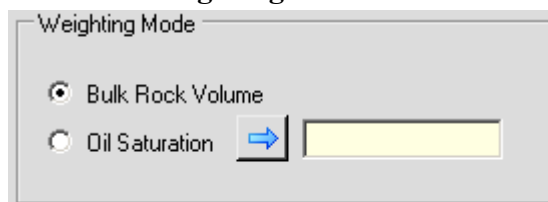
4. Highlight **permeability, porosity, NTG** and **SATNUM** one by one and then drag them to the corresponding drop boxes.



5. Select the desired upgridding mode. Please click on the radio button to enable the mode.



6. Select the **Weighting Mode**



If oil saturation is selected, a parameter containing the oil saturation values should be drag/dropped into the drop box.

7. Setup the maximum number of layers that are allowed in a single coarsened layer.

Geological Restrictions

Maximum number of layers to group:

This function helps to control upgridding resolution.

8. Setup the zonation and marker information.

Zonation and Markers

Unit top layers and Markers

For each of the geologic zones, please import the top layer number (fine scale). Upgridding will not occur across different zones.

9. Pick the desired coarsening layer options. SWIFT will calculate the optimal choice for the final number of layers if the Automatic method is selected. Otherwise, the user may specify the output layer design manually.

10. Select the output files

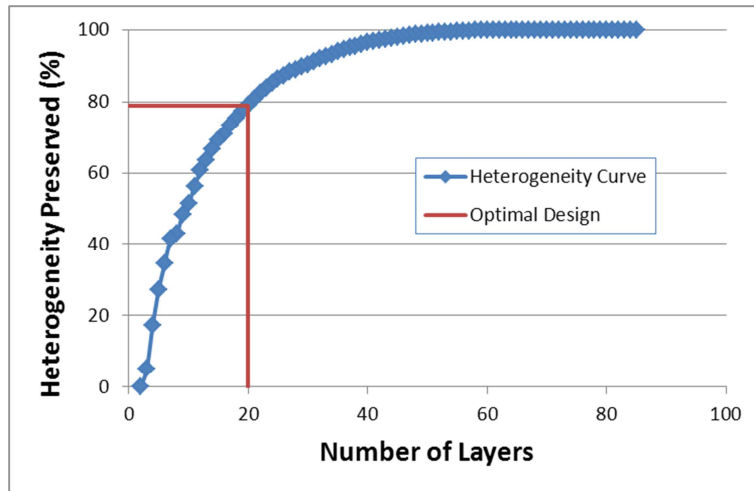
Output to Simulator(s)

Petrel     VIP  
 Eclipse     Generic

Diagnostics

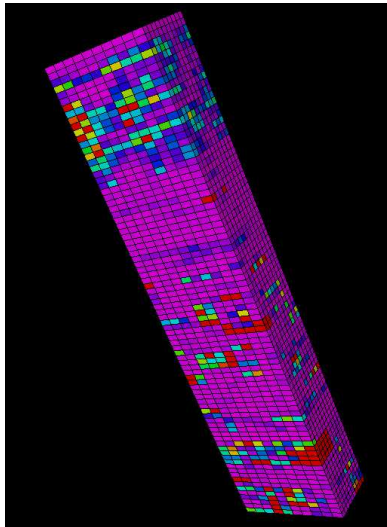
1D Diagnostic  
 3D Diagnostic

11. 1D Diagnostic



Plot is generated in Excel using the data in “1D\_Diagnostics.dat” file.

## 12. 3D Diagnostic



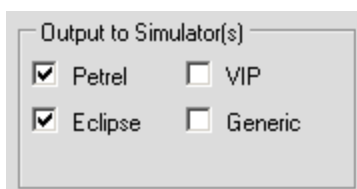
Each fine cell is populated with the “Within Cell” heterogeneity values. The data can be imported to Petrel as **Generic ECLIPSE style parameter**.

13. After setting up the necessary parameters, SWIFT is ready to fly.



## How to visualize the coarse model with Petrel

Detailed discussion of upgridding and upscaling processes can be found in the Petrel manual. Here we provide that portion of the instructions related to the use of the SWIFT output files.

1. SWIFT will automatically generate a coarsened grid from the fine scale model, if **Petrel** is checked in the **Output to Simulator(s)** panel.



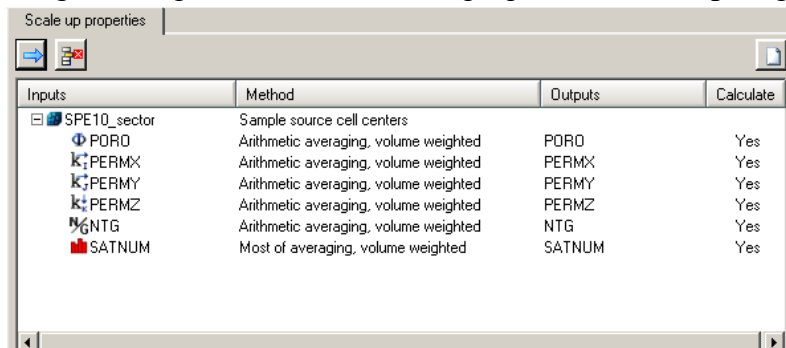
2. Coarsened model will be named as “Coarsened\_”+ original grid name.

 **Coarsened\_10x10x85.grdecl**  
 10x10x85.grdecl

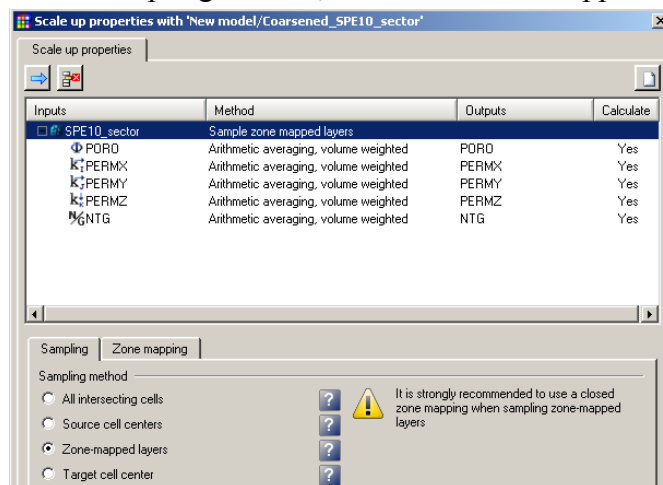
SWIFT bypasses the **Scale up structure** procedures and generates the coarsened grids. **Note:** SWIFT coarsens structures while honoring the horizontal information that the new layers will follow the original horizons.

3. In the **Processes** panel, double click **Scale up properties** and make sure the properties icon from SPE\_10\_sector (fine scale) is highlighted.

4. Drag and drop the fine scale model properties to the **Inputs** panel.

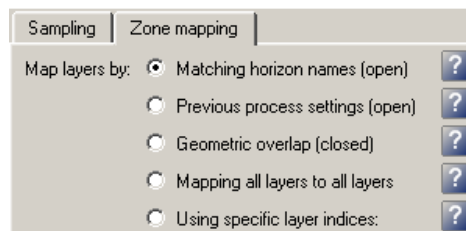


5. Left click on “SPE10\_sector” inside the Inputs panel to activate the **Sampling and Zone mapping functions**.
6. In the Sampling Section, check the Zone-Mapped Layers.



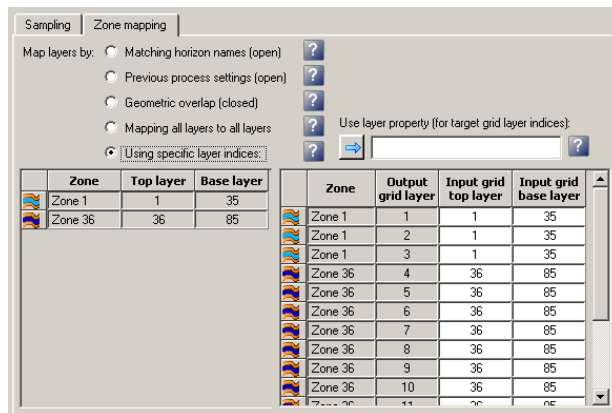
7. Zone mapping setting

If the model is imported from simulation results and the zones are not modified before running SWIFT, it is OKAY to use **Matching horizon names (open)**.



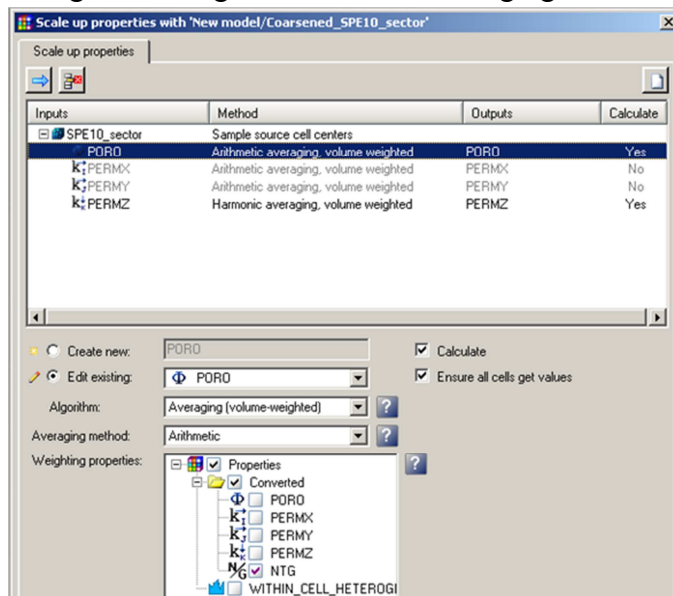


If the model is NOT imported from simulation results or the zones are modified before running SWIFT, it is recommended to use **“Using specific layer indices”**

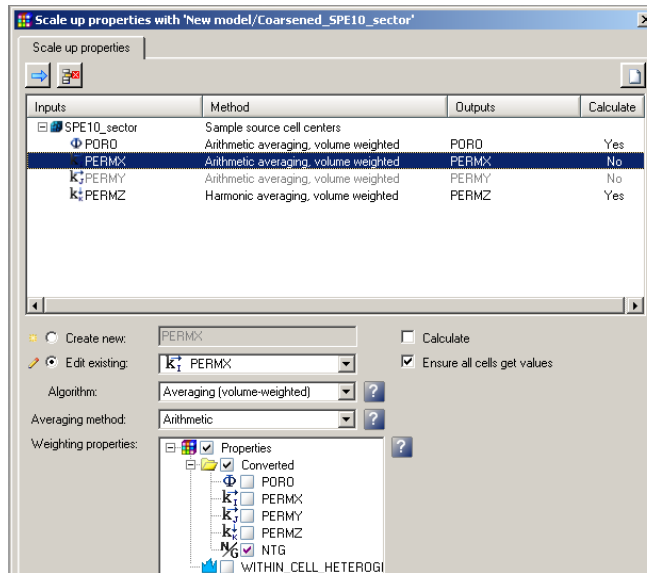


If choosing **“Using specific layer indices”**, copy and paste the corresponding columns from **“Petrel\_Output.dat”** file to the Input grid top layer and Input grid base layer columns.

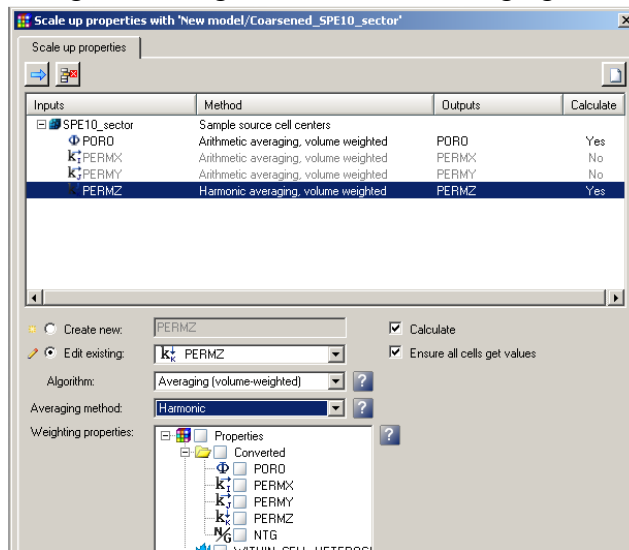
#### 8. Using NTG weighted arithmetic averaging for coarsened porosity calculation.



#### 9. Using NTG weighted arithmetic averaging for PERMX and PERMY calculation.

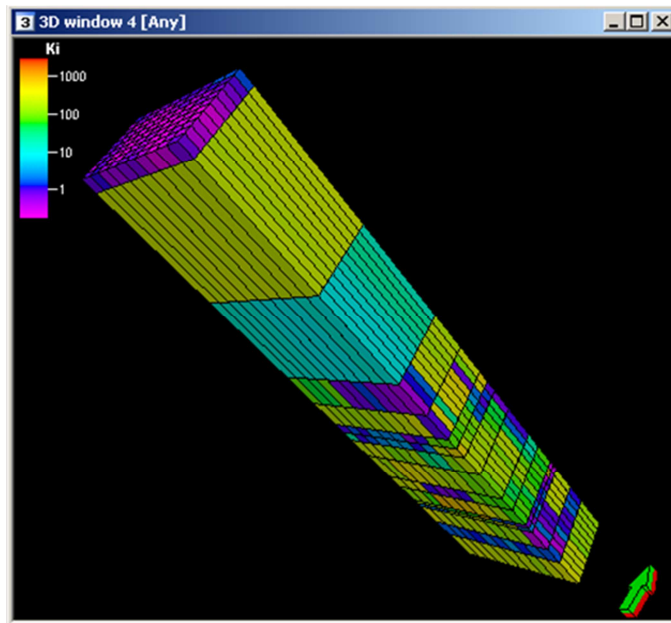


10. Using NTG weighted arithmetic averaging for PERMZ calculation.



11. Click “Apply” or “OK” to activate the property upscaling.

12. Visualize the upscaled property and grid in a new 3D window.



### SWIFT.SIP Sample

```

--*****
--*****
--** This file provides the required input **
--** data to run SWIFT upgridding Program. **
--*****
--**          Plug-in developed by          **
--**          Song Du                       **
--*****
--*****

```

#### OPTIMAL\_LAYER\_CHOICE

```

-- Choices for layering design:
--1- Keyword: LAYER & followed by target value.
--2- Keyword: OPT & followed by total number of layers.
--3- Keyword: PERCENTAGE & followed by followed by target value (30,
80...DO NOT use %).
--4- Keyword: LOW_RES.
--5- Keyword: HIGH_RES.
--6- Keyword: UNIFORM & followed by number of fine layers to be
combined uniformly.
OPT

```

#### ALGORITHM

```

--VELOCITY or SLOWNESS or VS
VS

```

## MARKER

-- marker locations

2/

1

36/

## 3DDiagnostic

-- "no\_output" for nothing to export

-- output for exporting 3d diagnostic files.

no\_output

## UNIT\_MAX

-- Maximum number of fine layers which are allowed to be combined.

40

## OUTPUT

-- Outputs are going to be generated in these formats.(PETREL, ECLIPSE,  
VIP OR GENERIC)

PETREL

ECLIPSE

## INIT\_FILE

SWIFT.INIT

## GRID

--NX

10

--NY

10

--NZ

85

## APPENDIX C: WORKFLOW OF THE MULTIPHASE UPSCALING

A general workflow of the multiphase upscaling is presented in Chapter 4. This section discusses the detailed workflow in which Petrel and Matlab program are involved. This method requires initial fine scale simulation runs on a sector model, and pseudo functions are applied to the full field coarse models. This sector model is a quarter of the SPE10 model containing a model dimension of 30x110x85. Two flow patterns are applied: a quarter of a five spot pattern (Q5) and line drive pattern. In the Q5 model, only one injector and one producer are placed at the corner of the sector model. In the line drive pattern, 30 injectors are placed in one end of the model, and 30 producers are placed in the other end of the model.

- 1) Run fine scale simulation on Eclipse 100 with a sector model which contains typical geologic features from the full field model. In our case study, we test both Q5 pattern and the line drive flow pattern. Restart files are requested at sufficient time steps.
- 2) Load simulation data into Petrel. For each time step, export the cumulative oil/water production, total water injection, water saturation, pressure and total oil/water flux for the outlet. The effective fractional flow calculation is based on the classic JBN analysis as described in Chapter 4. For each of the coarsened model, only one fractional flow curve is calculated using the pore volume based average value.
- 3) Calculate the effective total mobility at the outlet using Equation 3-18. This equation has a simplified assumption regarding the model geometry and global permeability rescaling. Flow path area, length and global permeability rescaling are calibrated with the sector coarse models. The sector coarse model contains the same vertical solution as the fine scale full field model. Therefore, for the same vertical grouping combinations, coarse scale sector

simulations are performed to calibrate the geometry and permeability impacts.

- 4) Another way of calculating the effective total mobility curve is based on the total fluid segregation analysis. A weighting factor is selected based on the sector model performance match. Sensitivity analysis is required for accurate factor selection.
- 5) As mentioned in the previous chapter of layer design, we are not considering the areal upgridding/upscaling. No numerical dispersion problem will be involved in this study.

## APPENDIX D: SWIFT\_PILLAR

### An IPL script for adaptive coarsening

#### User Interface

#### Main Window

When SWIFT\_PILLAR\_PILLAR IPL starts up, a main board, as shown in Figure D- 1, will provide the all major function information. Technical support is provided by the MCERI at Texas A&M University.

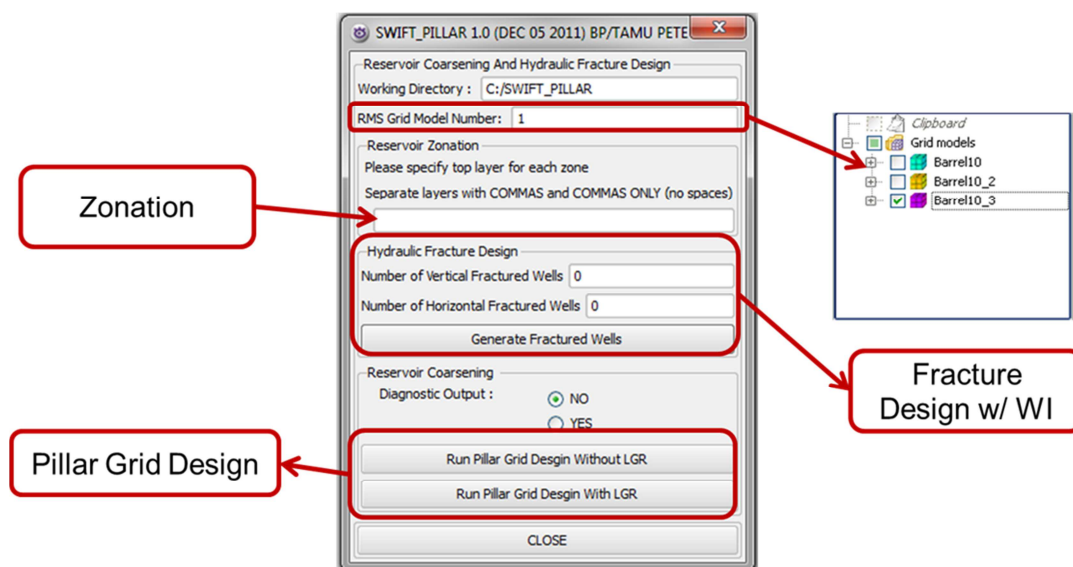


**Figure D- 1 Home page of the Swift\_Pillar**

#### Functions

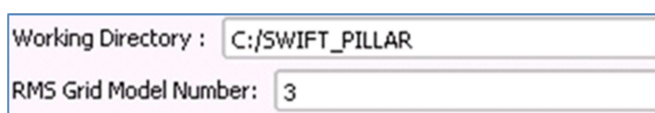
The main window is created when the process starts, as shown in , and will lead users to the individual function windows. At this version of SWIFT\_PILLAR, all of the functionality can be accessed from this single window.

SWIFT\_PILLAR IPL obtains its input data from a RMS grid model and its properties. Depending upon the choice of functions, it provides the files for Well Index manipulations, for LGR and Transmissibility Modifiers and diagnostic RMS parameters.

In this section, the main window will be introduced piece by piece.

### Project Settings

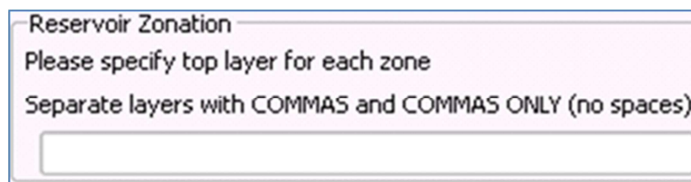
Ensure that the grid is active when you open the **SWIFT\_PILLAR** process and the default working directory is set to “C:/SWIFT\_PILLAR”. All the output files will be saved to the target folder. Since there may be more than one grid model in the “GridModel” folder under RMS tree, the default is set to the last one.



Working Directory : C:/SWIFT\_PILLAR  
RMS Grid Model Number: 3

**Figure D- 2 Working directory and model number**

The geologic constraint is very important to preserve reservoir zonation. For different zones, top layer of each zone is asked for in the **Reservoir Zonation** section. A comma and comma only is used to separate two entries. This will affect both the WI and LGR design.



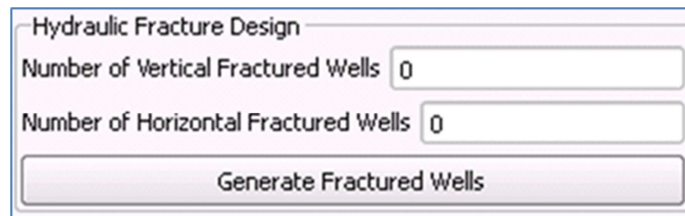
Reservoir Zonation  
Please specify top layer for each zone  
Separate layers with COMMAS and COMMAS ONLY (no spaces)

**Figure D- 3 Reservoir zonation setting**

### Fracture Design with Well Index

SWIFT\_PILLAR is able to represent hydraulic fractures with modified WI, the detailed methodology is provided in SPE 122793. Files containing WELLSPEC keyword will be generated and saved to the target working directory.





The image shows a dialog box titled "Hydraulic Fracture Design". It contains two input fields: "Number of Vertical Fractured Wells" and "Number of Horizontal Fractured Wells", both with the value "0" entered. Below these fields is a button labeled "Generate Fractured Wells".

**Figure D- 4 Hydraulic Fracture Design**

SWIFT\_PILLAR supports both the vertical and horizontal well design and the number of each type of the wells can share the same window. Default numbers are set to zeros. Due to the computer monitor size and resolution, the IPL will allow no more than 5 wells for hand typing. For more than 5 wells, files prepared by the users are going to be required, as seen in Figure D- 5. Imported files are also required in the popup window, as seen in Figure D- 6, if both the well numbers are set to zero. Those input files should contain exactly the same information as the input panel showing in Figure D- 6 and different parameters should be separated with spaces. No "TAB" is going to be accepted if they exist in the files.

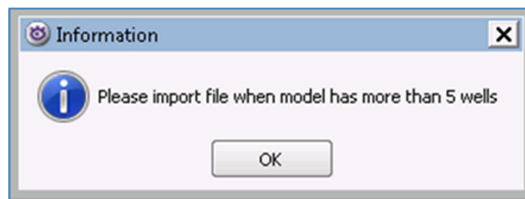


**Figure D- 5 Information Box**

Vertical Well(s)					
Well Names	X Location	Y Location	Zone #	Orientation(I/J)	Half Length
# 1 VWell_1	7.4069e+005	2.713e+005	*	J	1000
# 2 VWell_2	7.4069e+005	2.713e+005	*	J	1000
# 3 VWell_3	7.4069e+005	2.713e+005	*	J	1000

Horizontal Well(s)							
Well Names	Heel-X	Heel-Y	Toe-X	Toe-Y	Zone #	Half Length	Number of Hydraulic Fractures/Proportions
# 1 HWell_1	7.4031e+005	2.7093e+005	7.4106e+005	2.7168e+005	*	1000	Uniform (4)
# 2 HWell_2	7.4031e+005	2.7093e+005	7.4106e+005	2.7168e+005	*	1000	Uniform (4)
# 3 HWell_3	7.4031e+005	2.7093e+005	7.4106e+005	2.7168e+005	*	1000	Uniform (4)
# 4 HWell_4	7.4031e+005	2.7093e+005	7.4106e+005	2.7168e+005	*	1000	Uniform (4)
# 5 HWell_5	7.4031e+005	2.7093e+005	7.4106e+005	2.7168e+005	*	1000	Uniform (4)

**Figure D- 6 Fracture setting**

For vertical wells, we require the items: Well name, X-location, Y-location, Zone Number, Orientation(I/J) and Half Length.

Well Name: Unique name for each well.

X-location: Well location in X axis. Default: Center of the X axis.

Y-location: Well location in Y axis. Default: Center of the Y axis.

Zone Number: For which zones the well penetrates. Use “\*” to identify the wells penetrating the whole reservoir. Again, a comma and comma only is used to separate two zone numbers.

Orientation: Current well design function supports hydraulic fractures orientated in either I or J direction.

Half Length: Half Length of the fracture. Fractures are supposed to have equal half-length for individual wells.

For horizontal wells, we require the items: Well name, Heel-X, Heel-Y, Toe-X, Toe-Y, Zone Number, Half Length, fracture distributions and number of fractures.

Well Name: Unique name for each well.

Heel-X(Y): Heel location in X(Y) axis. Default: Calculated based on the well length, fracture numbers and distributions.

Toe-X(Y): Toe location in X(Y) axis. Default: Calculated based on the well length, fracture numbers and distributions.

Zone Number: For which zones the well penetrates. Use “\*” to identify the wells penetrating the whole reservoir. Again, a comma and comma only is used to separate two zone numbers.

Half Length: Half Length of the fracture. Fractures are supposed to have equal half-length for individual wells.

Distributions: Two types of fracture distributions are supported: uniform and proportional. If “Uniform” is selected, the total number of fractures for each well be uniformly distributed along the horizontal well from heel to toe. If “Proportional” is selected, the distribution portion is required, either float or integer values can be used for the proportional distribution assignments. Two typical well distributions: proportional distribution of 1:5:10 and fracture crossing be seen in Figure D- 7.

Number of Fractures: Total number of fractures from each well.

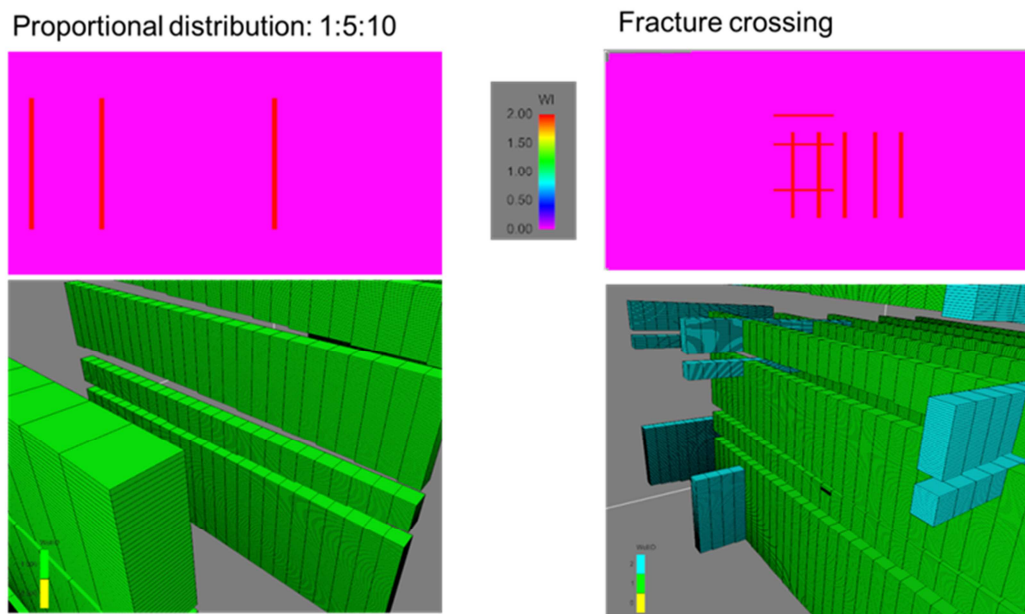


**Figure D- 7 Typical well design**

### Pillar Based Coarsening

In the **Reservoir Coarsening** section, as seen in Figure D- 8, we provide the Diagnostic Output for diagnostic output parameter for RMS models directly. This section also includes two different grid design algorithms including the novel pillar adaptive grid design as the first option and the grid design with LGR around the wells and fractures as the section option.

Reservoir Coarsening

Diagnostic Output :  NO  YES

Run Pillar Grid Desgin Without LGR

Run Pillar Grid Desgin With LGR

**Figure D- 8 Reservoir coarsening**

The first option, coarsening without LGR, will generate the “COARSEN” keyword for grid coarsening through the entire reservoir model and “FTRANS” for transmissibility modifiers for Nexus simulation model in the RECURRENT section. The detailed algorithm discussions are excluded from this manual. The following files are generated in the target folder: PILLAR\_COARSEN.inc, PILLAR\_SWIFT.inc, FTRANS\_COARSE@REC.inc and FTRANS\_COARSE@GRID.inc.

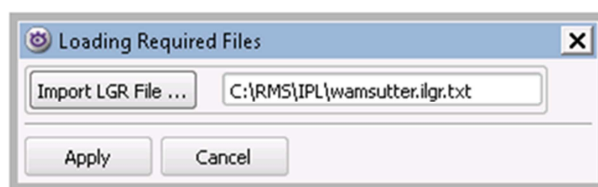


**Figure D- 9 LGR file import**

The second option, coarsening with LGR, requires input of the LGR distribution files (.ilgr file provided by BP), as seen in Figure D- 9, to preserve the necessary grids. No other property file is needed for adaptive gridding resolution control. Files containing COARSEN, LGR and FTRANS(at RECURRENT section) should be included at the same time to show the effect from different gridding resolutions. The following files will be generated in the target folder: PILLAR\_COARSEN.inc, PILLAR\_SWIFT.inc, FTRANS\_COARSE@REC.inc and FTRANS\_COARSE@GRID.inc.

Output from SWIFT\_PILLAR

**PILLAR\_SWIFT.inc:** File contains the keyword cards for Nexus. This file can be included in the input section of a Nexus Run

**PILLAR\_COARSEN.inc:** File contains the “COARSEN” keyword cards for Nexus. This file can be included in the GRID section of a Nexus Run

**FTRANS\_COARSEN@REC.inc:** File contains the transmissibility multipliers for coarsened grids. This file should be used in the RECURRENT section.

**FTRANS\_COARSEN@GRID.inc:** File contains the transmissibility multipliers for coarsened grids. This file should be used in the GRID section.

**Horizontal\_WELLSPEC.inc:** File contains WELLSPEC keyword information for horizontal wells. This file can be included in a Nexus Run.

**Vertical\_WELLSPEC.inc:** File contains WELLSPEC keyword information for vertical wells. This file can be included in a Nexus Run.

### A Step by Step Tutorial

This section will give a step by step tutorial in using SWIFT\_PILLAR. The model loaded in this tutorial is called “Sector”

1. In the **IPL** panel, load the SWIFT\_PILLAR file (.ipl) into the tree to view the ipl file.

2. Click the **Run** tab at the left bottom section to launch the main window.

3. Setup the working directory in the main window.

Working Directory :

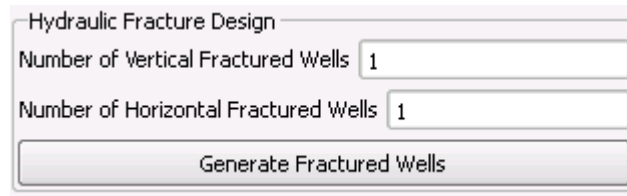
4. Setup the target grid model will be used:

RMS Grid Model Number:

5. Defining the reservoir zonation:

Reservoir Zonation  
Please specify top layer for each zone  
Separate layers with COMMAS and COMMAS ONLY (no spaces)

6. Using WI representing hydraulic fractures. Here we set the vertical and horizontal well to 1 and use the default well parameters. Files content for both vertical wells and horizontal wells are provided here.

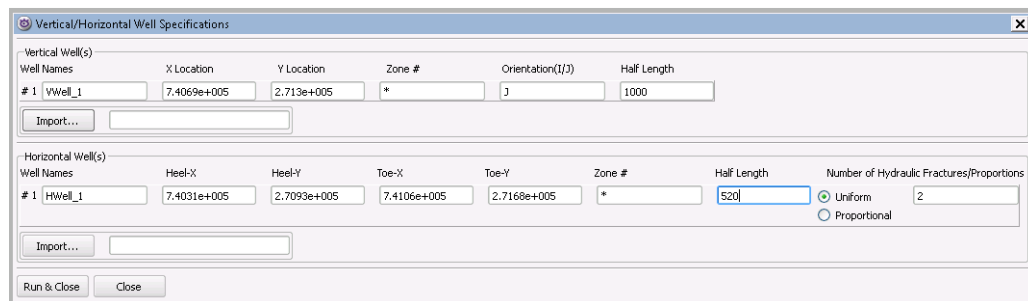


Hydraulic Fracture Design

Number of Vertical Fractured Wells

Number of Horizontal Fractured Wells

Well information can be seen as soon as the “Generate Fractured Wells” is clicked.



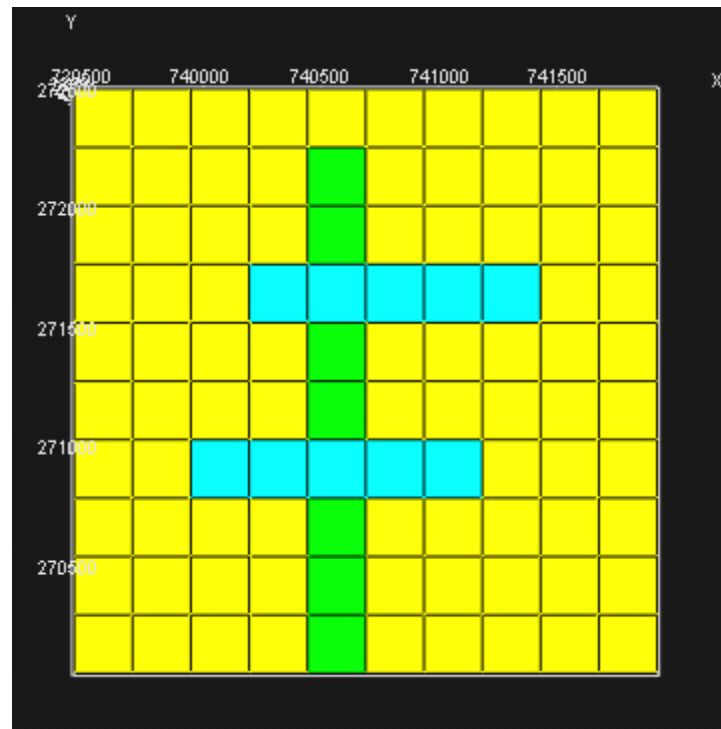
Vertical/Horizontal Well Specifications

Vertical Well(s)					
Well Names	X Location	Y Location	Zone #	Orientation(I/J)	Half Length
# 1   VWell_1	7.4069e+005	2.713e+005	*	J	1000

Horizontal Well(s)							
Well Names	Heel-X	Heel-Y	Toe-X	Toe-Y	Zone #	Half Length	Number of Hydraulic Fractures/Proportions
# 1   HWell_1	7.4031e+005	2.7093e+005	7.4106e+005	2.7168e+005	*	520	2

Uniform

To check the results, user can click on the “WELLID” parameter to visualize the created fractures for further modification. Fractures from different wells are labeled with different colors. As seen the following figure, we have one vertical well (fracture) labeled in green and one horizontal well with two fractures shown in blue. The horizontal well itself is not labeled.



Typical input file content for horizontal well and assuming we have at least 5 zones in this model:

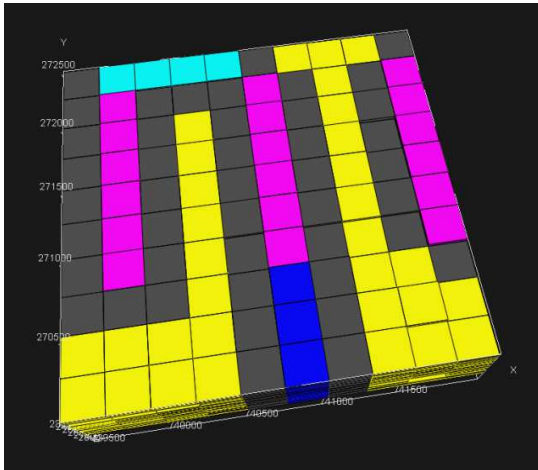
```
HorizontalWell_a 736000 327500 741000 327500 2,3 2000 Proportional 1,5,10,20
HorizontalWell_b 737000 332500 737000 324500 2,3,5 2000 Uniform 3
```

Typical input file content for vertical well:

```
VWell_a 741000 330000 1,3 J 3000
VWell_b 741000 330000 4,5 i 3000
```

7. Reservoir Coarsening. The grids are going to be different if the users are going to preserve the LGR regions or not. The LGR distribution file is provided by BP and no further modification is needed. The LGR affected cells and their adjacent cells are not going to be coarsened. Coarsening happens in the regions away from the LGR regions. As seen in the following figure. Light blue, dark blue and purple regions represent different LGR regions. Gray area shows the adjacent cells that preserved as a simulator transition zone required by Nexus and yellow zones labeled the area pillar-based upscaling can happen.





As mentioned previously, four files are going to be generated and three of them, PILLAR\_COARSEN.inc, PILLAR\_SWIFT.inc, FTRANS\_COARSE@REC.inc are going to be included in a Nexus run.